NREL/NASA Ames Science Panel - Blind Comparison Participants

Legend Identifier*	Participants (Attendees in Bold)	Organizations	Codes	Incomplete Output Files	Code Type
UIUC/Enron-C* UIUC/Enron-UIUC*	**Michael Selig Philippe Giguere**	University of Illinois/ Enron	PROPID-C PROPID-UI	No yaw, pitch moments.	Performance model with BEM and Corrigan stall delay model Performance model with BEM and UIUC stall delay model
ROTABEM-DTU	**Martin Hansen** Takis Chaviaropoulos	Tech Univ of Denmark/ CRES Greece	ROTABEM	No yaw, no downwind, no pitch moments.	Performance model with BEM using 3-D corrected airfoil data based on a quasi-3D Navier-Stokes solver
Global Energy Concepts, LLC	**David Malcolm, Tim McCoy, Dayton Griffin**	Global Energy Concepts	ADAMS	No pitch moments.	Multi-body aeroelastic model using "AeroDyn" aerodynamics (BEM/Leishman-Beddoes)
Loughborough University	**James Shawler**	Loughborough University CREST UK	YAWDYN	No dynamic pressure.	Aeroelastic model with rigid blade flapping hinge blade using "AeroDyn" aerodynamics (BEM/Leishman-Beddoes)
Windward (1) Windward (2) Windward (3)	**Craig Hansen, Dave Laino**	Windward Engineering	ADAMS		Multi-body aeroelastic model using "AeroDyn" aerodynamics (equilibrium wake, BEM/Leishman-Beddoes) Multi-body aeroelastic model using "AeroDyn" aerodynamics (dynamic inflow, BEM/Leishman-Beddoes) Multi-body aeroelastic model using "AeroDyn" aerodynamics (dynamic inflow and delayed stall, BEM/Leishman-Beddoes)
Garrad Hassan	**Robert Rawlinson -Smith**	Garrad-Hassan	*BLADED*	No pitch moment, root bending, torque, yaw moment.	Assumed modes aeroelastic model with BEM/Beddoes-Leishman aerodynamics
NASA Ames	**Wayne Johnson**	NASA Ames	Camrad II		Aero-mechanical rotorcraft analysis tool
RISOE – HAWC RISOE – HAWC3D	**Helge Madsen**	Risoe	HawC HawC-3D	No yaw. Yaw only.	Aeroelastic model with BEM theory Aeroelastic model with 3D CFD actuator disc model
ECN	Herman Snel, **Koert Lindenburg**	ECN	PHATAS		Aeroelastic model with BEM theory
Teknikgruppen AB	**Bjorn Montgomerie**, Anders Bjorck, **Hans Ganander**	FFA/ Nordic Windpower/ Teknikgruppen	VIDYN		Aeroelastic code with "AerForce" aerodynamics and "DynStall" dynamic stall (BEM/Leishman-Beddoes)
Risoe NNS	**Niels Sorensen**	Risoe	EllipSys3D	No yaw, no downwind	3D incompressible Navier-Stokes model
DTU1	**Robert Mikkelsen**	Tech.Univ. of Denmark	ADDWANS	No pitch moment, no yaw, no downwind	Combined Navier-Stokes BEM approach
Georgia Tech	Lakshmi Sankar **Guanpeng Xu**	Georgia Tech	Hybrid CFD	No yaw, no downwind,	3D multi-domain analysis unsteady Navier-Stokes model
CRES-NTUA	**Michael Belessis Spyros Voutsinas**	CRES-NTUA	GENUVP	No pitch moment, root bending, torque, yaw moment, downwind.	Vortex element, free wake model
Glasgow University	Frank Coton, Tongguang Wang, **Roddy Galbraith**	University of Glasgow	HawtDawg		Prescribed wake model (Horizontal Axis Wind Turbine Directly Allocated Wake Geometry)
TU Delft*	**Gerard Van Bussel**	Tech. Univ. of Delft	PREDICDYN	No S1500600, no pitch moments.	Assymptotic acceleration potential model
CRES-NTUA NS3D	**Michael Belessis Spyros Voutsinas**	CRES-NTUA	NS3D	S1000000 only, Cn, Ct only.	3D steady RANS finite volume formulation, Chimera mesh

* Did not provide documentation as specified in Blind Comparison Overview

Description of code and airfoil data used for the NREL 10-m Wind Turbine

Associate Professor Martin O.L.Hansen

Technical University of Denmark

Departmen t of Energy Engineering, Fluid Mec hanics Section Build. 403, DK-2800 Lyngby Denmark

Code description

The computations w ere done using a standard Blade Elemen t Mometnum method (BEM) as e.g. described in [1] including Prandtl's tip loss correction and a Glauert correction for high values of the thrust coefficien tC_T. Only stationary computations of the cases s0700000, s1000000, s1300000, s1500000, s2000000, s2500000 are performed using follo wing discretization of the blade

r [m]	twist	chord [m]
1.343	18.074	0.728
1.510	14.292	0.711
1.648	11.909	0.697
1.952	7.979	0.666
2.257	5.308	0.636
2.343	4.715	0.627
2.562	3.425	0.605
2.867	2.083	0.574
3.172	1.150	0.543
3.185	1.115	0.542
3.476	0.494	0.512
3.781	-0.015	0.482
4.023	-0.381	0.457
4.086	-0.475	0.451
4.391	-0.920	0.420
4.696	-1.352	0.389
4.780	-1.469	0.381
5.000	-1.775	0.358

A global pitch of 4.775^o is specified, i.e. the angle between the rotor plane and the tip chord is 3°. The results are put in the EX CEL file.

Airfoil data

The output of the BEM code depends strongly on the specified airfoil data and this is considered the main contribution of DTU1 (Technical University of Denmark) and a short description of how these are obtained and altered for 3-D effects are given. In the first step 2-D data was extracted from the measurements from Delft University of Technology Low Speed Laboratory low-turbulence wind tunnel Re=1·10^6, which are provided on http://wind2.nrel.gov/amestest/. These date are used up to an angle of attack of 20.16^o, but the point at 11.21^o is discarded since it is not believed that the drag has a local peak. For the higher angles of attack values of the lift and drag coefficients are extrapolated up to 90°. The lift is believed to be flat up to approximately 40° before it drops off smoothly to 0 at 90°. The drag coefficient is extrapolated from the measured data and it is assumed that the maximum value for an angle of attack of 90° is 1.3. The 2-D airfoil data are given in the table below

α	C_l	C_d
-1.04	0.019	0.0095
-0.01	0.139	0.0094
1.02	0.258	0.0096
2.05	0.378	0.0099
3.07	0.497	0.0100
4.10	0.617	0.0100
5.13	0.736	0.0097
6.16	0.851	0.0095
7.18	0.913	0.0127
8.20	0.952	0.0169
9.21	0.973	0.0247
10.20	0.952	0.0375
12.23	1.007	0.0636
13.22	1.031	0.0703
14.23	1.055	0.0828
15.23	1.062	0.1081
16.22	1.043	0.1425
17.21	0.969	0.1853
18.19	0.938	0.228
20.16	0.923	0.284
25.00	0.923	0.42
30.00	0.922	0.55
40.00	0.911	0.75
50.00	0.800	0.90
70.00	0.500	1.15
90.00	0.000	1.30

The 2-D airfoil data are corrected for 3-D rotational effects using a method derived by Chaviaropoulos and Hansen [2], valid for both the lift (x=l) and drag (x=d) coefficien ts.

$$C_{x,3D} = C_{x,2D} + a(c/r)^h cos^n(twist)\Delta C_x,$$

where

$$\Delta C_l = C_{l,INV} - C_{l,2D} \text{ and } \Delta C_d = C_{d,2D} - C_{d,2D-min}.$$

The constants are $a = 2.2$, $h = 1.3$ and $n = 4$. But since this implies that the lift coefficien t is not small for angles of attac k close to 90 the corrections are further m ultiplied by a function $f(\alpha)$, which is 1 for the lower angles of attack and 0 for the higher values. In this work the function is

$$f = 1 \qquad\qquad \alpha < 15^o$$
$$f = 0.5(cos(\pi\frac{\alpha-15}{25-15}) + 1) \qquad 15^o < \alpha < 25^o$$
$$f = 0 \qquad\qquad \alpha > 25^o.$$

With this function $f(\alpha)$ the 3-D rotational effects are only active for $\alpha < 25^o$. In Figure 1 is shown a comparison bet ween the pure 2-D and the 3-D corrected lift coefficien t as a function of the angle of attack for the spanwise position of r/R=0.3.
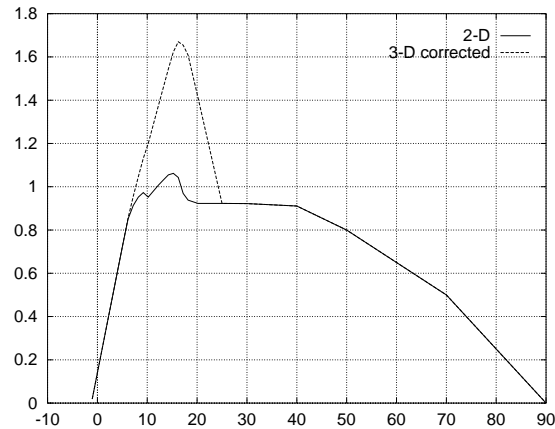

Figure 1: *Comparison bet ween pure 2-D and 3-D corrected airfoil data at r/R=0.30.*

References

[1] Hansen, M.O.L., 'Aerodynamics of Wind Turbines', James & James (Science Publishers) Ltd, 2000

[2] Chaviaropoulos, P.K. and Hansen, M.O.L., 'Investigating Three-Dimensional and Rotational Effects on Wind Turbine Blades by Means of a Quasi-3D Navier-Stokes Solver', Journal of Fluids Engineering, Vol. 122, pp. 330-337, June 2000.

Conceptual and Preliminary Design and
Modeling of Large-Scale Advanced Research Turbine (ART)

NREL Subcontract No. YAM-8-18208-01

NREL Advanced Research Turbine (ART)

Aerodynamic Loads Uncertainty Evaluation

November 13, 2000

Authors: Timothy J. McCoy
David J. Malcolm

Global Energy Concepts, LLC
5729 Lakeview Drive NE Suite 100
Kirkland, Washington 98033-7340
(425) 822-9008

1. Introduction

1.1 Background

Global Energy Concepts, LLC (GEC) has been working on the Advanced Research Turbine Project (ART) for the National Renewable Energy Laboratory (NREL) since the spring of 1998. In that time, a large quantity of loads data has been generated from various sources and analyzed by various methods. The sources for the data include field measurements, hand calculations, and several ADAMS™ models.

While it is believed that this information is reliable, it is worth investigating the uncertainty level of the load information by running the ADAMS model against a well characterized set of measurements. High quality wind turbine aerodynamic and structural load measurements have been made recently on the Unsteady Aerodynamics Experiment (UAE) turbine in the AMES/NASA wind tunnel.

1.2 Objective

The objective of this task was to make a blind comparison of the capability of the ADAMS and AeroDyn models to predict wind turbine aerodynamic and structural loads. The ADAMS model was created based on geometrical and structural information about the UAE turbine, and on adjusted two dimensional aerodynamic characteristics from wind tunnel testing. The results will be compared to the measured data after the modeling is complete.

1.3 Results

As requested by NREL, the results are in the file OutputFileFormat.xls.

1.4 References

1. "NREL/NWTC Aerodynamics Code Blind Comparison", September 7, 2000.
2. Malcolm, David J., Notebook "How to Use ADAMS DM/WT"
3. Hansen, Craig, "User's Guide for YawDyn and AeroDyn for ADAMS", University of Utah, January, 1996.
4. McCoy, Timothy J., Notebook "UAE Code Runoff ADAMS Modeling", October, 2000.

2. Modeling Approach

2.1 ADAMS

The results presented in this document are based on ADAMS™ modeling of the turbine. ADAMS is a proprietary general purpose, commercially available simulation package, available from MDI, Inc of Ann Arbor, Michigan. ADAMS is used for the dynamic analysis of mechanisms and structures. All runs were performed with ADAMS version 10.0 and AeroDyn version GEC0101which is a GEC derivative of the NREL AeroDyn version 10.

The following details the aspects of the model in regard to complexity and computation times:

- The model has 233 kinematic degrees of freedom.
- Each case is a simulation of 45 seconds of real time that includes 10 seconds of startup time, 5 seconds of "settling" time and 30 seconds of turbine operation.
- Computation times: 1300 to 1400 seconds of CPU time on a Pentium II 300 MHz per case.

2.2 Aerodynamic modeling

The aerodynamic model used in AeroDyn is the basic induction factor method with a skewed wake correction [3]. The model calculates the aerodynamic forces 500 times a second, or approximately every 0.864 degrees of rotor rotation.

Dynamic stall is modeled with the Beddoes model. Tip loss is accounted for with the Prandtl model.

The tower shadow is modeled as a velocity deficit on the freestream flow with a $\cos^2$ shape. The deficit is 30% and the width is 1 meter at a location 1 meter behind the tower centerline. The deficit decreases and the width increases with the square root of the distance from the tower.

2.3 Coordinate Systems and Rotations

The model uses a ground coordinate system with the x axis positive downwind, the z axis positive up and the y axis for a right handed system. The origin of this system is at the bottom of the semi-span mount on the tower centerline. The model uses local coordinate systems for the nacelle, shaft, hubs, and blades that are right hand rotations of the yaw, azimuth, flap hinges, and pitch bearings respectively. These differ from the standard wind turbine conventions that use left handed rotations for nacelle yaw and blade pitch. However, all rotation signal outputs are corrected as necessary to match the measurement convention of the UAE turbine. Otherwise the coordinate system is per IEC recommendations.

Because the AeroDyn model requires that the rotor rotate as a right handed system (CW looking downwind for both upwind and downwind rotors), the model rotates in the opposite direction to the actual turbine. It is believed that this will not cause any difficulties, however, to adjust appropriately, the yaw angle is also reversed relative to the actual turbine. All outputs are signed so as to compare directly with the wind tunnel test results.

2.4 Results Processing

ADAMS will output results at virtually any location and in any coordinate system. The results for this analysis were output directly at the various blade stations and load points. The required post processing consisted of calculating statistics, azimuth averaging, and calculating the aerodynamic coefficients, Cn, Ct, and Cm from the per unit span forces and the blade station dynamic pressures. The Cm results are zero since the AeroDyn model used by GEC has no built in provision for handling blade aerodynamic moments.

3. Model Description

3.1 Blade Aerodynamic Model

Table 3-1 describes the turbine blade geometry and Tables 3-2 and 3-3 present the adjusted lift and drag curves, respectively, for the blade stations. Aerodynamic moment coefficients were set to zero. The Corrigan post stall model was used to adjust the 2D airfoil data for 3D effects. The 2D data from the Delft wind tunnel at Re=1,000,000 were used at all blade stations.

Table 3-1 Blade Geometry

	Radius	Twist	Chord	Thickness	Airfoil
Station	m	Deg	m	% of chord	
1	0.432	0.00	0.080	100	Cylinder, no aero
2	0.754	0.00	0.203	100	Root transition
3	1.257	20.04	0.737	20.95	S809
4	1.508	14.34	0.711	20.95	S809
5	1.926	8.32	0.669	20.95	S809
6	2.344	4.71	0.627	20.95	S809
7	2.766	2.53	0.584	20.95	S809
8	3.183	1.12	0.542	20.95	S809
9	3.621	0.25	0.498	20.95	S809
10	4.023	-0.38	0.457	20.95	S809
11	4.400	-0.93	0.419	20.95	S809
12	4.778	-1.47	0.381	20.95	S809

Table 3-2 Airfoil Lift Coefficients

	--Blade Station --									
AOA	1	2	3	4	5	6	7	8	9	10	11
-180	0.000	-0.170	-0.170	-0.170	-0.170	-0.170	-0.170	-0.170	-0.170	-0.170	-0.170
-170	0.320	0.640	0.640	0.640	0.640	0.640	0.640	0.640	0.640	0.640	0.640
-160	0.440	0.840	0.840	0.840	0.840	0.840	0.840	0.840	0.840	0.840	0.840
-150	0.490	1.080	1.080	1.080	1.080	1.080	1.080	1.080	1.080	1.080	1.080
-140	0.540	1.150	1.150	1.150	1.150	1.150	1.150	1.150	1.150	1.150	1.150
-130	0.530	1.090	1.090	1.090	1.090	1.090	1.090	1.090	1.090	1.090	1.090
-120	0.460	0.880	0.880	0.880	0.880	0.880	0.880	0.880	0.880	0.880	0.880
-110	0.360	0.600	0.600	0.600	0.600	0.600	0.600	0.600	0.600	0.600	0.600
-100	0.250	0.310	0.310	0.310	0.310	0.310	0.310	0.310	0.310	0.310	0.310
-90	0.000	0.000	0.000	0.000	0.000	0.000	0.000	0.000	0.000	0.000	0.000
-80	-0.250	-0.310	-0.310	-0.310	-0.310	-0.310	-0.310	-0.310	-0.310	-0.310	-0.310
-70	-0.360	-0.600	-0.600	-0.600	-0.600	-0.600	-0.600	-0.600	-0.600	-0.600	-0.600
-60	-0.460	-0.880	-0.880	-0.880	-0.880	-0.880	-0.880	-0.880	-0.880	-0.880	-0.880
-50	-0.530	-1.090	-1.090	-1.090	-1.090	-1.090	-1.090	-1.090	-1.090	-1.090	-1.090
-40	-0.540	-1.150	-1.150	-1.150	-1.150	-1.150	-1.150	-1.150	-1.150	-1.150	-1.150
-30	-0.500	-1.080	-1.080	-1.080	-1.080	-1.080	-1.080	-1.080	-1.080	-1.080	-1.080
-20	-0.440	-0.840	-0.840	-0.840	-0.840	-0.840	-0.840	-0.840	-0.840	-0.840	-0.840
-10	-0.320	-0.640	-0.640	-0.640	-0.640	-0.640	-0.640	-0.640	-0.640	-0.640	-0.640
-6	-0.190	-0.558	-0.573	-0.578	-0.573	-0.564	-0.553	-0.541	-0.530	-0.519	-0.507
-4	-0.130	-0.325	-0.325	-0.325	-0.325	-0.325	-0.325	-0.325	-0.325	-0.325	-0.325
-3	-0.095	-0.209	-0.209	-0.209	-0.209	-0.209	-0.209	-0.209	-0.209	-0.209	-0.209
-1	-0.026	0.019	0.019	0.019	0.019	0.019	0.019	0.019	0.019	0.019	0.019
0	0.010	0.139	0.139	0.139	0.139	0.139	0.139	0.139	0.139	0.139	0.139
1	0.041	0.258	0.258	0.258	0.258	0.258	0.258	0.258	0.258	0.258	0.258
2	0.072	0.378	0.378	0.378	0.378	0.378	0.378	0.378	0.378	0.378	0.378
4	0.151	0.643	0.664	0.673	0.665	0.652	0.636	0.618	0.601	0.585	0.569
5	0.187	0.763	0.784	0.793	0.785	0.772	0.756	0.738	0.721	0.705	0.689
6	0.220	0.882	0.903	0.912	0.904	0.891	0.875	0.857	0.840	0.824	0.808
7	0.245	0.997	1.018	1.027	1.019	1.006	0.990	0.972	0.955	0.939	0.923
8	0.273	1.059	1.080	1.089	1.081	1.068	1.052	1.034	1.017	1.001	0.985
9	0.304	1.096	1.118	1.126	1.119	1.105	1.090	1.072	1.055	1.039	1.022
10	0.336	1.119	1.141	1.149	1.142	1.128	1.112	1.095	1.078	1.061	1.045
11	0.371	1.139	1.161	1.169	1.162	1.148	1.133	1.115	1.098	1.081	1.065
12	0.399	1.157	1.179	1.187	1.180	1.167	1.151	1.133	1.116	1.100	1.083
13	0.420	1.173	1.195	1.203	1.196	1.182	1.167	1.149	1.132	1.116	1.099
14	0.435	1.187	1.208	1.216	1.209	1.196	1.180	1.162	1.145	1.129	1.112
15	0.445	1.198	1.219	1.227	1.220	1.207	1.191	1.173	1.156	1.140	1.123
16	0.452	1.206	1.228	1.236	1.229	1.216	1.200	1.182	1.165	1.149	1.132
17	0.457	1.189	1.210	1.219	1.211	1.198	1.182	1.164	1.147	1.131	1.115
20	0.440	0.840	0.840	0.840	0.840	0.840	0.840	0.840	0.840	0.840	0.840
30	0.490	1.080	1.080	1.080	1.080	1.080	1.080	1.080	1.080	1.080	1.080
40	0.540	1.150	1.150	1.150	1.150	1.150	1.150	1.150	1.150	1.150	1.150
50	0.530	1.090	1.090	1.090	1.090	1.090	1.090	1.090	1.090	1.090	1.090
60	0.460	0.880	0.880	0.880	0.880	0.880	0.880	0.880	0.880	0.880	0.880
70	0.360	0.600	0.600	0.600	0.600	0.600	0.600	0.600	0.600	0.600	0.600
80	0.250	0.310	0.310	0.310	0.310	0.310	0.310	0.310	0.310	0.310	0.310
90	0.000	0.000	0.000	0.000	0.000	0.000	0.000	0.000	0.000	0.000	0.000
100	-0.250	-0.310	-0.310	-0.310	-0.310	-0.310	-0.310	-0.310	-0.310	-0.310	-0.310
110	-0.360	-0.600	-0.600	-0.600	-0.600	-0.600	-0.600	-0.600	-0.600	-0.600	-0.600
120	-0.460	-0.880	-0.880	-0.880	-0.880	-0.880	-0.880	-0.880	-0.880	-0.880	-0.880
130	-0.530	-1.090	-1.090	-1.090	-1.090	-1.090	-1.090	-1.090	-1.090	-1.090	-1.090
140	-0.540	-1.150	-1.150	-1.150	-1.150	-1.150	-1.150	-1.150	-1.150	-1.150	-1.150
150	-0.490	-1.080	-1.080	-1.080	-1.080	-1.080	-1.080	-1.080	-1.080	-1.080	-1.080
160	-0.440	-0.840	-0.840	-0.840	-0.840	-0.840	-0.840	-0.840	-0.840	-0.840	-0.840
170	-0.320	-0.640	-0.640	-0.640	-0.640	-0.640	-0.640	-0.640	-0.640	-0.640	-0.640
180	0.000	-0.170	-0.170	-0.170	-0.170	-0.170	-0.170	-0.170	-0.170	-0.170	-0.170

Table 3-3 Airfoil Drag Coefficients

--Blade Station --

AOA	1	2	3	4	5	6	7	8	9	10	11
-180	0.7384	0.0200	0.0200	0.0200	0.0200	0.0200	0.0200	0.0200	0.0200	0.0200	0.0200
-170	0.7409	0.0500	0.0500	0.0500	0.0500	0.0500	0.0500	0.0500	0.0500	0.0500	0.0500
-160	0.7961	0.3100	0.3100	0.3100	0.3100	0.3100	0.3100	0.3100	0.3100	0.3100	0.3100
-150	0.9000	0.6200	0.6200	0.6200	0.6200	0.6200	0.6200	0.6200	0.6200	0.6200	0.6200
-140	1.0676	0.9600	0.9600	0.9600	0.9600	0.9600	0.9600	0.9600	0.9600	0.9600	0.9600
-130	1.1992	1.3000	1.3000	1.3000	1.3000	1.3000	1.3000	1.3000	1.3000	1.3000	1.3000
-120	1.2983	1.5200	1.5200	1.5200	1.5200	1.5200	1.5200	1.5200	1.5200	1.5200	1.5200
-110	1.3618	1.6600	1.6600	1.6600	1.6600	1.6600	1.6600	1.6600	1.6600	1.6600	1.6600
-100	1.4052	1.7600	1.7600	1.7600	1.7600	1.7600	1.7600	1.7600	1.7600	1.7600	1.7600
-90	1.4439	1.8000	1.8000	1.8000	1.8000	1.8000	1.8000	1.8000	1.8000	1.8000	1.8000
-80	1.4052	1.7600	1.7600	1.7600	1.7600	1.7600	1.7600	1.7600	1.7600	1.7600	1.7600
-70	1.3618	1.6600	1.6600	1.6600	1.6600	1.6600	1.6600	1.6600	1.6600	1.6600	1.6600
-60	1.2983	1.5200	1.5200	1.5200	1.5200	1.5200	1.5200	1.5200	1.5200	1.5200	1.5200
-50	1.1992	1.3000	1.3000	1.3000	1.3000	1.3000	1.3000	1.3000	1.3000	1.3000	1.3000
-40	1.0676	0.9600	0.9600	0.9600	0.9600	0.9600	0.9600	0.9600	0.9600	0.9600	0.9600
-30	0.9000	0.6200	0.6200	0.6200	0.6200	0.6200	0.6200	0.6200	0.6200	0.6200	0.6200
-20	0.7961	0.3100	0.3100	0.3100	0.3100	0.3100	0.3100	0.3100	0.3100	0.3100	0.3100
-10	0.7417	0.0500	0.0500	0.0500	0.0500	0.0500	0.0500	0.0500	0.0500	0.0500	0.0500
-6	0.7403	0.0100	0.0100	0.0100	0.0100	0.0100	0.0100	0.0100	0.0100	0.0100	0.0100
-4	0.7389	0.0098	0.0098	0.0098	0.0098	0.0098	0.0098	0.0098	0.0098	0.0098	0.0098
-3	0.7386	0.0095	0.0095	0.0095	0.0095	0.0095	0.0095	0.0095	0.0095	0.0095	0.0095
-1	0.7383	0.0095	0.0095	0.0095	0.0095	0.0095	0.0095	0.0095	0.0095	0.0095	0.0095
0	0.7384	0.0094	0.0094	0.0094	0.0094	0.0094	0.0094	0.0094	0.0094	0.0094	0.0094
1	0.7384	0.0096	0.0096	0.0096	0.0096	0.0096	0.0096	0.0096	0.0096	0.0096	0.0096
2	0.7384	0.0099	0.0099	0.0099	0.0099	0.0099	0.0099	0.0099	0.0099	0.0099	0.0099
4	0.7384	0.0100	0.0100	0.0100	0.0100	0.0100	0.0100	0.0100	0.0100	0.0100	0.0100
5	0.7385	0.0100	0.0100	0.0100	0.0100	0.0100	0.0100	0.0100	0.0100	0.0100	0.0100
6	0.7388	0.0097	0.0097	0.0097	0.0097	0.0097	0.0097	0.0097	0.0097	0.0097	0.0097
7	0.7397	0.0095	0.0095	0.0095	0.0095	0.0095	0.0095	0.0095	0.0095	0.0095	0.0095
8	0.7404	0.0127	0.0127	0.0127	0.0127	0.0127	0.0127	0.0127	0.0127	0.0127	0.0127
9	0.7407	0.0169	0.0169	0.0169	0.0169	0.0169	0.0169	0.0169	0.0169	0.0169	0.0169
10	0.7411	0.0247	0.0247	0.0247	0.0247	0.0247	0.0247	0.0247	0.0247	0.0247	0.0247
11	0.7415	0.0375	0.0375	0.0375	0.0375	0.0375	0.0375	0.0375	0.0375	0.0375	0.0375
12	0.7420	0.0725	0.0725	0.0725	0.0725	0.0725	0.0725	0.0725	0.0725	0.0725	0.0725
13	0.7425	0.0636	0.0636	0.0636	0.0636	0.0636	0.0636	0.0636	0.0636	0.0636	0.0636
14	0.7436	0.0703	0.0703	0.0703	0.0703	0.0703	0.0703	0.0703	0.0703	0.0703	0.0703
15	0.7454	0.0828	0.0828	0.0828	0.0828	0.0828	0.0828	0.0828	0.0828	0.0828	0.0828
16	0.7508	0.1081	0.1081	0.1081	0.1081	0.1081	0.1081	0.1081	0.1081	0.1081	0.1081
17	0.7600	0.1425	0.1425	0.1425	0.1425	0.1425	0.1425	0.1425	0.1425	0.1425	0.1425
20	0.7961	0.3100	0.3100	0.3100	0.3100	0.3100	0.3100	0.3100	0.3100	0.3100	0.3100
30	0.9319	0.6200	0.6200	0.6200	0.6200	0.6200	0.6200	0.6200	0.6200	0.6200	0.6200
40	1.0676	0.9600	0.9600	0.9600	0.9600	0.9600	0.9600	0.9600	0.9600	0.9600	0.9600
50	1.1992	1.3000	1.3000	1.3000	1.3000	1.3000	1.3000	1.3000	1.3000	1.3000	1.3000
60	1.2983	1.5200	1.5200	1.5200	1.5200	1.5200	1.5200	1.5200	1.5200	1.5200	1.5200
70	1.3618	1.6600	1.6600	1.6600	1.6600	1.6600	1.6600	1.6600	1.6600	1.6600	1.6600
80	1.4052	1.7600	1.7600	1.7600	1.7600	1.7600	1.7600	1.7600	1.7600	1.7600	1.7600
90	1.4439	1.8000	1.8000	1.8000	1.8000	1.8000	1.8000	1.8000	1.8000	1.8000	1.8000
100	1.4052	1.7600	1.7600	1.7600	1.7600	1.7600	1.7600	1.7600	1.7600	1.7600	1.7600
110	1.3618	1.6600	1.6600	1.6600	1.6600	1.6600	1.6600	1.6600	1.6600	1.6600	1.6600
120	1.2983	1.5200	1.5200	1.5200	1.5200	1.5200	1.5200	1.5200	1.5200	1.5200	1.5200
130	1.1992	1.3000	1.3000	1.3000	1.3000	1.3000	1.3000	1.3000	1.3000	1.3000	1.3000
140	1.0676	0.9600	0.9600	0.9600	0.9600	0.9600	0.9600	0.9600	0.9600	0.9600	0.9600
150	0.9000	0.6200	0.6200	0.6200	0.6200	0.6200	0.6200	0.6200	0.6200	0.6200	0.6200
160	0.7961	0.3100	0.3100	0.3100	0.3100	0.3100	0.3100	0.3100	0.3100	0.3100	0.3100
170	0.7409	0.0500	0.0500	0.0500	0.0500	0.0500	0.0500	0.0500	0.0500	0.0500	0.0500
180	0.7384	0.0200	0.0200	0.0200	0.0200	0.0200	0.0200	0.0200	0.0200	0.0200	0.0200

Table 3-4 Blade Structural and Inertial Properties

ADAMS Part ID#	Beam ID#	CG Radius (m)	Beam length (m)	Density (kg/m)	Part mass (kg)	I1 (kg.m^2/m)	I2 (kg.m^2/m)	Chordwise cg offset m (y dir)	Aero center m (y dir)	Elastic axis offset m (y dir)	Principal axis twist (deg)	EA (N)	Flap Elyy (N.m^2)	Edge Elxx (N.m^2)	GJ (N.m^2)	GA (N)
5100		0.432		40.00	6.44	1.60E-02	1.60E-02	0	0		0	5.03E+08	2.37E+05	2.37E+05	1.80E+05	1.91E+08
	5100		0.322													
10100		0.754		19.08	7.87	2.71E-03	6.57E-02	0	0	0.018	10.020	2.04E+07	1.16E+06	4.06E+06	8.12E+05	1.16E+06
	10100		0.503													
10200		1.257		18.64	7.03	2.00E-02	8.44E-01	0.037	-0.037	0.036	17.189	2.28E+06	2.28E+06	7.78E+06	7.78E+05	4.56E+05
	10200		0.251													
10300		1.508		16.93	5.66	3.13E-02	7.13E-01	0.036	-0.036	0.034	11.326	1.71E+08	2.28E+06	7.78E+05	4.56E+05	4.56E+05
	10300		0.418													
10400		1.926		14.08	5.88	2.30E-02	5.24E-01	0.033	-0.033	0.032	6.512	1.80E+08	1.24E+06	6.66E+05	2.49E+05	7.78E+05
	10400		0.418													
10500		2.344		13.13	5.52	1.89E-02	4.30E-01	0.031	-0.031	0.030	3.618	1.66E+08	6.66E+05	5.64E+05	9.58E+04	6.66E+05
	10500		0.422													
10600		2.766		12.51	5.25	1.56E-02	3.56E-01	0.029	-0.029	0.028	1.824	1.49E+08	4.79E+05	4.99E+05	8.13E+04	5.64E+05
	10600		0.417													
10700		3.183		11.77	5.03	1.27E-02	2.88E-01	0.027	-0.027	0.026	0.686	9.77E+07	1.73E+05	2.80E+05	3.45E+04	4.99E+05
	10700		0.438													
10800		3.621		11.00	4.62	9.96E-03	2.27E-01	0.025	-0.025	0.024	-0.064	1.15E+08	2.61E+05	3.69E+05	5.23E+04	3.45E+05
	10800		0.402													
10900		4.023		10.22	3.98	7.81E-03	1.78E-01	0.023	-0.023	0.022	-0.657	8.22E+07	1.15E+05	2.18E+05	2.31E+04	2.80E+05
	10900		0.377													
11000		4.400		9.49	3.58	6.10E-03	1.39E-01	0.021	-0.021	0.020	-1.199	1.10E+08	2.16E+05	3.25E+05	4.32E+04	3.69E+05
	11000		0.378													
11100		4.778		9.29	1.75	4.93E-03	1.12E-01	0.019	-0.019							3.25E+05
Total					62.6											

3.2 Structural Model

3.2.1 ADAMS

The ADAMS structural model is made up of three primary elements: parts, beams, and joints. Parts are entities that have mass and inertial properties but no flexibility. Parts are connected to one another via either beams or joints. Beams are flexible members with no mass that can connect two parts. Joints are connections between parts that allow some combination of rigid body translations and/or rotations. In the figures the parts are outlined with a fine line and the beams are indicated with a heavy line. Beam connection points are indicated with a large dot.

3.2.2 Blades

The blade is modeled as a series of 12 parts connected by 11 beams. Table 3-4 presents the mass, inertial and structural properties of the blade assigned to the individual parts and beams. The center of gravity of each part outboard of the maximum chord locations has been estimated to be at the 35% chord location. The elastic centers for each beam have also been estimated to be at the 35% chord locations.

The blade flapwise stiffness was increased by 3.5 times the original specification in order to match the modal test results. Aerodynamic forces are applied to all of the parts except the most inboard part. These are applied at the aerodynamic center, estimated to be at the 25% chord location.

The local blade section origin is the pitch line, at 50% chord for the first two stations and at 30% chord outboard. The y direction referred to in Table 3-4 is the local blade y axis along the chord line, positive towards the trailing edge. A plan view schematic of the blade model is shown in Figure 3-1.

3.2.3 Hub

The flapping hub is modeled with two parts (one for each blade) connected to the shaft part by revolute joints (no translational and one rotational degree of freedom) for flap motion. These joints are used to set the rotor coning as necessary. The hub parts are connected to the pitch shaft parts via revolute joints to model the pitch bearings. The tables below describe the hub parts. The CG coordinates are in the ground (same as tower) reference frame. The boom and camera are modeled as a single part connected to the end of the shaft.

The hub itself is modeled as a rigid part. A beam, representing the flexibility of the pitch shaft, is used to connect the pitch shaft part to the first blade part. This beam is fixed to the pitch shaft part at the strain gage location, 0.432 m from the center of rotation. The beam axes are rotated 2.5 degrees to align with the tip chord. This beam is detailed in Table 3-6. A schematic of the model is shown in Figure 3-2.

Table 3-5 Hub Model – Parts

Item	ID #	CGx,y,z	Mass, kg	Ix, kg.m^2	Iy, kg.m^2	Iz, kg.m^2
Blade 1 hub	4100	±1.401, 0, 14.484	147.5	4.86	4.86	3.15
Blade 2 hub	4200	±1.401, 0, 13.984	147.5	4.86	4.86	3.15
Pitch shaft 1	5150	±1.401, 0, 14.484	10.0	0.16	0.16	0.10
Pitch shaft 2	5250	±1.401, 0, 13.984	10.0	0.16	0.16	0.10
Boom/camera	3600	±2.0, 0, 14.234	141.9	3.50	4.00	4.00

± Refers to downwind/upwind orientation

Table 3-6 Hub Model – Beam

Item	Beam ID	Endpoint x,y,z	Endpoint x,y,z	Length, m	Area, m^2	EI, m^4	GJ, m^4
Pitch shaft 1	5150	±1.401, 0, 14.584	-1.401, 0, 14.666	0.082	0.050	2.0E-5	4.0E-5
Pitch shaft 1	5250	±1.401, 0, 13.884	-1.401, 0, 13.802	0.082	0.050	2.0E-5	4.0E-5

± Refers to downwind/upwind orientation

3.2.4 Drive Train

The drive train is modeled with parts, joints, and beams representing the shaft, bearings, and generator. There is no gearing modeled, all motions and loads are in the low speed frame of reference. The four shaft parts and three beams are "in series". The shaft is split this way to allow accurate modeling of the bearing connections to the mainframe. The motor part is connected to the end of the shaft with a fixed (no flexibility) connection. The shaft beam connections are intended to represent the entire drivetrain flexibility. Tables 3-7, 3-8 and 3-9 below describe the drive train parts, joints, and beams. The CG coordinates are in the ground (same as tower) reference frame. A schematic of the model is shown in Figure 3-2.

Table 3-7 Drive Train Model – Parts

Item	ID #	CGx,y,z	Mass, kg	Ix, $kg.m^2$	Iy, $kg.m^2$	Iz, $kg.m^2$
Shaft 1	3400	±1.242, 0, 14.234	2.05	9.3E-4	0.32	0.32
Shaft 2	3300	±0.99, 0, 14.234	0.25	1.1E-4	5.2E-4	5.2E-4
Shaft 3	3200	±0.635, 0, 14.234	3.0	1.4E-3	1.0	1.0
Shaft 4	3100	±0.18, 0, 14.234	0.925	4.2E-4	0.12	0.12
Generator	3500	-/+1.0, 0, 14.234	179.0	150.0*	20.0	20.0

* Reflects multiplication by gear ratio squared
± Refers to downwind/upwind orientation

Table 3-8 Drivetrain Model - Bearings

Item	Joint ID	Location x,y,z	Constraint	Connected Between Parts
Rotor end	2203	±0.99, 0, 14.234	Fy, Fz	3300 and 2200
Gearbox end	2202	±0.28, 0, 14.234	Fx, Fy, Fz	3100 and 2200
Generator	2301	-/+1.0, 0, 14.234	Fy, Fz	3500 and 2300

± Refers to downwind/upwind orientation

Table 3-9 Shaft Model – Beams

Item	Beam ID	Endpoint x,y,z	Endpoint x,y,z	Length, m	Area, m^2	EI, m^4	GJ, m^4
Shaft	3400	±1.469, 0, 14.234	±0.99, 0, 14.234	0.479	5.72E-4	1.3E-6	2.6E-6
Shaft	3300	±0.99, 0, 14.234	±0.635, 0, 14.234	0.355	5.72E-4	1.3E-6	2.6E-6
Shaft	3200	±0.635, 0, 14.234	±0.28, 0, 14.234	0.355	5.72E-4	1.3E-6	2.6E-6

± Refers to downwind/upwind orientation

3.2.5 Nacelle

The mainframe is modeled with three parts representing the box beam structure, the bedplate (which is a plate that connects the box beam to the yaw column), and a third part for additional nacelle mass. The flexibility of the box beam structure is represented by a beam which connects the rotor end of the box beam to the bedplate. The yaw column is modeled with a part and a beam. The beam connects the bedplate to the bottom of the yaw column (yaw bearing end). The yaw bearing is modeled with a revolute joint connecting the bottom end of the yaw column to the top of the tower. Tables 3-10 and 3-11 below describe the parts and beams. The nacelle structure is depicted schematically in Figure 3-2.

Table 3-10 Nacelle Model – Parts

Item	ID #	CGx,y,z	Mass, kg	Ix, kg.m^2	Iy, kg.m^2	Iz, kg.m^2
Box beam	2200	0, 0, 13.911	300	20	200	200
Bedplate	2100	0, 0, 13.911	40	1	1	1
Yaw column	2000	0, 0, 13.55	106.5	5.68	5.68	2.40
Nacelle mass	2300	0, 0, 14.234	815	2700	1887	1887

Table 3-11 Nacelle Model – Beams

Item	Beam ID	Endpoint x,y,z	Endpoint x,y,z	Length, m	Area, m^2	EI, m^4	GJ, m^4
Box beam	2200	±0.99, 0, 13.911	0, 0, 13.911	0.99	0.01136	1.03E-4, 1.05E-3	1.28E-4
Yaw column	2000	0, 0, 13.911	0, 0, 13.20	0.711	0.0191	2.156E-4	4.31E-4

3.2.6 Generator model

The generator torque, T, is modeled with the following function, where a = rpm/42.

$$T[N.m] = 29.5*a/(0.02428a^2 + 0.00106*a + 0.0002)$$

This equation represents a slip of 1.69% at a rated torque of 2620 N.m. The torque is in the low speed frame of reference.

3.2.7 Tower

The tower is modeled with a series of parts and beams. The total mass was reduced by 18% from the specified mass to obtain natural frequencies matching the modal test. The parts and beams are described in the Table 3-12 and depicted in Figure 3-3.

Table 3-12 Tower Structural and Inertial Properties

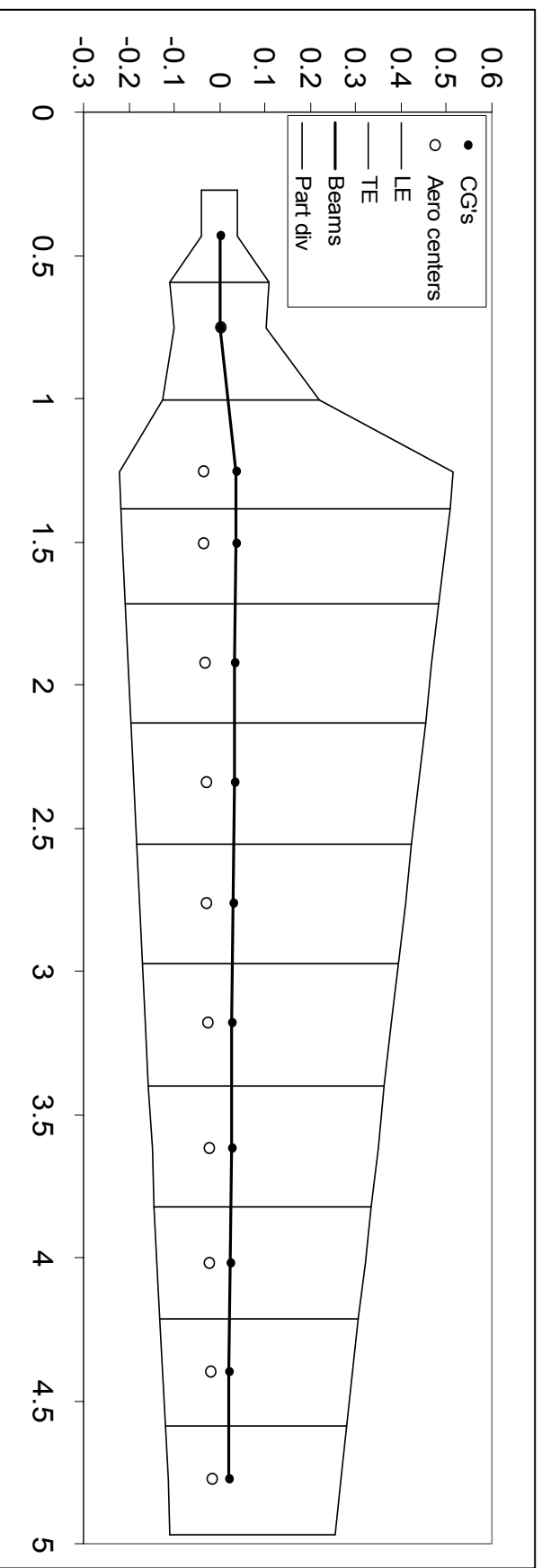| ADAMS part ID	CG Height	Beam ID	Beam connect	Tube_id	Wall thickness	Beam length	Section area	Section Iyy,Izz	Section J	Beam mass	Non-struct mass	Part mass	Part Ix,y	Part Ix,y
	m		m	m	m	m	m^2	m^4	m^4	kg	kg	kg	kg.m^2	kg.m^2
1	0.000	11	0.000	0.000	0.000	0.000	0.000	0.000	0.000	0.000	0.0	0.0	0.000	0.000
1100	0.850	1101	1.700	1.829	0.0175	1.700	9.959E-02	4.086E-02	8.171E-02	1346.1	8.5	1354.6	881.9	1111.4
1200	2.550	1201	3.400	0.6096	0.0175	1.700	3.255E-02	1.428E-03	2.856E-03	451.4	8.5	459.9	130.9	40.3
1300	4.250	1301	5.100	0.6096	0.0175	1.700	3.255E-02	1.428E-03	2.856E-03	451.4	8.5	459.9	130.9	40.3
1400	5.350	1401	5.600	0.508	0.0214	0.500	3.271E-02	9.701E-04	1.940E-03	133.4	2.5	135.9	6.86	8.06
1500	6.480	1501	7.360	0.4064	0.0214	1.760	2.588E-02	4.811E-04	9.621E-04	375.2	8.8	384.0	106.26	14.27
1600	8.120	1601	8.880	0.4064	0.0214	1.520	2.588E-02	4.811E-04	9.621E-04	324.0	7.6	331.6	70.02	12.33
1700	9.540	1701	10.200	0.4064	0.0214	1.320	2.588E-02	4.811E-04	9.621E-04	281.4	6.6	288.0	47.17	10.71
1800	10.775	1801	11.350	0.4064	0.0214	1.150	2.588E-02	4.811E-04	9.621E-04	245.2	5.8	250.9	32.32	9.33
1900	11.845	1901	12.340	0.4064	0.0214	0.990	2.588E-02	4.811E-04	9.621E-04	211.1	5.0	216.0	21.66	8.03
1950	12.770	1951	13.200	0.4064	0.0214	0.860	2.588E-02	4.811E-04	9.621E-04	183.3	4.3	187.6	15.05	6.98
									Totals (kg)		58	2714		

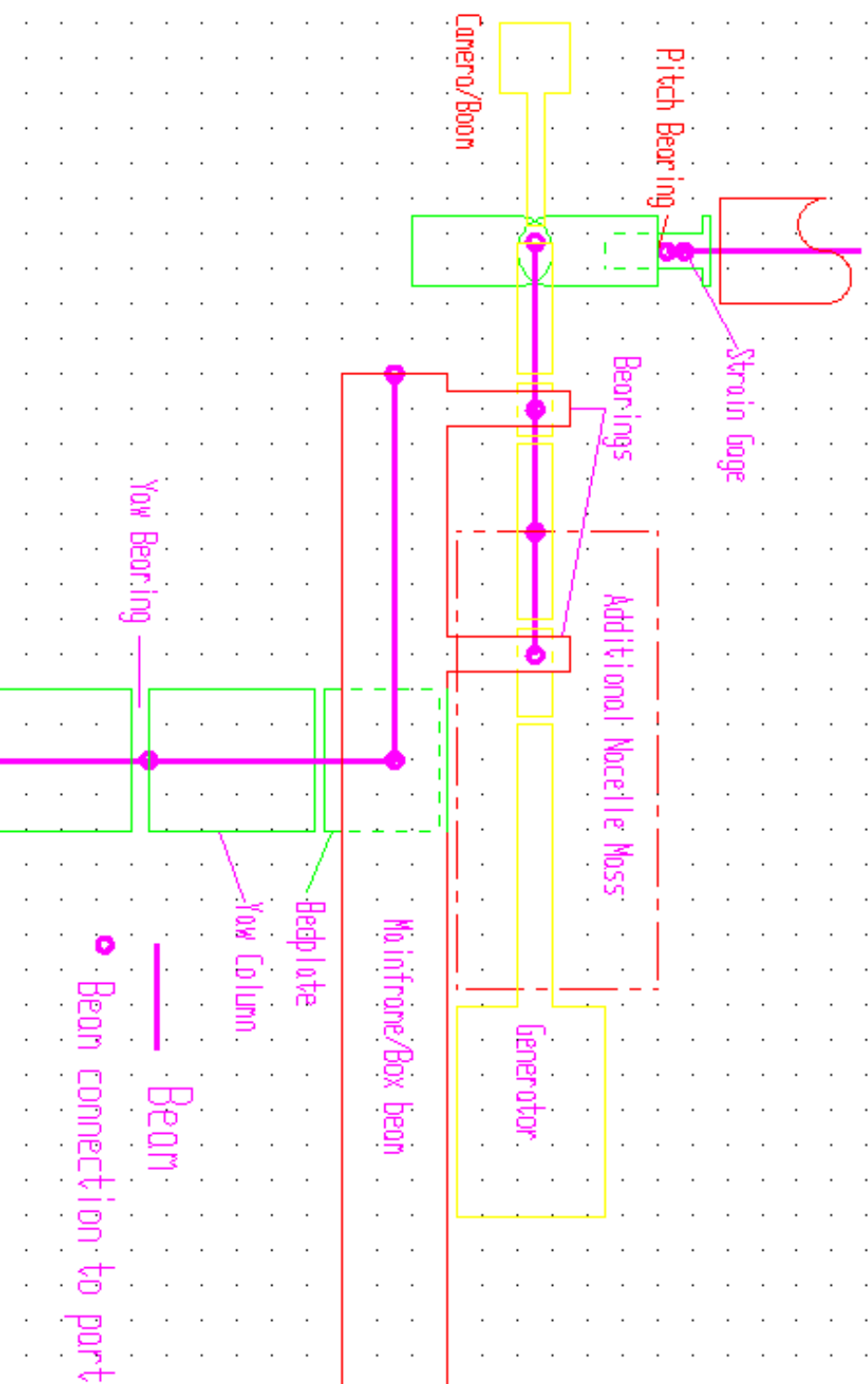**Figure 3–1 Schematic of ADAMS structural model of the blade**

Global Energy Concepts, LLC
ADAMS/AeroDyn

Figure 3-2 Schematic of ADAMS structural model of the hub, mainframe, and yaw column

Camera/Boom

Pitch Bearing

Strain Gage

Bearings

Additional Nacelle Mass

Generator

Yaw Bearing

Yaw Column

Bedplate

Mainframe/Box beam

Beam

Beam connection to part

Yaw Bearing

Tunnel floor

Semi-span mount
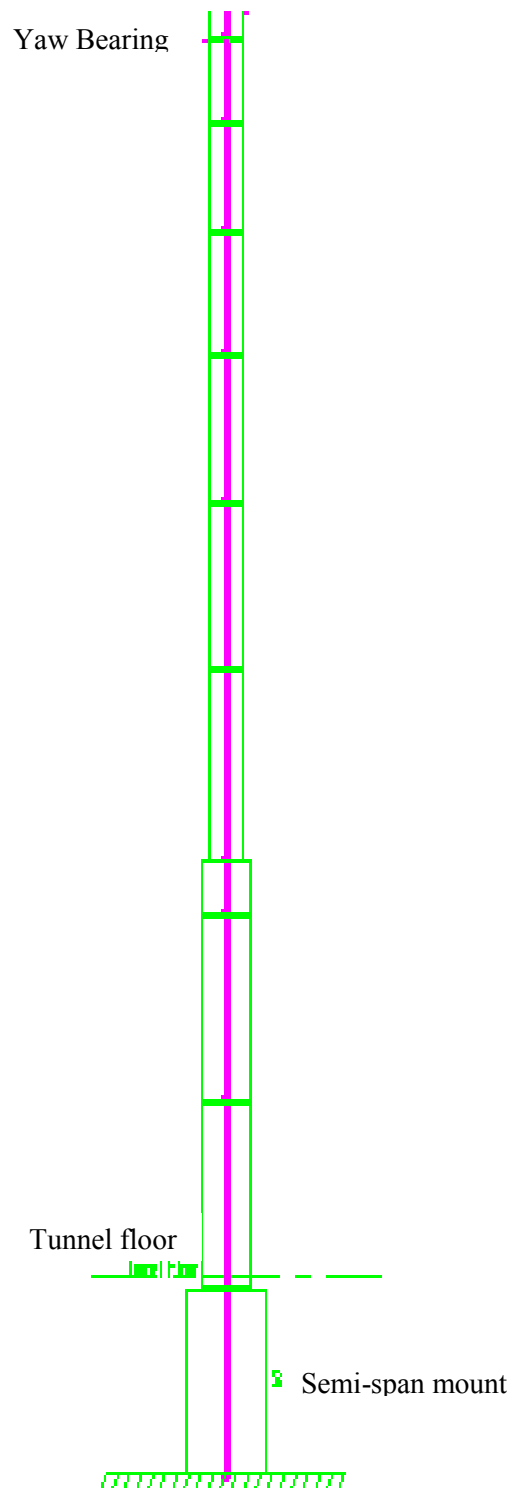
Figure 3–3 Schematic of ADAMS structural model of the tower

Blind Code Runoff: Initial Yawdyn Model Description and Definitions

James R Shawler
Centre for Renewable Energy Systems Technology,
Loughborough University, United Kingdom.

12th November 2000

1. Bl ind Code Yawdyn Model

This is an brief report on the structure of a YAWDYN model constructed for the NREL blind code runoff.

It is intended to present the details of the model as constructed and the assumptions made for the 20 case simulations.

The model used has a rigid hub with flapping hinges for the blades and the rotor has a fixed rotational speed and a fixed yaw angle.

1.1. Blade Calculations

1.1.1. Blade Mass and Inertial Calculations

The mass distribution used for the blade was based upon the one given in the Turbine Properties document for the mass distribution of the twisted, constant chord Phase V blades (Table A9).

This was modified to improve the correlation with the measured physical properties of the twisted, tapered blades which were used for the NASA Ames tests, the distribution of lumped masses used is given in table 1.1.

Which gives a total blade mass of 60.22Kg.

The flapping hinge in the model was positioned at the same radial distance as the strain gauges for edge and flap moments, 0.432m.

These figures give the resulting physical properties:

Blade centre of gravity from the centre of rotation: 2.253m.

Blade centre of gravity from the flapping hinge: 1.821m.

Blade moment of inetia around centre of rotation: 395.4Kgm^2.

Blade moment of inertia around the flapping hinge: 289.3Kgm^2.

This means that the rotational inertia of the rotor is 395.4*2 = 790.8Kgm^2. Which is a bit lower than the quoted inertia of 949Kgm^2 for the rotor because the mass and inertia of the hub and instrumentation is missing.

The stiffness of the flapping hinge was calculated from equation 1.1.

Radial Distance (m)	Mass (Kg)
0.6285	2.89606
0.8775	5.348195
1.2575	15.767015
1.7605	7.368115
2.2635	6.16966
2.7665	5.810015
3.269	5.15575
3.7715	4.504615
4.2745	3.816705
4.7775	3.390355

Table 1.1: Blade lumped mass distribution

$$Frequency = \frac{1}{2\pi}\sqrt{\frac{K}{I}} \tag{1.1}$$

Using a desired of frequency of 7.3Hz and the value of the blades inertia around the hinge of 289.3Kgm^2, a hinge stiffness of 608,588 Nm/rad was obtained.

This gave a rotating first flap frequency of 6.18P.

1.1.2. Blade Aerodynamic Assumptions

The blade was divided up into 15 elements for the application of Blade Element Momentum theory, these started from a radial distance of 1.257m and ran outwards to 5.029m.

Curve fits were applied to the Twist and Chord distributions given for the twisted/tapered blades, based upon radial distance.

Certain elements were chosen to be centred upon the 5 radial positions which had the pressure taps, these are elements 2,5,8,11 and 14, these elements also have span lengths of 0.2m. Details of the blade elements used for the Yawdyn model are given in Table 1.2.

1.2. 2D Section Data Used

A quick set of calculations based upon rotational speed and wind speed showed the reynolds numbers at the blade elements to be close to 1 million for the 20

Element No	Radial Distance (RELM)	Span (DR)	chord	Twist
1	1.333	0.152	0.729	18.18
2	1.509	0.2	0.711	14.44
3	1.773	0.328	0.685	10.16
4	2.1005	0.327	0.651	6.49
5	2.364	0.2	0.625	4.49
6	2.615	0.302	0.599	3.13
7	2.917	0.302	0.569	1.95
8	3.168	0.2	0.544	1.23
9	3.432	0.328	0.517	0.62
10	3.7595	0.327	0.484	0.01
11	4.023	0.2	0.457	-0.42
12	4.262	0.278	0.433	-0.78
13	4.5395	0.277	0.405	-1.15
14	4.778	0.2	0.381	-1.46
15	4.9535	0.151	0.363	-1.68

Table 1.2: Blade Element data

cases considered.

It was decided to use the profile coefficients from the DUT wind tunnel tests at a reynolds number of 1 million (Table A8) for the Yawdyn simulations of the 20 cases. In order to obtain the necessary parameters to enable the Beddoes/Leishman dynamic stall model to be used in the simulations the set of data from Table A8 was processed with Foilcheck software.

Figures 1.1, 1.2 and 1.3 show plots of the extrapolated data sets and attached to this report is a copy of the coefficients data file used for all elements in all test cases.

1.3. Turbine Setup

The model was set up as follows for the 20 cases:

Tower Shadow could only be applied in Yawdyn on the downwind cases, of these, the cases at 7m/s had a shadow applied of twice the width of the tower and a centre line deficit of 10% of the freestream velocity at the rotor plane. The 17m/s cases had a shadow applied of the same width as the tower diameter, with a centre line deficit of 20% of the free stream velocity, these were the values at
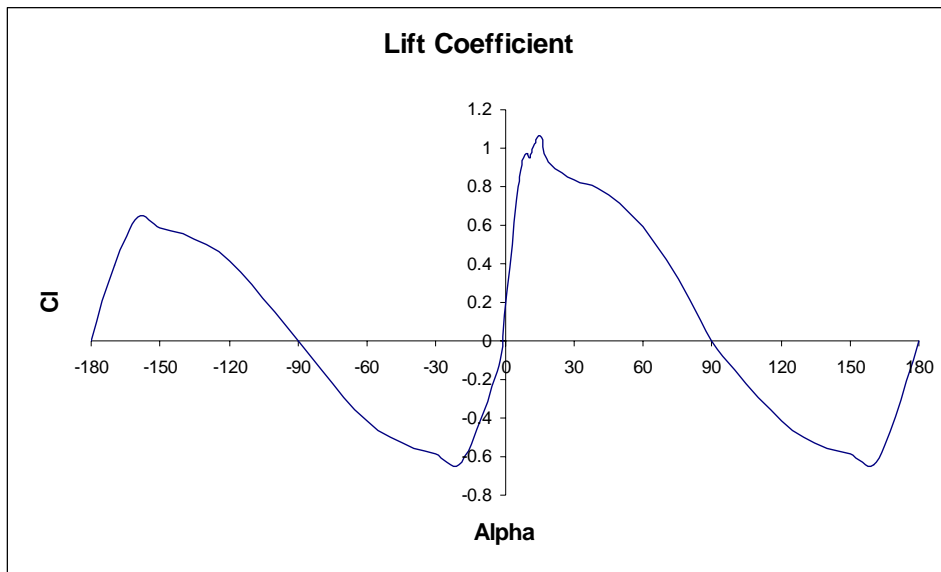
3

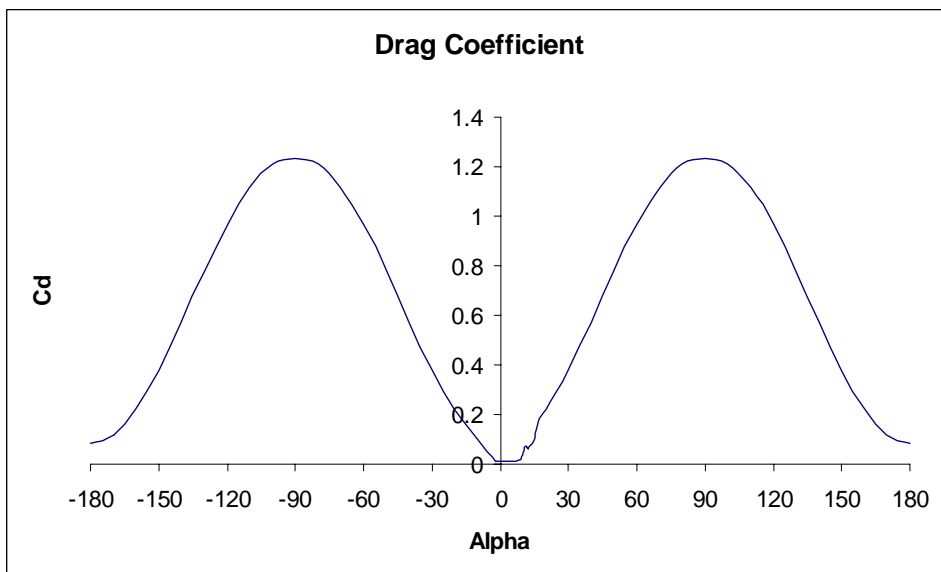Figure 1.1: Lift Coefficient extrapolated from DUT data

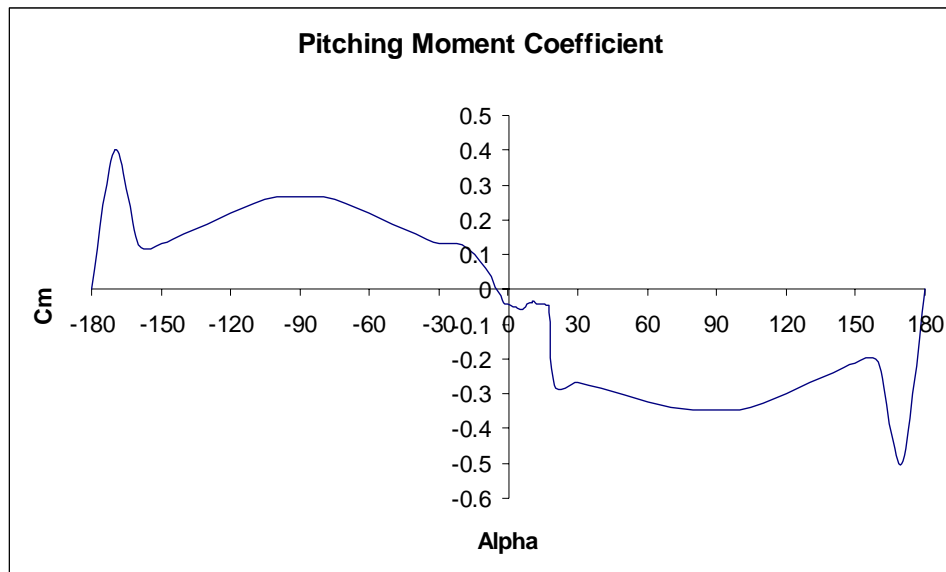Figure 1.2: Drag Coefficient extrapolated from DUT data

4

Figure 1.3: Pitching Moment Coefficient extrapolated from DUT data

the rotor plane.

Air Density was changed to match the individual case conditions

Hub Height above the ground 12.192m although irrelevent given the steady wind input.

Distance from Yaw axis to Hub, 1.401m

Number of aerofoil data files used, 1 (see attached)

Flapping hinges were used on the blades, giving 2 structural degrees of freedom.

Data output at every azimuth angle, (0 to 360).

Time of simulation, 8 secs. The simulation was run until transients had died out, 2 complete revolutions were then plotted to check this. Then results from one complete revolution were used for post-processing.

Trim solution Tolerance 0.02

Rotational Speed fixed at that for the case being simulated

Blade Pitch angles, 3 degs at the tip, this means that the root set angle in Yawdyn was set at 4.775 degs, since (3+1.775=4.775).

Mass Moment of inetia about the yaw axis was a dummy value (10Kgm^2) since the Yaw was fixed.

The dynamics of the blade/flap hinge were set up as already outlined.

5

Yaw stiffness, damping and Friction were given large dummy values, again because the yaw angle is fixed for each test case.

1.4. YAWDYN Options used

Interactive mode was selected.

Beddoes/Leishman dynamic Stall was used based on the parameters given in the attached data file at the end of this report.

Pitching Moments were calculated.

Tangential and Axial induction factors were calculated.

Pitt and Peters dynamic Inflow model used, applied across the rotor.

Hub Height wind files were used.

Aerodynamics time step was 0.005 sec.

1.5. Post Processing

In order to calculate the output channels required the following calculations were made:

- Yaw Angle, this was as input into Yawdyn, however it was reversed based on the fact that a Yawdyn model always rotates clockwise when viewed from upwind (whether or not the rotor is upwind or downwind of the tower), and the test rotor always rotated anticlockwise when viewed from upwind (whether or not the rotor is upwind or downwind of the tower).

- Tunnel Speed, as input into the relevent hub height wind file, (from Table 1).

- Blade 3 Azimuth, this was taken from the blade 1 output of Yawdyn and all readings adjusted by 180 degrees to match the test cases convention.

- Blade 3 Flap Angle, again taken from the blade 1 output of Yawdyn.

- Blade 3 Pitch angle, this is unchanged for all of the cases run at 4.775 degrees, (3+1.775).

- RPM, again this is fixed for all the test cases according to the relevent value from Table 1.

- Blade 3 Flap Bending Moment, this was calculated from the output for blade 1 from the Yawdyn model, since the strain gauges used in the test were aligned perpendicular to the tip chord, the values from Yawdyn had to be resolved by 3 degrees incorporating both in plane and out of plane moments from Yawdyn:

$$FlapMom = \cos(3\deg).OutPlane + \sin(3\deg).inplane$$

- Blade 3 Edge Bending moment, again this had to resolved from in and out of plane bending moments from the blade 1 Yawdyn output

$$EdgeMom = \cos(3\deg).inPlane - \sin(3\deg).Outplane$$

- Low speed Shaft Torque, this was calculated from the Power output from the Yawdyn by dividing by the fixed rotational speed given in Rads/sec.

$$Torque = \frac{P}{\omega}$$

- Nacelle Yaw Moment, the convention for both Yawdyn and the test turbine is for a positive clockwise yaw moment when the turbine is viewed from above, since the direction of rotation and yaw angle are reversed for the Yawdyn model compared to the test turbine, the sign of the Yaw Moment also had to be reversed.

- No Local Dynamic Pressures were calculated.

- Normal Force coefficients, these were calculated for the relevent blade element by resolving the relevent lift and drag data output by Yawdyn for a given blade element.

$$C_N = \cos(alpha).C_L + \sin(alpha).C_D$$

- Tangential force coefficients, again these were resolved from the output lift and drag data for a given blade element.

$$C_T = \cos(alpha).C_D - \sin(alpha).C_L$$

7

- Pitching Moment Coefficient, this was available directly from the Yawdyn output for a given blade element

- Normal Force, Tangential Force and Pitching Moment, these were calculated for the required blade elements by taking the values ouput by Yawdyn for the appropriate blade element and multiplying by 5. The elements centred on the radial stations of interest were selected to have a span of 0.2m hence multiplying the output forces by 5 gives the forces/moments per metre span.

Delft Wind Tunnel Data, S809 Aerofoil, Table A8 (Somers 1997)
Re = 1 million, 2D section data, extrapolated with Foilcheck
1 Number of airfoil tables in this file
0.00 Table ID parameter
15.23 Stall angle (deg)
0.00 No longer used, enter zero
0.00 No longer used, enter zero
0.00 No longer used, enter zero
-1.22 Zero lift angle of attack (deg)
6.61471 Cn slope for zero lift (dimensionless)
1.8984 Cn at stall value for positive angle of attack
-0.8000 Cn at stall value for negative angle of attack
-0.0100 Angle of attack for minimum CD (deg)
0.0094 Minimum CD value

-180.00	0.000	0.0809	0.0000
-170.00	0.394	0.1169	0.4000
-160.00	0.641	0.2204	0.1293
-150.00	0.585	0.3786	0.1338
-140.00	0.554	0.5719	0.1578
-130.00	0.501	0.7762	0.1890
-120.00	0.415	0.9661	0.2208
-110.00	0.295	1.1175	0.2476
-100.00	0.152	1.2110	0.2646
-90.00	0.000	1.2342	0.2684
-80.00	-0.152	1.2110	0.2646
-70.00	-0.295	1.1175	0.2476
-60.00	-0.415	0.9661	0.2208
-50.00	-0.501	0.7762	0.1890
-40.00	-0.554	0.5719	0.1578
-30.00	-0.585	0.3786	0.1338
-20.00	-0.641	0.2204	0.1293
-10.00	-0.388	0.1015	0.0598
-2.08	-0.100	0.0095	-0.0370
-1.04	0.019	0.0095	-0.0408
-0.01	0.139	0.0094	-0.0435
1.02	0.258	0.0096	-0.0462
2.05	0.378	0.0099	-0.0487

3.07	0.497	0.0100	-0.0514
4.10	0.617	0.0100	-0.0538
5.13	0.736	0.0097	-0.0560
6.16	0.851	0.0095	-0.0571
7.18	0.913	0.0127	-0.0506
8.20	0.952	0.0169	-0.0439
9.21	0.973	0.0247	-0.0374
10.20	0.952	0.0375	-0.0397
11.21	0.947	0.0725	-0.0345
12.23	1.007	0.0636	-0.0420
13.22	1.031	0.0703	-0.0420
14.23	1.055	0.0828	-0.0419
15.23	1.062	0.1081	-0.0418
16.22	1.043	0.1425	-0.0452
17.21	0.969	0.1853	-0.0458
20.00	0.916	0.2204	-0.2742
30.00	0.836	0.3786	-0.2685
40.00	0.791	0.5719	-0.2836
50.00	0.716	0.7762	-0.3039
60.00	0.592	0.9661	-0.3234
70.00	0.422	1.1175	-0.3388
80.00	0.217	1.2110	-0.3478
90.00	0.000	1.2342	-0.3487
100.00	-0.152	1.2110	-0.3450
110.00	-0.295	1.1175	-0.3280
120.00	-0.415	0.9661	-0.3012
130.00	-0.501	0.7762	-0.2694
140.00	-0.554	0.5719	-0.2382
150.00	-0.585	0.3786	-0.2142
160.00	-0.641	0.2204	-0.2096
170.00	-0.394	0.1169	-0.5000
180.00	0.000	0.0809	0.0000

Windward Engineering UAE Blind Test Simulations—Equilibrium Wake Model

The UAE Blind Test simulations conducted by Windward Engineering utilized an ADAMS (v 10.0) model and the AeroDyn (v 12.0beta) aerodynamics package. The ADAMS model of the UAE turbine is a modified model of that used for the predictions made for the wind tunnel experiments. It was originally constructed by Kirk Pierce of NREL, and modified by Windward Engineering.

The ADAMS model has a flexible tower and low-speed-shaft. However, these degrees of freedom are expected to have minimal effect on the results for this study (especially in a fixed yaw configuration), and thus mass and inertia of the tower and nacelle were not updated to reflect any changes in that data. The blades were modified to reflect the data provided by NREL for this test. The blades are rigid with a root spring that was chosen to provide flap and edge frequencies reported by NREL for the phase VI blades.

Using ADAMS Linear, modal results were provided for a cantilevered blade, and for the full system. The focus for these tests was blade and rotor frequencies. The results are shown in Table 1.

TABLE 1 - ADAMS Linear Results

Model	Frequency (Hz)	Mode
Cantilevered Blade	7.3	1st Flap
	9.0	1st Edge
Full System Model (Rotor parked vertically)	1.81	1st Twr F-A
	1.82	1st Twr Lateral
	3.03	LSS Torsion
	3.48	LSS Bending - vertical
	6.10	LSS Bending - horizontal
	7.47	1st Symmetric Flap
	9.21	1st Symmetric Edge

The aerodynamic properties for the blade are the same as those used for the test predictions. This data was based upon the OSU data at Re=0.75 million, clean roughness, as reported in NREL/TP-442-7817.

The baseline AeroDyn options (including the EQUIL or equilibrium wake option) and blade geometry properties used in the analyses are found in the sample input file shown in Appendix A. In addition to this baseline case, another set of results was achieved using the DYNIN (dyamic inflow) option on line 7 of the input file. A third set was accomplished by applying delayed stall criteria to the 7 inboard blade sections of the model. To do this, the airfoil file was altered based upon our modifications to the procedure outlined by Du and Selig [1].

The results of the 20 simulations requested for this study are presented in the format requested by NREL in three files. These are named:

(1) 'Windward EQUIL Results.xls',   - Equilibrium wake calculation
(2) 'Windward DYNIN Results.xls', and   - Dynamic Inflow considered
(3) 'Windward DYNIN_DelayStall Results.xls'.   - Dynamic Inflow and Delayed Stall considered

The numbers correspond to the numbers on each spreadsheet, and can be used to differentiate the results.

There is one item of note regarding this data: The azimuth averaged values are not in bins centered on integer angles as requested. Crunch (v2.32) was used to calculate the azimuth averages and it does not allow for selection of bin centers. We hope this will not be an inconvenience. The raw data used in the post-processing encompassed 30 seconds of operation.

The blade aerodynamic data is provided at 5 span locations in close proximity to the pressure taps on the test turbine. A comparison is presented in Table 2.

TABLE 2 - Span-wise Location Comparison

Span Location (Distance from axis of rotation) for Aerodynamic Data	
Test Turbine	Windward Model
30.0%	30.0% (1.50 m)
46.6%	46.6% (2.34 m)
63.3%	63.3% (3.19 m)
80.0%	80.2% (4.04 m)
95.0%	97.1% (4.88 m)

The AeroDyn routines use BEMT to calculate the aerodynamic forces at discrete positions along each blade. An equilibrium wake assumption is used in calculating the rotor induced velocities in both the axial and tangential directions. The Bedoes dynamic stall model was used for all simulations. A Prandtl tip loss model is also applied in the analyses. For more information on the AeroDyn Code see the User's Guide [2].

Wind input to the model is a steady, uniform flow across the rotor disk.

All simulations were conducted on PC's with a ratio of roughly 10:1 simulation to real time. 50 seconds were simulated for each case, with the first 20 seconds discarded from the final data set. Post-processing was accomplished using Crunch (v2.32) [3] for the azimuth averaging calculations.

REFERENCES

[1] Du, Z. and Selig, M.S., "A 3-D Stall-Delay Model for Horizontal Axis Wind Turbine Performance Prediction," AIAA-98-0021, Proceedings of the 1998 ASME Wind Energy Symposium, Reno, Nevada, pp. 9-19.

[2] Hansen, A.C. & Laino, D.J., User's Guide to the Wind Turbine Dynamics Computer Programs YawDyn and AeroDyn for ADAMS®, http://wind2.nrel.gov/designcodes/papers/ydguide11.pdf.

[3] Buhl, M.L., "Crunch Read Me file", http://wind2.nrel.gov/designcodes/crunch/readme.txt.

APPENDIX A
Sample AeroDyn Input File

```
TITLE
BATCH          Simulation mode:   INTERACTive, BATCH
BEDDOES        Dynamic stall model:   BEDDOES, STEADY
USE_CM         Aerodynamic pitching moment included?: USE_CM or NO_CM
SWIRL          Induction Factor Model: NONE, WAKE, SWIRL
0.005          ATOLER, Tolerance for induction factor convergence (0.005)
EQUIL          Dynamic inflow model:   DYNIN, EQUILibrium
HH             Wind data file type: HH (Hub height) or FF (Full Field)
yawdyn.wnd
SI             SIUNIT, select units: SI or ENGLISH
0.35           Tower shadow deficit fraction
0.4            Tower shadow width
2              Number of blades
1.225          Air density
12.011         Hub height above ground
1.421          Distance from yaw axis to hub
0              Shaft tilt angle (deg)
3.5            Rotor precone angle (deg)
0.002          Aerodynamics time step (sec)
1              Number of airfoil data files you wish to use
../aerodata/s809_cln.dat
16             Number of blade elements per blade
0.64909    0.2822    5.5402    0.3110    1    NOPRINT    RELM and Twist not used by ADAMS
0.93128    0.2822    13.1195   0.5101    1    NOPRINT    but must be present in the dataset
1.21347    0.2822    15.5933   0.6240    1    NOPRINT    RELM, DR,Twist, Chord, Airfoil#
1.49566    0.2822    16.2351   0.7075    1    PRINT
1.77784    0.2822    12.4393   0.6842    1    NOPRINT
2.06003    0.2822    8.7559    0.6556    1    NOPRINT
2.34222    0.2822    6.6653    0.6271    1    PRINT
2.62441    0.2822    4.9565    0.5986    1    NOPRINT
2.90659    0.2822    3.8470    0.5701    1    NOPRINT
3.18878    0.2822    3.0044    0.5415    1    PRINT
3.47097    0.2822    2.3348    0.5130    1    NOPRINT
3.75316    0.2822    1.8147    0.4845    1    NOPRINT
4.03534    0.2822    1.3302    0.4560    1    PRINT
4.31753    0.2822    0.9303    0.4275    1    NOPRINT
4.59972    0.2822    0.5419    0.3989    1    NOPRINT
4.88191    0.2822    0.1858    0.3704    1    PRINT
END of ADAMS input, (the word END must appear in the first three cols)
```

2. AERODYNAMICS

The modelling of rotor aerodynamics provided by **Bladed** is based on the well established treatment of combined blade element and momentum theory [2.1]. Two major extensions of this theory are provided as options in the code to deal with the unsteady nature of the aerodynamics. The first of these extensions allows a treatment of the dynamics of the wake and the second provides a representation of dynamic stall through the use of a stall hysteresis model.

The theoretical background to the various aspects of the treatment of rotor aerodynamics provided by **Bladed** is given in the following sections.

2.1 Combined blade element and momentum theory

At the core of the aerodynamic model provided by **Bladed** is combined blade element and momentum theory. The features of this treatment of rotor aerodynamics are described below.

2.1.1 Actuator disk model

To aid the understanding of combined blade element and momentum theory it is useful initially to consider the rotor as an "actuator disk". Although this model is very simple, it does provide valuable insight into the aerodynamics of the rotor.

Wind turbines extract energy from the wind by producing a step change in static pressure across the rotor-swept surface. As the air approaches the rotor it slows down gradually, resulting in an increase in static pressure. The reduction in static pressure across the rotor disk results in the air behind it being at sub atmospheric pressure. As the air proceeds downstream the pressure climbs back to the atmospheric value resulting in a further slowing down of the wind. There is therefore a reduction in the kinetic energy in the wind, some of which is converted into useful energy by the turbine.

In the actuator disk model of the process described above, the wind velocity at the rotor disk U_d is related to the upstream wind velocity Uo as follows:

$$U_d = (1 - a)U_o$$

The reduced wind velocity at the rotor disk is clearly determined by the magnitude of a, the axial flow induction factor or inflow factor.

By applying Bernoulli's equation and assuming the flow to be uniform and incompressible, it can be shown that the power P extracted by the rotor is given by :

$$P = 2\rho A U_o^3 a(1 - a)^3$$

where ρ is the air density and A the area of the rotor disk.

The thrust T acting on the rotor disk can similarly be derived to give:

$$T = 2\rho A U_o^2 a(1-a)$$

The dimensionless power and thrust coefficients, C_P and C_T are respectively:

$$C_P = P / (\tfrac{1}{2}\rho A U_o^3) = 4a(1-a)^2$$

and:

$$C_T = T / (\tfrac{1}{2}\rho A U_o^2) = 4a(1-a)$$

The maximum value of the power coefficient C_P occurs when a is $^1/_3$ and is equal to $^{16}/_{27}$ which is known as the Betz limit.

The thrust coefficient C_T has a maximum value of 1 when a is $^1/_2$.

2.1.2 Wake rotation

The actuator disk concept used above allows an estimate of the energy extracted from the wind without considering that the power absorbed by the rotor is the product of torque Q and angular velocity Ω of the rotor. The torque developed by the rotor must impart an equal and opposite rate of change of angular momentum to the wind and therefore induces a tangential velocity to the flow. The change in tangential velocity is expressed in terms of a tangential flow induction factor a'. Upstream of the rotor disk the tangential velocity is zero, at the disk the tangential velocity at radius r on the rotor is $\Omega r a'$ and far downstream the tangential velocity is $2\Omega r a'$. Because it is produced in reaction to the torque, the tangential velocity is opposed to the motion of the blades.

The torque generated by the rotor is equal to the rate of change of angular momentum and can be derived as:

$$Q = \pi\rho R^4 (1-a)a' U_o \Omega$$

2.1.3 Blade element theory

Combined blade element and momentum theory is an extension of the actuator disk theory described above. The rotor blades are divided into a number of blade elements and the theory outlined above used not for the rotor disk as a whole but for a series of annuli swept out by each blade element and where each annulus is assumed to act in the same way as an independent actuator disk. At each radial position the rate of change of axial and angular momentum are equated with the thrust and torque produced by each blade element.

The thrust dT developed by a blade element of length dr located at a radius r is given by:

$$dT = \tfrac{1}{2}\rho W^2 (C_L \cos\phi + C_D \sin\phi)cdr$$

where W is the magnitude of the apparent wind speed vector at the blade element, ϕ is known as the inflow angle and defines the direction of the apparent wind speed vector relative to the plane of rotation of the blade, c is the chord of the blade element and C_L and C_D are the lift and drag coefficients respectively.

The lift and drag coefficients are defined for an aerofoil by:

$$C_L = L / (\tfrac{1}{2}\rho V^2 S)$$

and

$$C_D = D / (\tfrac{1}{2}\rho V^2 S)$$

where L and D are the lift and drag forces, S is the planform area of the aerofoil and V is the wind velocity relative to the aerofoil.

The torque dQ developed by a blade element of length dr located at a radius r is given by:

$$dQ = \tfrac{1}{2}\rho W^2 r(C_L \sin\phi - C_D \cos\phi)cdr$$

In order to solve for the axial and tangential flow induction factors appropriate to the radial position of a particular blade element, the thrust and torque developed by the element are equated to the rate of change of axial and angular momentum through the annulus swept out by the element. Using expressions for the axial and angular momentum similar to those derived for the actuator disk in Sections 2.1.1 and 2.1.2 above, the annular induction factors may be expressed as follows:

$$a = g_1 / (1 + g_1)$$

and

$$a^{\cdot} = g_2 / (1 - g_2)$$

where

$$g_1 = \frac{Bc}{2\pi r} \frac{(C_L \cos\phi + C_D \sin\phi)}{4F \sin^2\phi} H$$

and

$$g_2 = \frac{Bc}{2\pi r} \frac{(C_L \sin\phi - C_D \cos\phi)}{4F \sin\phi \cos\phi}$$

Here B is the number of blades and F is a factor to take account of tip and hub losses, refer Section 2.1.4.

The parameter H is defined as follows:

for $a \leq 0.3539, \quad H = 1.0$

for $a > 0.3539, \quad H = \frac{4a(1-a)}{(0.6 + 0.61a + 0.79a^2)}$

In the situation where the axial induction factor a is greater than 0.5, the rotor is heavily loaded and operating in what is referred to as the "turbulent wake state". Under these conditions the actuator disk theory presented in Section 2.1.1 is no longer valid and the expression derived for the thrust coefficient:

$$C_T = 4a(1-a)$$

must be replaced by the empirical expression:

$$C_T = 0.6 + 0.61a + 0.79a^2$$

The implementation of blade element theory in **Bladed** is based on a transition to the empirical model for values of a greater than 0.3539 rather than 0.5. This strategy results in a smoother transition between the models of the two flow states.

The equations presented above for a and $a^{'}$ can only be solved iteratively. The procedure involves making an initial estimate of a and $a^{'}$, calculating the parameters g_1 and g_2 as functions of a and $a^{'}$, and then using the equations above to update the values of a and $a^{'}$. This procedure continues until a and $a^{'}$ have converged on a solution. In **Bladed** convergence is assumed to have occurred when:

$$a_k - a_{k-1} \leq tol$$

and

$$a_k^{'} - a_{k-1}^{'} \leq tol$$

where *tol* is the value of aerodynamic tolerance specified by the user.

2.1.4 Tip and hub loss models

The wake of the wind turbine rotor is made up of helical sheets of vorticity trailed from each rotor blade. As a result the induced velocities at a fixed point on the rotor disk are not constant with time, but fluctuate between the passage of each blade. The greater the pitch of the helical sheets and the fewer the number of blades, the greater the amplitude of the variation of induced velocities. The overall effect is to reduce the net momentum change and so reduce the net power extracted. If the induction factor a is defined as being the value which applies at the instant a blade passes a given point on the disk, then the average induction factor at that point, over the course of one revolution will be aF_t, where F_t is a factor which is less than unity.

The circulation at the blade tips is reduced to zero by the wake vorticity in the same manner as at the tips of an aircraft wing. At the tips, therefore the factor F_t becomes zero. Because of the analogy with the aircraft wing , where losses are caused by the vortices trailing from the tips, F_t is known as the tip loss factor.

Prandtl [2.2] put forward a method to deal with this effect in propeller theory. Reasoning that, in the far wake, the helical vortex sheets could be replaced by solid disks, set at the same pitch as the normal spacing between successive turns of the sheets, moving downstream with the speed of the wake.

The flow velocity outside of the wake is the free stream value and so is faster than that of the disks. At the edges of the disks the fast moving free stream flow weaves in and out between them and in doing so causes the mean axial velocity between the disks to be higher than that of the disks themselves, thus simulating the reduction in the change of momentum.

The factor F_t can be expressed in closed solution form:

$$F_t = \frac{2}{\pi} arccos[exp(-\frac{\pi s}{d})]$$

where s is the distance of the radial station from the tip of the rotor blade and d is the distance between successive helical sheets.

A similar loss takes place at the blade root where, as at the tip, the bound circulation must fall to zero and therefore a vortex must be trailed into the wake, A separate hub loss factor F_h is therefore calculated and the effective total loss factor at any station on the blade is then the product of the two:

$$F = F_t F_h$$

The combined tip and hub loss factor is incorporated in the equations of blade element theory as indicated in Section 2.1.3 above.

2.2 Wake models

2.2.1 Equilibrium wake

The use of blade element theory for time domain dynamic simulations of wind turbine behaviour has traditionally been based on the assumption that the wake reacts instantaneously to changes in blade loading. This treatment, known as an equilibrium wake model, involves a re-calculation of the axial and tangential induction factors at each element of each rotor blade, and at each time step of a dynamic simulation. Based on this treatment the induced velocities along each blade are computed as instantaneous solutions to the particular flow conditions and loading experienced by each element of each blade.

Clearly in this interpretation of blade element theory the axial and tangential induced velocities at a particular blade element vary with time and are not constant within the annulus swept out by the element.

The equilibrium wake treatment of blade element theory is the most computationally demanding of the three treatments described here.

2.2.2 Frozen wake

In the frozen wake model, the axial and tangential induced velocities are computed using blade element theory for a uniform wind field at the mean hub height wind speed of the simulated wind conditions. The induced velocities, computed according to the mean, uniform flow conditions, are then assumed to be fixed, or "frozen" in time. The induced velocities vary from one element to the next along the blade but are constant within the annulus swept out by the element. As a consequence each blade experiences the same radial distribution of induced flow..

It is important to note that it is the axial and tangential induced velocities aU_o and $a'r\Omega$ and not the induction factors a and a' which are frozen in time.

2.2.3 Dynamic wake

As described above, the equilibrium wake model assumes that the wake and therefore the induced velocity flow field react instantaneously to changes in blade loading. On the other hand, the frozen wake model assumes that induced flow field is completely independent of changes in incident wind conditions and blade loading. In reality neither of these treatments is strictly correct. Changes in blade loading change the vorticity that is trailed into the rotor wake and the full effect of these changes takes a finite time to change the induced flow field. The dynamics associated with this process is commonly referred to as "dynamic inflow".

The study of dynamic inflow was initiated nearly 40 years ago in the context of helicopter aerodynamics. In brief, the theory provides a means of describing the dynamic dependence of the induced flow field at the rotor upon the loading that it experiences. The dynamic inflow model used within **Bladed** is based on the work of Pitt and Peters [2.3] which has received substantial validation in the helicopter field, see for example Gaonkar et al [2.4].

The Pitt and Peters model was originally developed for an actuator disk with assumptions made concerning the distribution of inflow across the disc. In **Bladed** the model is applied at blade element or actuator annuli level since this avoids any assumptions about the distribution of inflow across the disc.

For a blade element, bounded by radii R_1 and R_2, and subject to uniform axial flow at a wind speed U_o, the elemental thrust, *dT*, can be expressed as:

$$dT = 2U_o am + U_o m_A \dot{a}$$

where *m* is the mass flow through the annulus, m_A is the apparent mass acted upon by the annulus and *a* is the axial induction factor.

The mass flow through the annular element is given by:

$$m = \rho U_o (1-a)dA$$

where *dA* is the cross-sectional area of the annulus.

For a disc of radius *R* the apparent mass upon which it acts is given approximately by potential theory, Tuckerman, [2.5]:

$$m_A = \frac{8}{3}\rho R^3$$

Therefore the thrust coefficient associated with the annulus can be derived to give:

$$C_T = 4a(1-a) + \frac{16}{3\pi U_o} \frac{(R_2^3 - R_1^3)}{(R_2^2 - R_1^2)} \dot{a}$$

This differential equation can therefore be used to replace the blade element and momentum theory equation for the calculation of axial inflow. The equation is integrated at each time step to give time dependent values of inflow for each blade element on each blade. The tangential inflow is obtained in the usual manner and so depends on the time dependent axial value. It is evident that the equation introduces a time lag into the calculation of inflow which is dependent on the radial station.

It is probable that the values of time lag for each blade element calculated in this manner will under-estimate somewhat the effects of dynamic inflow, as each element is treated independently with no consideration of the three dimensional nature of the wake or the possibly dominant effect of the tip vortex. The treatment is, however, consistent with blade element theory and provides a simple, computationally inexpensive and reasonably reliable method of modelling the dynamics of the rotor wake and induced velocity flow field.

2.3 Steady stall

The representation and to some extent the general understanding of aerodynamic stall on a rotating wind turbine blade remain rather poor. This is a rather extraordinary situation in view of the importance of stall regulation to the industry.

Stall delay on the inboard sections of rotor blades, due to the three dimensionality of the incident flow field, has been widely confirmed by measurements at both model and full scale. A number of semi-empirical models [2.6, 2.7] have been developed for correcting two dimensional aerofoil data to account for stall delay. Although such models are used for the design analysis of stall regulated rotors, their general validity for use with a wide range of aerofoil sections and rotor configurations remains, at present, rather poor. As a consequence *Bladed* does not incorporate models for the modification of aerofoil data to deal with stall delay, but the user is clearly able to apply whatever correction of the aerofoil data he believes is appropriate prior to its input to the code.

2.4 Dynamic stall

Stall and its consequences are fundamentally important to the design and operation of most aerodynamic devices. Most conventional aeronautical applications avoid stall by operating well below the static stall angle of any aerofoils used. Helicopters and stall regulated wind turbines do however operate in regimes where at least part of their rotor blades are in stall. Indeed stall regulated wind turbines rely on the stalling behaviour of aerofoils to limit maximum power output from the rotor in high winds.

A certain degree of unsteadiness always accompanies the turbulent flow over an aerofoil at high angles of attack. The stall of a lifting surface undergoing unsteady motion is more complex than static stall.

On an oscillating aerofoil, where the incidence is increasing rapidly, the onset of the stall can be delayed to an incidence considerably in excess of the static stall angle. When dynamic stall does occur, however, it is usually more severe than static stall. The attendant aerodynamic forces and moments exhibit large hysteresis with respect to the instantaneous angle of attack, especially if the oscillation is about a mean angle close to the static stall angle. This represents an important contrast to the quasi-steady case, for which the flow field adjusts immediately, and uniquely, to each change in incidence.

Many methods of predicting the dynamic stall of aerofoil sections have been developed, principally for use in the helicopter industry.

The model adopted for inclusion of unsteady behaviour of aerofoils is that due to Beddoes [2.8]. The Beddoes model was developed for use in helicopter rotor performance calculations and has been formulated over a number of years with particular reference to dynamic wind tunnel testing of aerofoil sections used on helicopter rotors. It has been used successfully by Harris [2.9] and Galbraith et al [2.10] in the prediction of the behaviour of vertical axis wind turbines.

The model used within ***Bladed*** is a development of the Beddoes model which has been validated against measurements from several stall regulated wind turbines. The model utilises the following elements of the method described in [2.8] to calculate the unsteady lift coefficient

- The indicial response functions for modelling of attached flow
- The time lagged Kirchoff formulation for the modelling of trailing edge separation and vortex lift

The use of the model of leading edge separation has been found to be inappropriate for use on horizontal axis wind turbines where the aerofoil characteristics are dominated by progressive trailing edge stall.

The time lag in the development of trailing edge separation is a user defined parameter within the model implemented in ***Bladed***. This time lag encompasses the delay in the response of the pressure distribution and boundary layer to the time varying angle of attack. The magnitude of the time lag is directly related to the level of hysteresis in the lift coefficient.

The drag and pitching moment coefficients are calculated using the quasi-steady input data along with the effective unsteady angle of attack determined during the calculation of the lift coefficient.
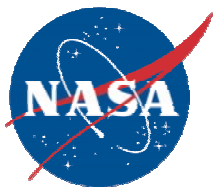
CAMRAD II Model of
NREL / NWTC Wind Turbine in
NASA Ames 80- by 120-Foot Wind Tunnel

Wayne Johnson
NASA Ames Research Center

November 2000
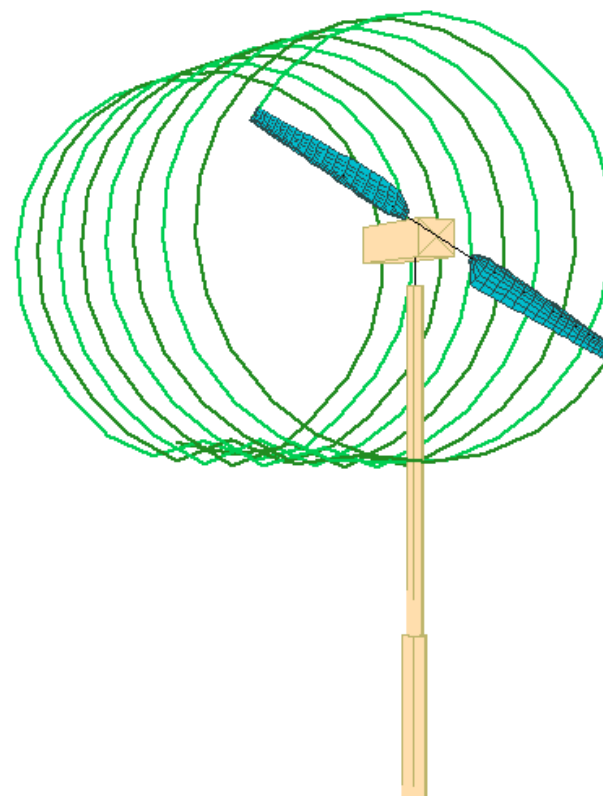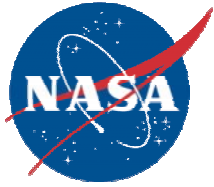
CAMRAD II Analysis

Calculations for Aerodynamics Code Blind Comparision performed using rotorcraft analysis CAMRAD II

This document describes the CAMRAD II model, and identifies correlation activities that will be considered when wind tunnel data are available

OPERATING CONDITIONS

Specified collective, yaw angle, rotor speed, temperature and density

Fixed rpm (no drive train)

Steady state, periodic solution; azimuth step = 5 deg

AERODYNAMIC MODEL

Second-order lifting line theory with vortex wake calculation of nonuinform induced velocity and free wake geometry

Two-dimensional airfoil tables, with corrections for sweep/yawed flow and static stall delay, and unsteady aerodynamics

20 aerodynamic panels, widths varying from .05R inboard to .02R at tip

Root cutout = 0.18R
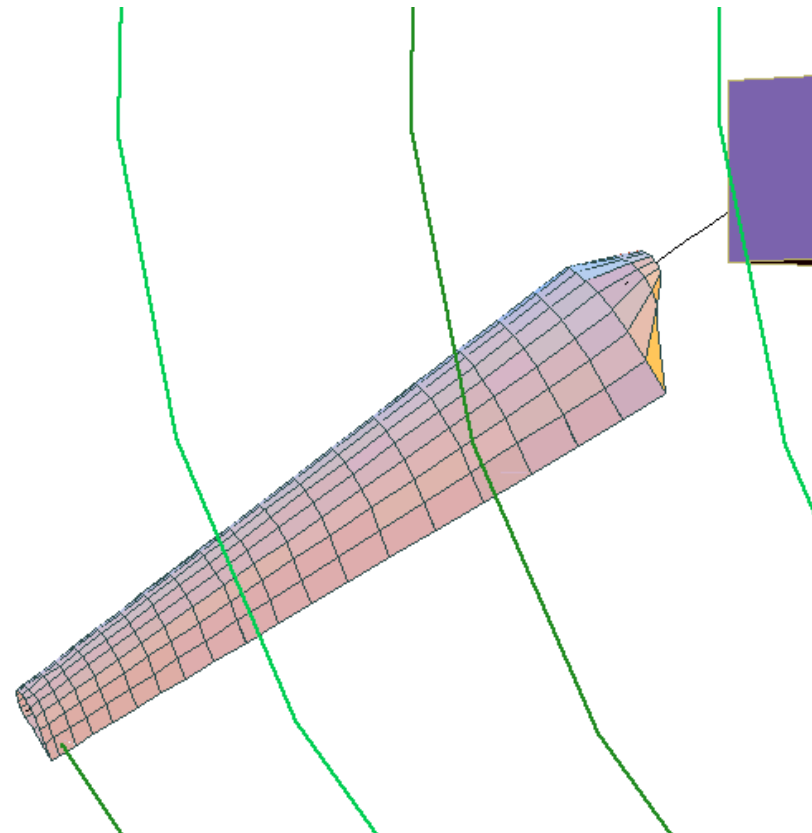
AERODYNAMIC MODEL

Aerodynamic twist, chord, pitch axis for Phase VI blades

Wind tunnel — no ground boundary layer or gust

Simple model of tower aerodynamic interference
potential flow about body, influencing blade angle of attack and
wake geometry

S809 airfoil table (outboard of r = 0.25R; root section table at r = 0.175R)
CSU 500000 data, modified so minimum c_d = 0.0080,
c_m from Re = 1020000 data

ISSUE: facility affects on airfoil data

S809 Airfoil Data
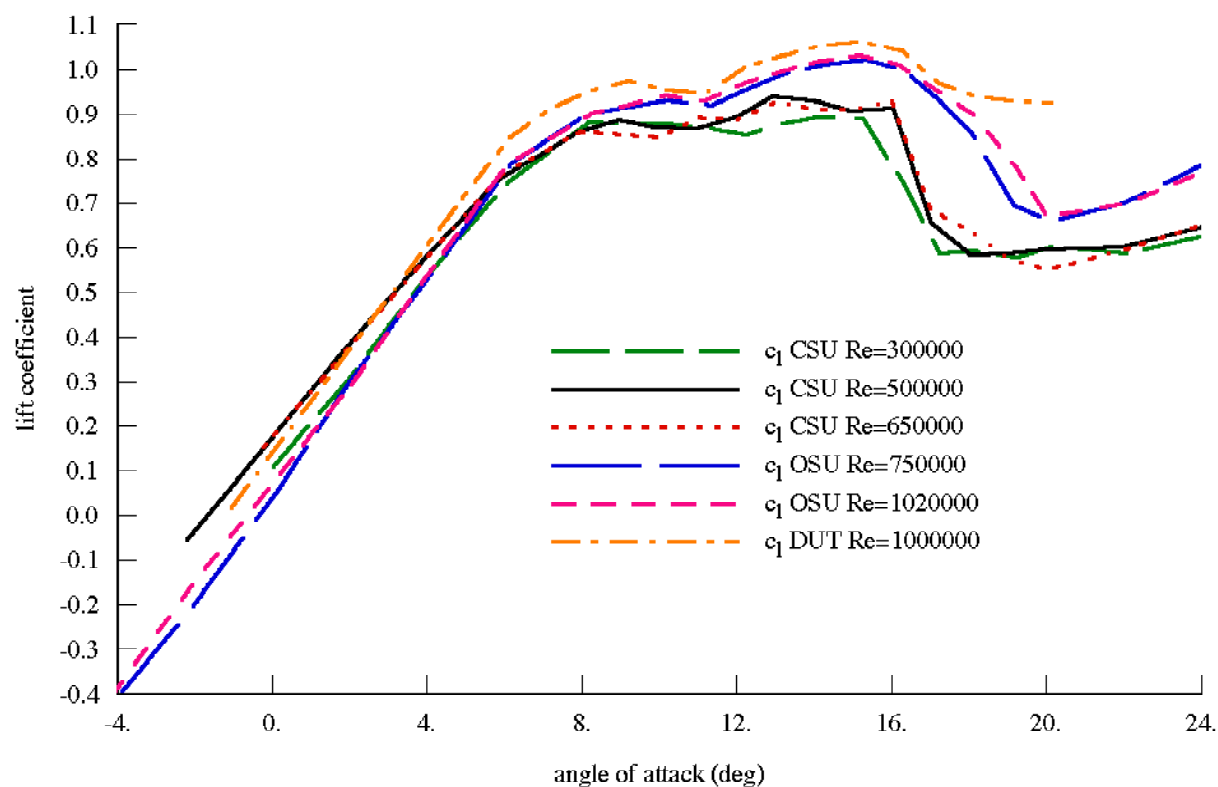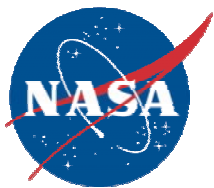
S809 Airfoil Data
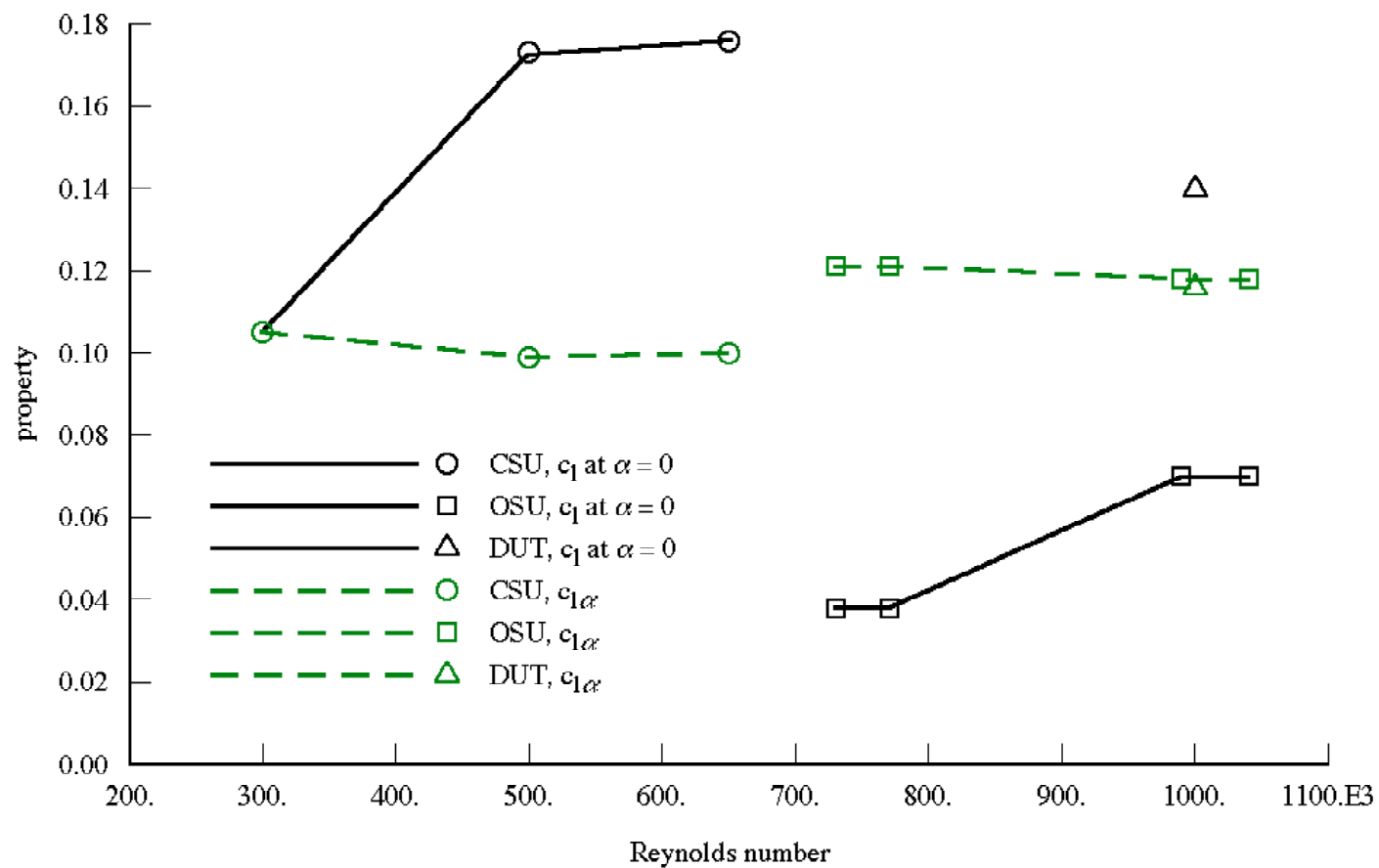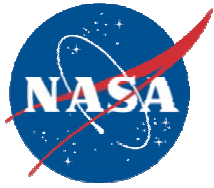
STALL DELAY

Stall delay modelled using input factors K_{sd} to modify the lift and drag coefficients obtained from airfoil tables:

$$c_l = (1 - K_{sdL})\, c_{l\,table} + K_{sdL}\; c_{l\,\alpha}\,(\alpha - \alpha_z)$$

$$c_d = (1 - K_{sdD})\, c_{d\,table} + K_{sdD}\; c_{dz}$$

$c_{l\,\alpha}$ is lift-curve slope

α_z is angle of attack at zero lift

c_{dz} is drag coefficient at zero lift

Stall delay factors evaluated using Raj-Selig functions

CORRELATION — Consider other stall delay models, factors
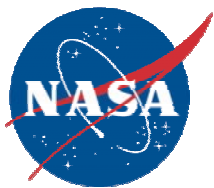
STALL DELAY FACTORS
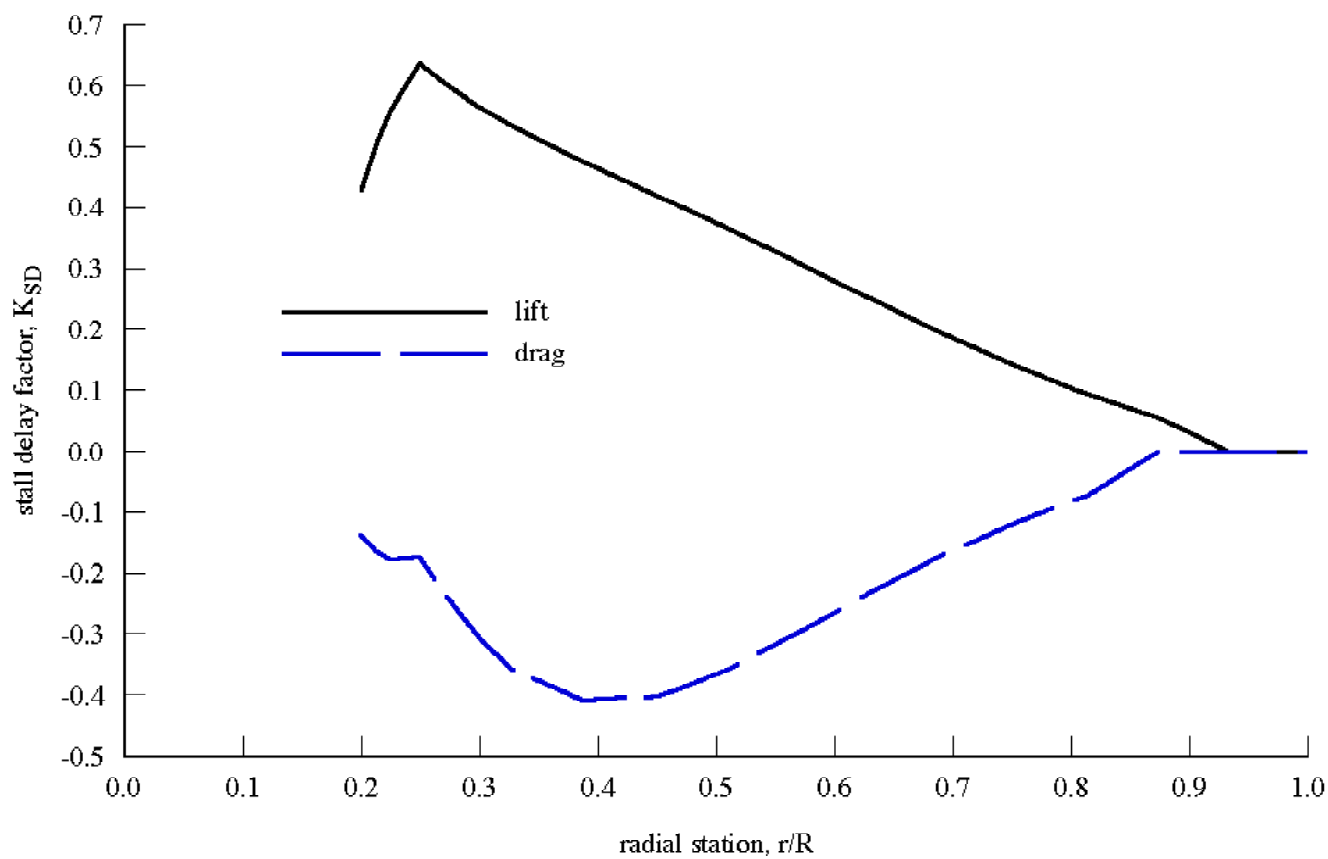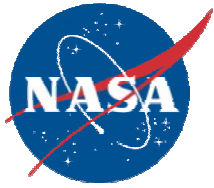
AERODYNAMIC MODEL

Vortex wake calculation of nonuniform induced velocity and free wake geometry

Unsteady aerodynamics: thin airfoil theory, no dynamic stall

CORRELATION — Use differential momentum theory

      With a lot of stall, free wake may not be essential

      Differential momentum theory faster

CORRELATION — Dynamic stall models

      Models available: Johnson, Boeing, Leishman-Beddoes,

      ONERA EDLIN, ONERA BH

BLADE STRUCTURAL MODEL

Elastic blade, consisting of 4 beam elements (rigid element inboard of pitch bearing)

nodes at r/R = 0.1014 (pitch bearing), 0.379, 0.7

Modal analysis, 1% structural damping assumed for each mode

blade frequencies = 4.0 (L1), 7.4 (F1), 19.1 (L2), 32.0 (T1) per-rev

Periodic solution

10 harmonics of structural degrees of freedom

72 time steps per revolution

Twist of structural and inertial principal axes = aerodynamic twist

Section mass and bending stiffness same as Phase II, IV blades

Estimated torsion stiffness and section pitch inertia

CORRELATION — Influence of blade elastic motion

Obtain measured blade stiffness and mass data?

Light-weight blade design and analysis?
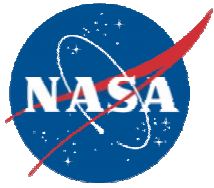
TOWER STRUCTURAL MODEL

Tower modelled as 2 beams, tower head as rigid body

Modal analysis, 5 modes used

Beam 1: length = 3.65 m (floor at 0.356 m)

Beam 2: length = 7.85 m, tower head at 11.5 m

Hub at 12.534 m from base, 1.401 m forward

Mass and inertia of tower head given

Section mass and torsion inertia of tower obtained from OD/ID and mass of tower

Tower stiffness and nacelle cg position determined by matching measured frequencies and mode shape of tower (without blades)

measured	calculated
1.34 Hz, yaw about tower	1.34 Hz
1.79 Hz, fore/aft	1.81 Hz
1.85 Hz, hub/tower motion	1.84 Hz

CORRELATION — Influence of tower dynamics

NREL/NWTC AERODYNAMICS CODE BLIND COMPARISON -- SIMULATIONS WITH HawC and HawC3D

Helge Aagaard Madsen

Risø National Laboratory, Roskilde
N0vember 2000

Contents

1 Models

The aeroelastic simulations from Risø have been run with two different codes: 1)HawC and 2)Hawc3D. The difference between the two codes is the computation of the induced flow field where two completely different models are used. In HawC the standard blade element momentum theory is used whereas in Haw3D the induced flow field is computed with a 3D actuator disc model. Below, a short description of the models is presented including references to more detailed papers and reports.

1.1 The HawC model

The development of the aeroelastic code Hawc (derived from horizontal axis wind turbine code) was initiated in a Ph.D. sturdy at Risø in 1986, and the first operational version of the model was ready in 1990 [1]. Since then the model has been continuously in use, mainly as a research code at Risø but recently also in the Danish wind turbine industry. The development has been accompanied with a continued verification process connected to several measurement programs. A short description including some validation results can be found in [2].

Structural modelling

The model is based on the finite element formulation formulation and a simple prismatic beam element is used. The wind turbine is divided into substructures comprising the tower, the shaft-nacelle and the rotor blades. The substructures are coupled at nodes where important bearing restrained degrees of freedom (DOFs) usually are located. In the model these bearings are treated as

Figure 1-1   The HawC model is a finite element representation of the turbine.

real DOFs, and they enter a general kinematic analysis together with elastic deformations –translations and rotations – at the tower top and at the shaft end. The kinematic analysis results in the accelerations of the material points on the substructures and subsequently in the inertia loads. The inertia loads are con-

sistenly transformed to the nodes resulting in expressions combined of matrices and vectors. The local dependency is expressed through the mass-, Coriolis-, and softening matrices. Due to the kinematic coupling additional inertia terms arise. They can be arranged in the equations of motion (EOMs) as additional matrices of the types above and vectors.

In general, the equations are nonlinear due to the rproduct terms of the DOFs. The kinematic analysis provides for the geometric compatibility between the substructures and the final EOMs are obtained by imposing force equilibrium at the two sets of substructure coupling nodes.

Finally, structural damping is represented as proportional damping.

Aerodynamic modelling

Computation of the induction is based on blade element momentum strip theory. The induction is updated and expanded in a truncated Taylor series, and is a function of wind speed, wind direction, yaw position, rotor speed and blade pitch angle. Further, the time constants introduce delay in the wake generation and in this way simulate dynamic inflow.

The Prandtl tip loss model is implemented and correction of the induction at high loading is based on the Glauert imperial formula.

Unsteady airfoil aerodynamics -dynamic stall

For simulation of local, unsteady aerodynamic effects at the airfoil section, three different models are presently implemented:

- the Beddoes-Leishman (BL) model
- the model of Stig Øye (The Technical University of Denmark)
- the fgh model (developed at Risø for anlysis of field rotor aerodynamic data)

In the present calculations on the NREL rotor the BL model has been used.

Three-dimensional (3D) effects

There is no general 3D correction model included in HawC but the airfoil input data are corrected, based on general experience with 3D effects [4], [5], [6]and in particular the field rotor experiments at Risø [7] and at NREL [8]. 3D Airfoil characteristics from these two experiments are shown in Figure 1-2 and Figure 1-3 and they show much of the same tendencies: 1) strongly delayed stall on the inner part of the blade but also with a strong increases in drag and 2) some increase of the lift coefficient in post stall so that there is little or no negative slope on the lift curve here. The final set of corrected airfoil data used for the present simulations are shown in Figure 1-6.
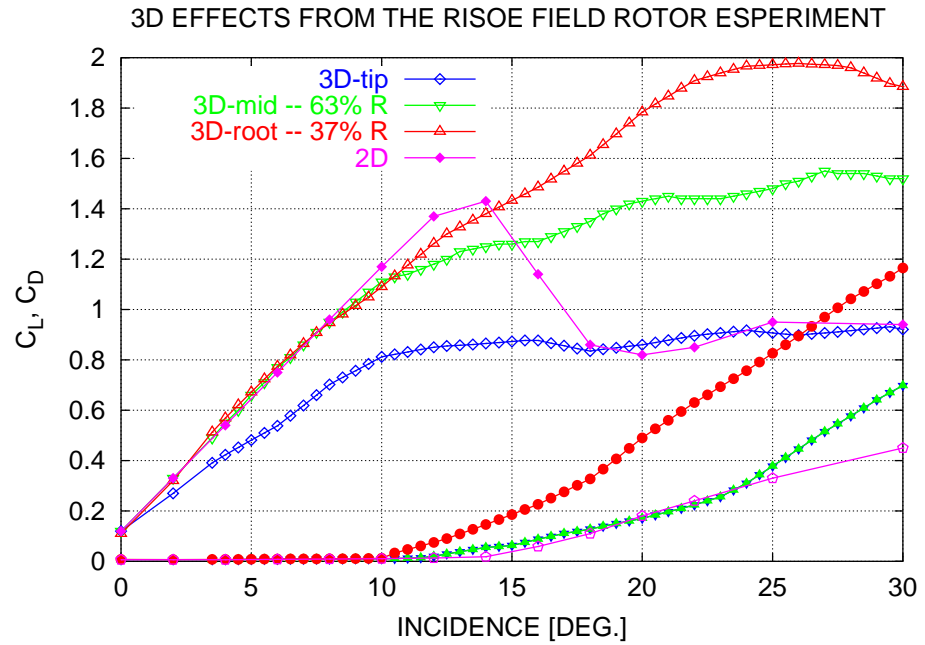
3D EFFECTS FROM THE RISOE FIELD ROTOR ESPERIMENT

Figure 1-2   3D-effects as derived from the field rotor experiment as Risoe.

Figure 1-3   3D airfoil characteristics measured during Phase II of the NREL combined experiment, [8].
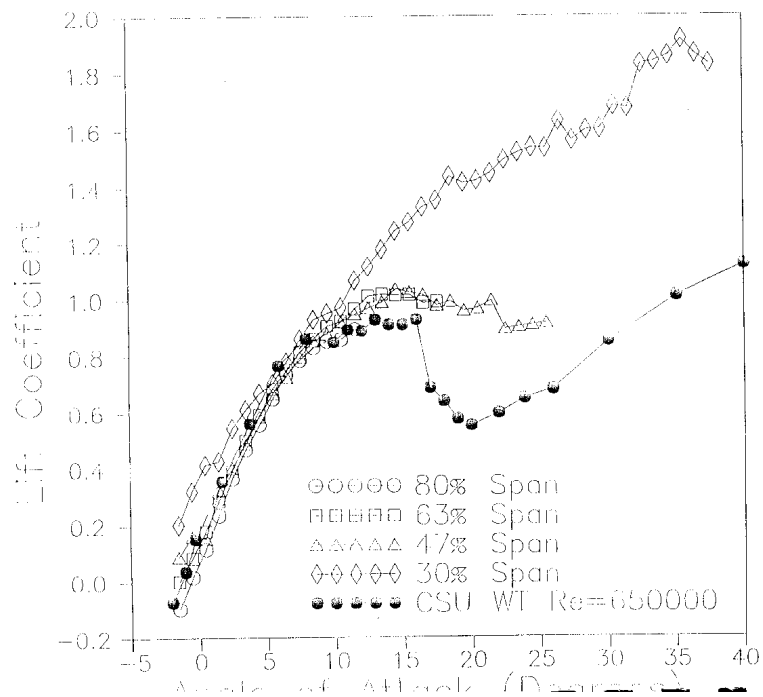

Figure 1-4   3D airfoil characteristics measured during Phase II of the NREL combined experiment, [8]. C_L curves.
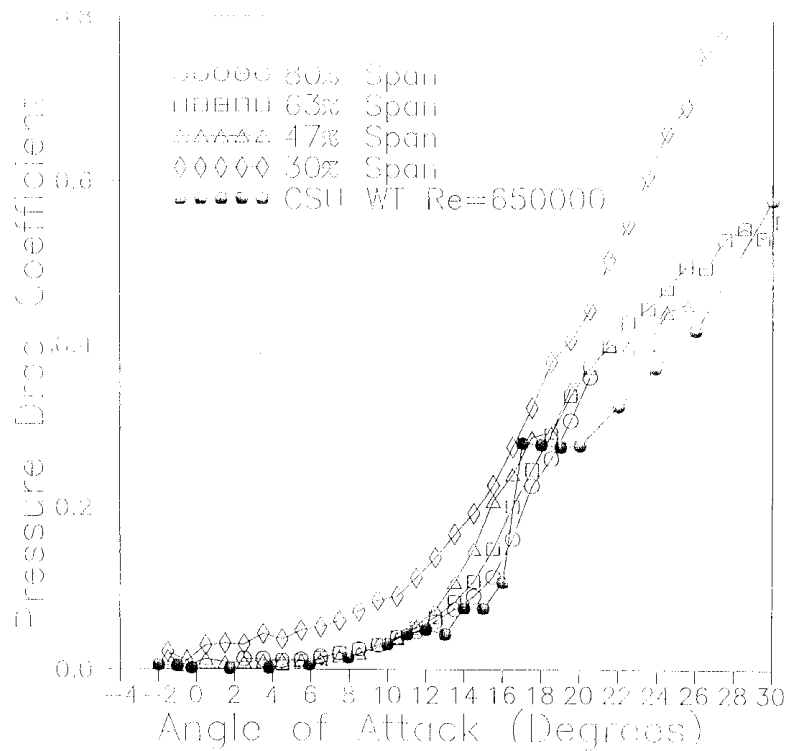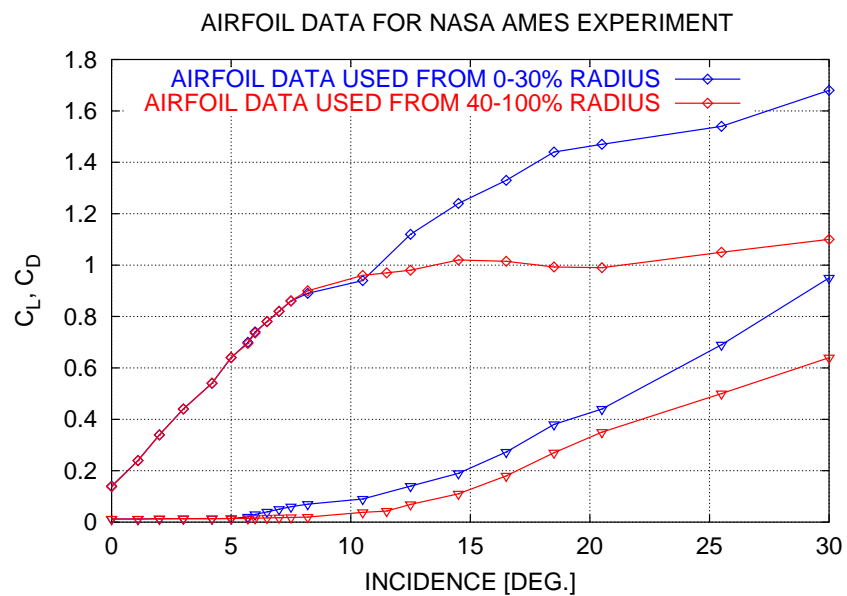
*Figure 1-5   3D airfoil characteristics measured during Phase II of the
NREL combined experiment, [8]. C$_D$ curves*

Figure 1-6   Corrected airfoil data used for the computations.

Tower flow model

A combined potential flow model and source flow model is used for simulation of the influence from the tower on the flow field, both upstream and down-stream. The reason to combine the potential flow model with a source model is 1) that the upstream influence from the wake of the cylinder in this way can be taken into account and 2) the source model computes a wake deficit behind the cylindrical tower.

The nondimensional velocity componetss *u* and *v* (non-dimensionalised with the free stream velocity) Figure 1-7 can be written as:

$$u = 1 - \frac{x^2 - y^2}{\left(x^2 + y^2\right)^2} \qquad\qquad (1\text{-}1)$$

$$v = 2\frac{xy}{\left(x^2 + y^2\right)^2} \qquad\qquad (1\text{-}2)$$
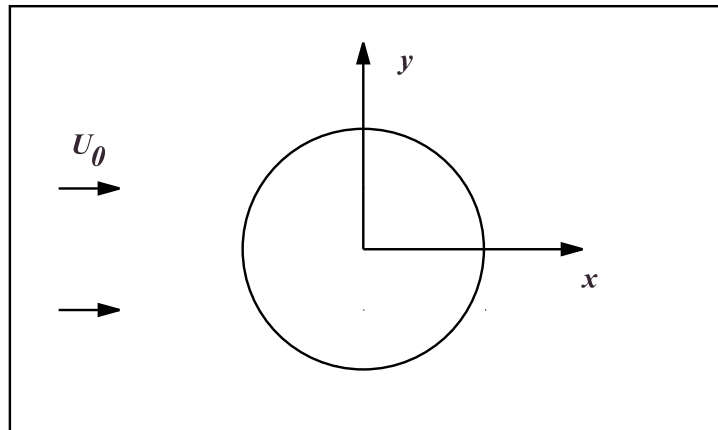

Figure 1-7   Potential flow around a circular cylinder.

In the source model radial volume forces are applied to the flow on a cylindrical surface Figure 1-8 and with an intensity which varies sinusoidal as shown in Figure 1-8 (actuator cylinder model).
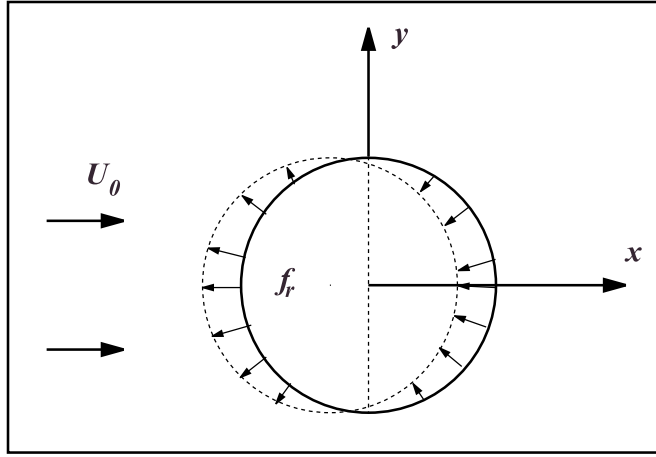
*Figure 1-8   In the source flow radial volume forces are applied on the cy-
               lindrical surface (actuator cylinder model) [9].*

The analytical solution for this flow problem [9] can be written as:

$$u = 1 + \frac{CD}{2\pi} \frac{x}{x^2 + y^2} \qquad (1\text{-}3)$$

$$v = \frac{CD}{2\pi} \frac{y}{X^2 + y^2} \qquad (1\text{-}4)$$

where $CD = F(f_r)$.

inside the cylinder:

$$u = 1 - \frac{CD}{2\pi} \left(x + 2\sqrt{1 - y^2} \right) \qquad (1\text{-}5)$$

$$v = \frac{CD}{2\pi} y \qquad (1\text{-}6)$$

in the wake:

$$u = 1 - \frac{CD}{2\pi} \left[\frac{x}{x^2 + y^2} - 4\sqrt{1 - y^2} \right] \qquad (1\text{-}7)$$

$$v = \frac{CD}{2\pi} \frac{y}{x^2 + y^2} \qquad (1\text{-}8)$$

Here the sum of the volume forces in streamwise direction is expressed through the drag coefficient CD for the cylinder. In the present simulations on the NREL rotor a value of 0.7 has been used.

The final flow field around the cylinder is now found as a sum of the two solutions. However to improve the solution close to the tower wall a coordinate shift in x of 0.1 (-0.1 for the flowfield upstream the cylinder and 0.1 for the flowfield downstream for the cylinder) is introduced.
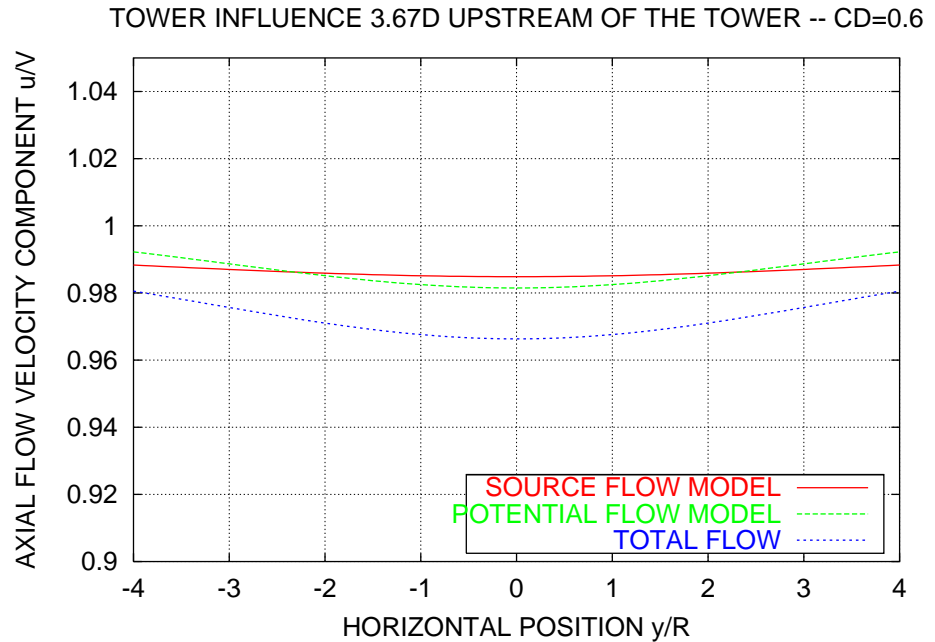

Figure 1-9   Modelled tower influence 3.67 tower diameters upstream.
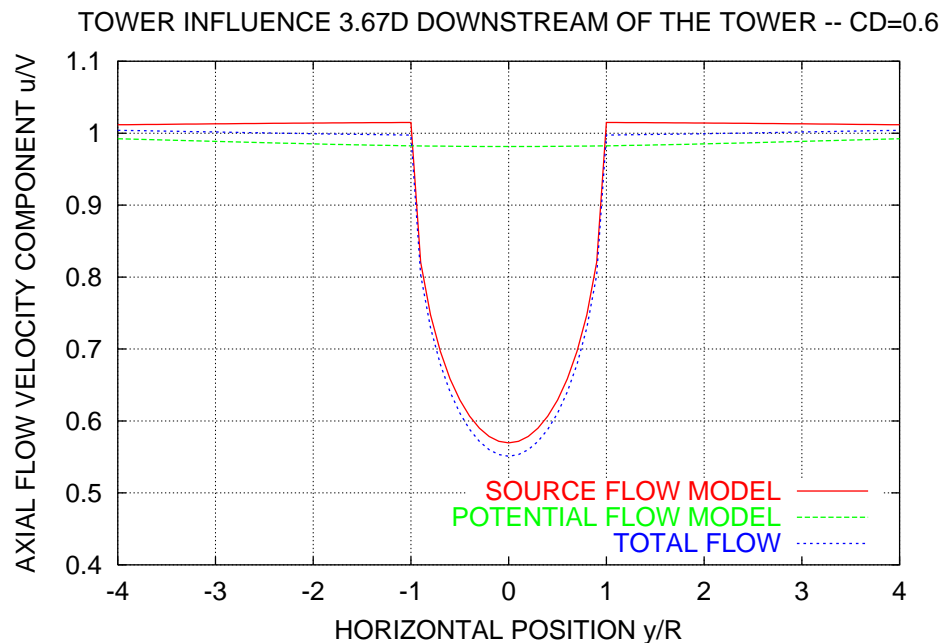

Figure 1-10   Modelled tower influence 3.67 tower diameters downstream.

Flow field

The deterministic wind field includes logarithmic or user-defined shear and turbulence can be simulated , either by use of the Sandia model [10] or the Mann model [11], giving a 3-dimensional and 3-component turbulence field.

Numerical Solution

The solution of the equations of motions is carried out by means of the Newmark implicit integration scheme in combination with Newton-Raphson iterations, performed to ensure equilibrium of the nonlinear equations at each time step, thus preventing the accumulation of errors.

   For the present simulations a 30 sec. time series for each test case was run with a time step 0f 0.002 sec.

1.2 The Hawc3D model

This model was developed in the period from 1998-1999 [15] but is based on previous work with 2D and 3D actuator disc models[12],[13] and [14]. The basic concept is that the induced flow field is calculated with a 3D actuator disc model instead of the blade element momentum (BEM) theory. The loading on the actuator disc is the aerodynamic forces from the aeroelastic code HawC, but run without the BEM model. Instead the induction in HawC is simulated with the full flow field from the 3D actuator model read into HawC as a shear field. As in a BEM model a few (5-10) iterations are run until the flow field and the aeroedynamic forces are balanced.
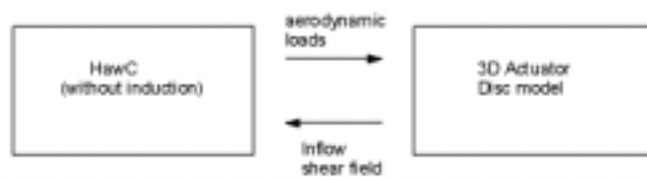

Figure 1-11   The basic principle in HawC3D is a coupling of a 3D actuator disc model with the aeroelastic code HawC. Based on a time simulation with HawC (without the BEM model) the aerodynamic rotor loading is computed. The loading is read into the 3D actuator disc model and the flow field around the actuator disc is computed. The flow filed is read in HawC as a shear field and a newaeroealstic simulation is run and a new aerodynamic rotor loading is computed. A few iterations are run until the the aerodynamic forces and the flow field are balanced.

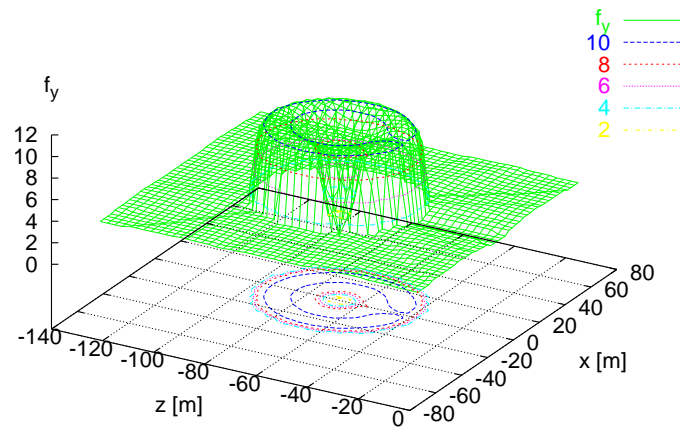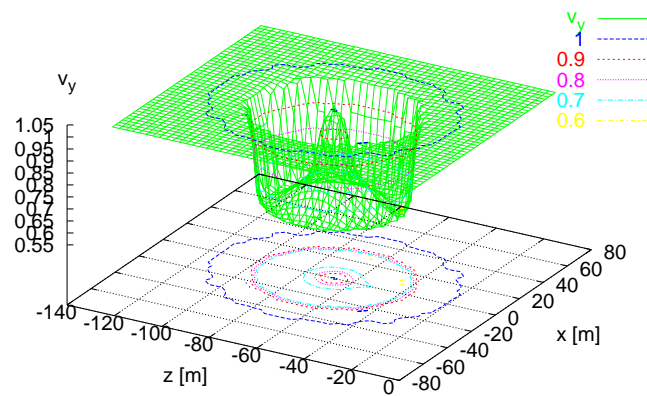VOLUMENKRAFTKOEFFICIENT UDSKREVET FRA HawC

*Figure 1-12   The aerodynamic loading perpendicular to the rotor plane
computed by the aeroelastic code HawC is input to the 3D ac-
tuator disc model.*

HASTIGHEDSFELT (AKSIEL KOMPOSANT) FRA ACTUATOR DISC

*Figur 5-3.   The computed flow field from the 3D actuator disc model is
read into HawC as a shear flow field..*

2 References

[1]   Petersen, J.T. *"Kinematically Nonlinear Finite Element Model of a Horizontal Axis Wind Turbine"*. Ph.D. Thesis. Dept. of Meteorology and Wind Energy, Risø National Laboratory. Roskilde, Denmark, 1990.

[2]   Petersen, J.T. *"The Aeroelastic Code HawC – Model and Comparisons"*. Paper presented at the 28th IEA Experts Meeting: `State of the Art of Aeroelastic Codes`. April 11-12 1996, Technical University of Denmark, Lyngby.

[3]   Petersen, J.T. *"HawC Wind Turbine Simulation Code User´s Guide"*. Version 99o.4.2000.0110, Risø-I-1408(EN), Risø National Laboratory, January 2000.

[4]   Madsen, H.A. and Rasmussen, F. *"Derivation of Three-Dimensional Airfoil Data on the Basis of Experiment and Theory"*. Paper presented at Windpower 88, September 18-22, 1988 Honolulu, Hawaii.

[5]   Madsen, H.A. and Christensen, H.F. *"On the relative importance of rotational, unsteady and three-dimensional effects on the HAWT rotor aerodynamics"*.Proceedings of European Community Wind Energy Conference held at Madrid, Spain 10-14 September 1990, pp 227-232.

[6]   Madsen, H.A. and Rasmussen, F. *"Stall Hysteresis and 3D Effects on Stall Regulated Wind Turbines: Experiment and Modelling"*. Paper presented at the 75th Fluid Dynamics Symposium held in Berlin, Germany, 10-13 October 1994. AGARD Conference Proceedings NO. 552, pp *9-1 to 9-9.*

[7]   Madsen, H.A. *"Aerodynamics of a Horizontal-Axis Wind Turbine in Natural Conditions"*. Risø-M-2903, Risø Natinal Laboratory, September 1991.

[8]   Butterfield, C.P. et al. *"NREL Combined Experiment Final Report – Phase II"*. Draft, NREL/TP-442-4807, NREL august 1992.

[9]   Madsen, H.A. "The actuator cylinder model". Aalborg University Centre, January 1982.

[10]   Veers, P. *"Three-dimensional Wind Simulation"*. Sandia report SAND88-015. Sandia National Laboratories. Alberquerque, New Mexico, 1988.

[11]   Mann, J. and Krenk, S. *"Fourier Simulation of a Non-Isotropic Wind Field Model"* . Paper no. 117/3/27. In Proceedings of the 6th International Conference on Structural Safety, ICOSSAR´93, Innsbruck, Austria, 9-13 August 1993.

[12]   Madsen, H.A. *"Application of Actuator Surface Theory on Wind Tur-bines"*. Proceedings of the 2nd IEA Symposium on Aerodynamics of Wind Turbines held at Lyngby 21-22. November 1988.

[13]   Madsen, H.A. and Paulsen, U.S. *"An Integrated Rotor and Wake Model compared with Experiment"*. Proceedings of the European Community Wind Energy Conference held at Madrid, Spain 10-14 September 1990.

[14]   Madsen, H.A. *"A CFD Analysis of the Actuator Disc Flow Compared with Momentum Theory results"*. Proceedings of the IEA Joint Action, Aerodynamics of Wind Turbines, 10th Symposium, held at the University of Edinburgh, December 16-17, 1997, pp. 109-124.

[15]   Madsen, H.A. *"Yaw Simulation using a 3D Actuator Disc Model Cou-pled to the Aeroelastic Code HawC"*. Proceedings of the IEA Joint Action, Aerodynamics of Wind Turbines, 13th Symposium, held at FFA, Stockholm, November 29.-30. 1999, pp. 133-146

MODELLING OF THE 10m NWTC
UNSTEADY AERODYNAMICS EXPERIMENT
FOR CALCULATIONS WITH PHATAS-IV

C. Lindenburg
ECN Wind Energy

November 9, 2000

1. INTRODUCTION

Basis for the turbine input file is mainly based on the documents on the web-site. The
program PHATAS-IV is applied with the models as are "Standard" used by colleagues.

2. AERODYNAMIC MODELLING

2.1 Airfoil Coefficients

2.1.1 NREL S809 airfoil
All airfoil coefficients files were copied and investigated.
It appeared that the angle of attack for the files from the
OHIO State University have an offset compared to those
from the Colorado State University and the Delft University.
After some discussions with Herman Snel and Nando Timmer tables
with airfoil coefficients were used of which the lift and drag
coefficients at small angles of attack were from the Delft
University while for large angles of attack they were from the
OHIO State University. For the latter coefficients the angle of
attack was decreased with 0.53 deg.
The moment coefficients were from the Delft University.
For angles of attack smaller than -17 deg and larger than 19 deg
the coefficients are derived with the program StC for an aspect
ratio of 6.97.
From the files with measured coefficients, it is found (as Nando
Timmer says) that the dependency on Reynolds number is weak.
It was however found that the maximum lift measured at the
Colorado State University is smaller than measured at the Ohio
State University and the Delft University.

2.1.2 Blade root
The blade root is modelled with the drag coefficient of a cylinder
for which the value 1.0 is used. Depending on the roughness and
turbulence this drag can be between 0.35 (rough) to 1.2 (smooth).

2.2 Blade Geometry
The blade is modelled from the rotor centre to the blade tip, which
has a radius of 5.029 m. The specified chord distribution is based
on the fact that this is linear over a large span.
Also the linearity of the blade twist distribution between 4.391 m
and 5.029 m is used to reduce the PHATAS input with chord-values.
The blade axis is modelled through the 30% chord locations.
The "Root Vortex Radius" is modelled at 1.21 m.
The aspect ratio is calculated from "Root Vortex Radius" as 6.97.
The aerodynamic solidity is calculated as 0.05853.

3. STRUCTURAL MODELLING

3.1 Blade Model
The mass distribution is derived from the distribution listed for
the constant chord blade by multiplication with 0.6*(1 - 0.14*R)'.
With this blade mass distribution the mass of one blade is 60.3 kg
of which the centre of gravity is 2.243m from the rotor centre.
The specifications give a mass of 60.2 kg with its centre at 2.266m.

The stiffness distribution is based on the stiffness distribution of
the constant-chord blade. The flat-wise bending stiffnesses are
multiplied with (3. - 0.25*r) and the edgewise bending stiffness
is multiplied with (1.4 - 0.12*r). For a radius up to 0.4m the
stiffnesses are very high. From r = 0.4m to r = 0.46m the stiffness
has the value for the strain gage device.

With the obtained stiffness distribution the first bending frequencies
are 7.26 Hz and 8.99 Hz (rotating), which correspond reasonably with
the specified values. The second blade flapping frequency is 31.4 Hz
which should be 30 Hz.

The Lock number for the first flapping mode is 0.992 which is small
for a wind turbine. A small Lock number indicates little aerodynamic
damping for structural dynamics, here blade flapping.
As long as the aerodynamic loads are measured directly this has
little effect.

3.2 Hub Model
The hub is rigid because the teeter hinge is locked.
The hub inertia is chosen at 118 kg*m*m such that the rotor inertia
has the specified value of 949 kg*m*m.

3.3 Nacelle Model

The nacelle mass is 1332kg which is the specified value of 1712 kg minus 379.7kg hub mass.
The nacelle yawing inertia has the specified value of 3798kg*m^2.

The shaft is modelled as rigid, despite of the factthat it may have bending flexibility.

3.4 Tower Model
The tower is described as a tubular tower in terms of diameters and wall thickness while the material properties of steel. The material density of the steel tower is increased to 9000 kg/m^3.
Following the "Frequently asked Questions" web-page the wall thickness of the lower part is 0.0175 m and of the upper part is 0.0214m. The conical section in between has a wall thickness 0.0214m.

The tower is modelled with two bending modes for which the first frequency (assuming a rigid rotor) is 1.74 Hz.

The drag coefficient of the tower (used for the strength of the tower wake) is 0.35, based on a Reynolds number between 0.4E+6 and 0.7E+6.
For the load cases with 7 m/s wind speed the Re- number is 0.28E+6 in which case the tower drag coefficient is guessed at 1.0.

 4. DRIVE TRAIN

4.1 Rotational Direction
In PHATAS the rotational direction is opposite to that of the test turbine. This is compensated by using yaw angles with opposite direction and to correct the structural loads for this model.

4.2 Generator Model
The generator is described as an asynchronous generator with a nominal rotor speed of 72.838 rpm and a nominal power of 20kW.
The nominal slip is 1.69%.
The time constant tau = 0.025s for the generator torque is used as:
    Qgen + tau * d(Qgen)/d(t) = Qgen(stationary)

4.3 Transmission
The transmission ratio is 25.13.
The generator inertia 143/(25.13)^2 = 0.22644 kg*m^2 is modelled at the fast shaft.
The shaft torsional stiffness is given the value of the lumped drive train flexibility of 199.E+3 N*m/rad.
The total drive train inertia should be between 144 and 179 kg*m^2.
Since 143kg*m^2 is from the generator the slow shaft inertia is

chosen roughly 17 kg*m^2.
For a disconnected generator the frequency is 6.07 Hz while for
normal operation the drive train inertia is 2.277 Hz.
The specified drive train frequency is 5.8 Hz.

4.4 Losses

The drive train efficiency was reported as 78%.
Calculation of the expression for full-load operation gives an
efficiency of 81.32%.
With the speficied relation for the efficiency, the loss of power
is calculated at full load and at 50% partial load. From these
values the linear expression for the loss a linear expression
for the loss of torque is derived
For simplicity the drive train efficiency is modelled as constant
value of 78%. This gives 22%/78% = 28.2% loss of generator torque.

5. NUMERICAL ASPECTS

5.1 Blade Discretisation

In PHATAS the rotor blade is modelled with a number of elements
of equal size. The aerodynamic state is described for the middle
of each of the elements. The number of elements is selected such
that the radial positions for the output variables matches best
with the middle locations of the elements:

R_out	20 el	19 el	18 el	17 el	16 el	15 el	14 el	13 el	12 el
1.510	1.383	1.455	1.537	1.627	1.414	1.509	1.616	1.354	1.467
2.343	2.389	2.250	2.375	2.219	2.357	2.514	2.335	2.514	2.305
3.185	3.143	3.044	3.213	3.106	3.300	3.185	3.053	3.288	3.143
4.023	3.897	4.103	4.051	3.994	3.929	3.856	4.131	4.062	3.981
4.780	4.904	4.896	4.889	4.881	4.872	4.861	4.849	4.836	4.819

From these element discretisations it was found that for 12 blade
elements the output locations have the smallest maximum difference
of 0.043m compared with the middle of the blade elements.

5.2 Time Increment

The time increment is 0.005 s which is sufficient to describe
frequencies up to 8.6 Hz.
Remind that the bending frequencies are 7.26 Hz and 8.99 Hz.
Within this time increment the blade tip travels 0.53 times its
chord, while the 80%-span section travels 0.43 times its chord
which means that dynamic stall phenomena can just be described.

6. OUTPUT

6.1 Time Span
As is prescribed the results are provided for a time span of 30s.
In order to have output of the stationary state, the calculations
are performed for 35s of which the first 5s are skipped.
In using PHATAS with a control algorithm it was found that about
5 to 6 revolutions are needed before stationary values of pitch
angle and rotor speed are obtained. Although the U.A.E. turbine
does not have a control algorithm, the Lock number is rather low
for which reason it is decided to skip also 5 to 6 revolutions.

6.1 Input properties
Pitch angle is read as the angle of the tip chord at R=5.029m with
respect to the rotor plane. This means that for a tip pitch angle
of 3 deg the blade (with twist distribution as specified) is
rotated over 1.185deg.
The wind speed and the yaw angle are treated as external conditions.
The rotor speed is used as initial value of the rotor speed
because in PHATAS the rotor speed results from equilibrium between
generator model and rotor torque, the specified rotor speed is
used as initial value for the calculation.
After completion of the calculations it appeared that for the
high wind speed load cases the rotor speed is somewhat larger
than the rotor speed as specified: 72.4 rpm for wind speed
values of 15m/s to 20m/s.

6.2 Output Properties
The blade chord used for the sectional forces and moments are
the chord values from the Turbine description. The values of
the local effective wind velocity are also expressed at the
radial positions (in meters) as specified.
The aerodynamic coefficients are evaluated for the middle of
the blade elements that are closest to the radial locations
of the instrumented section.

6.3 Rotor-azimuth Bin averaging
The program for rotor-azimuth bin-averaging used at ECN takes
for each revolution one value of the output time-series in each
of the 360 bins. Here the bins are centered at the integer
values of the azimuth.

7. AERODYNAMIC MODEL DESCRIPTION

7.1 Blade Element Momentum Theory.
Dynamic equations for axial- and tangential induced velocities.
The drag coefficient is not included in the description of the

induced velocity at the rotor plane. The wake filaments from profile-drag are considered to be thin

The stationary state without the induced velocity is calculated with the local wind velocity, excluding the influence of tower stagnation. The influence of the tower stagnation however is included in the local velocity acting on the airfoil.

Instationary effects in terms of annulus-average velocity are implemented on bases of conservation of axial momentum.

Distribution of induced velocity with the rule derived in the project "Ontwikkeling van een Engineering Model voor
        Scheefstand op Basis van Wind Tunnel Metingen".

The local induced velocity on a blade element is expressed with Tip loss factor of Prandtl.

Turbulent wake state described with the linear relation of Wilson.

Effects of rotation with the empirical rule of Snel et.al.
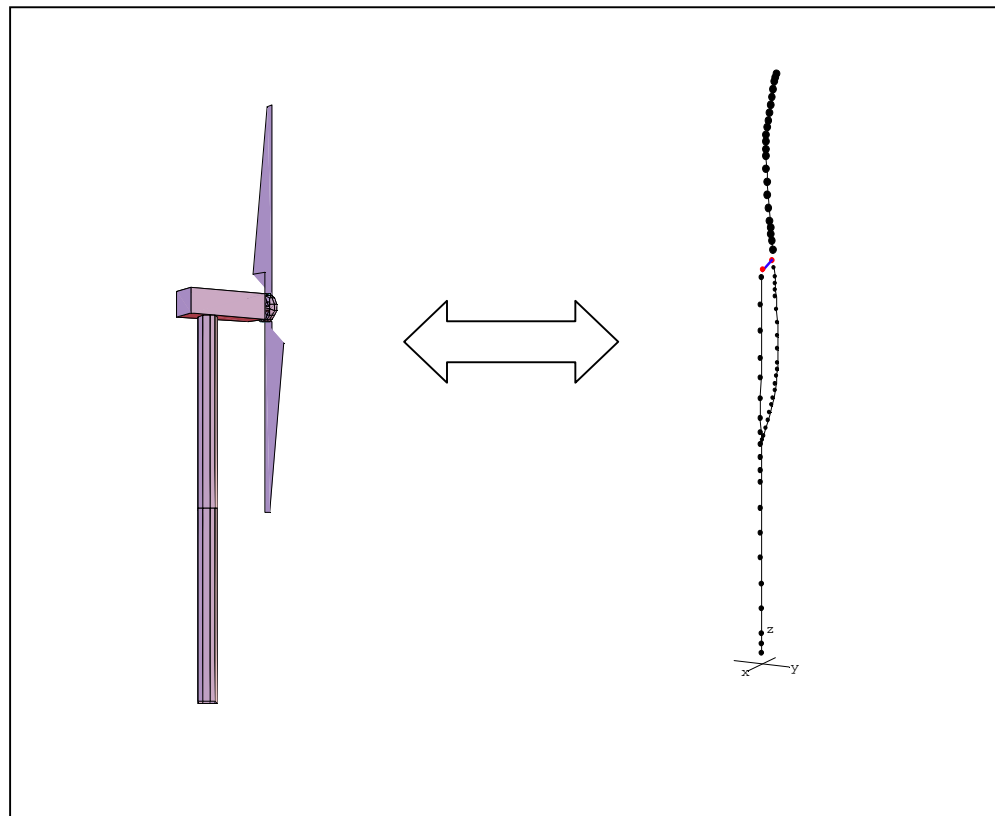which has a dependency on $(c/r)^2$.

Dynamic stall effects with the first-order Heuristic model formulated by H. Snel.

----------------------- KOERT LINDENBURG -----------------------

VIDYN version V824

Analysis of two bladed horisontal axis wind turbines

Description of structural model and new features of the Vidyn system

September 2000
Hans Ganander

Teknikgruppen AB   Tel: +46 8 444 5120
Box 21   Fax: +46 8 444 5129
S-191 21 Sollentuna   e-mail: hans@teknikgruppen .se
SWEDEN

Content

1. Introduction.

The main reason for development of a new version of the Vidyn wind turbine simulation code is the need for more accurate model of structure dynamics. The increase of the size of the turbines increases the motions due to flexibilities, which in turn means stronger dynamic coupplings. More acturatetly descibed flexible blade, nacelle and tower components are therefore important to achieve more reliable behaviour of the model of the turbines. There is as well a need for possibilities to change chosen principles of the models, as degrees of freedom and new geometric parameters. Reduction of calculation run time is allways asked for, and the desire to perform optimization makes that even more important.

These were most of the needs to meet. The method used to reach these ambitions is to use

- Improved descriptions of the flexibilities of the component
- Derive the equations according to Lagrange equation
- Use Mathematica   code for the derivation of th edynamic equations
- Make use of the possiblity to minimize the numerics of the derived subroutines

What has now been achieved?

- A system for derivation of the dynamic equations
- Generating numerically optimized Fortran subroutines, which are compiled and assembled together with the rest of the Vidyn system
- Two and three bladed models have been derived, tested and used
- Eigenvalue solutions have been calculated and verified
- Development of a tuning method
- Typical number of degrees of freedom is around 20 –25, as for example:
  - 3 blade deformation functions per blade, each one with flap, edge and pitch deformation components
  - teeter angle if needed
  - turbine and generator azimuthal positions
  - 6 dof nacelle support
  - yaw angle
  - 4 tower bending functions
- calculation speed is about 1-2 times real time on a 200 Mhz Pentium Pro

2. Coordinate systems.

Refering to fig 1 the turbine is composed of components, as tower, nacelle and blades. To describe the position of parts of these components several coordinate systems are used. DEgrees of freedom are shown within []. The systems used are:

- Tower, index t
- Yaw part of the nacelle, index y
- Nacelle, index n
- Couppling between nacelle and rotor, index p
- Non rotating 'rotor' system, index nc
- Rotating rotor system, index rc
- Rotor, index α
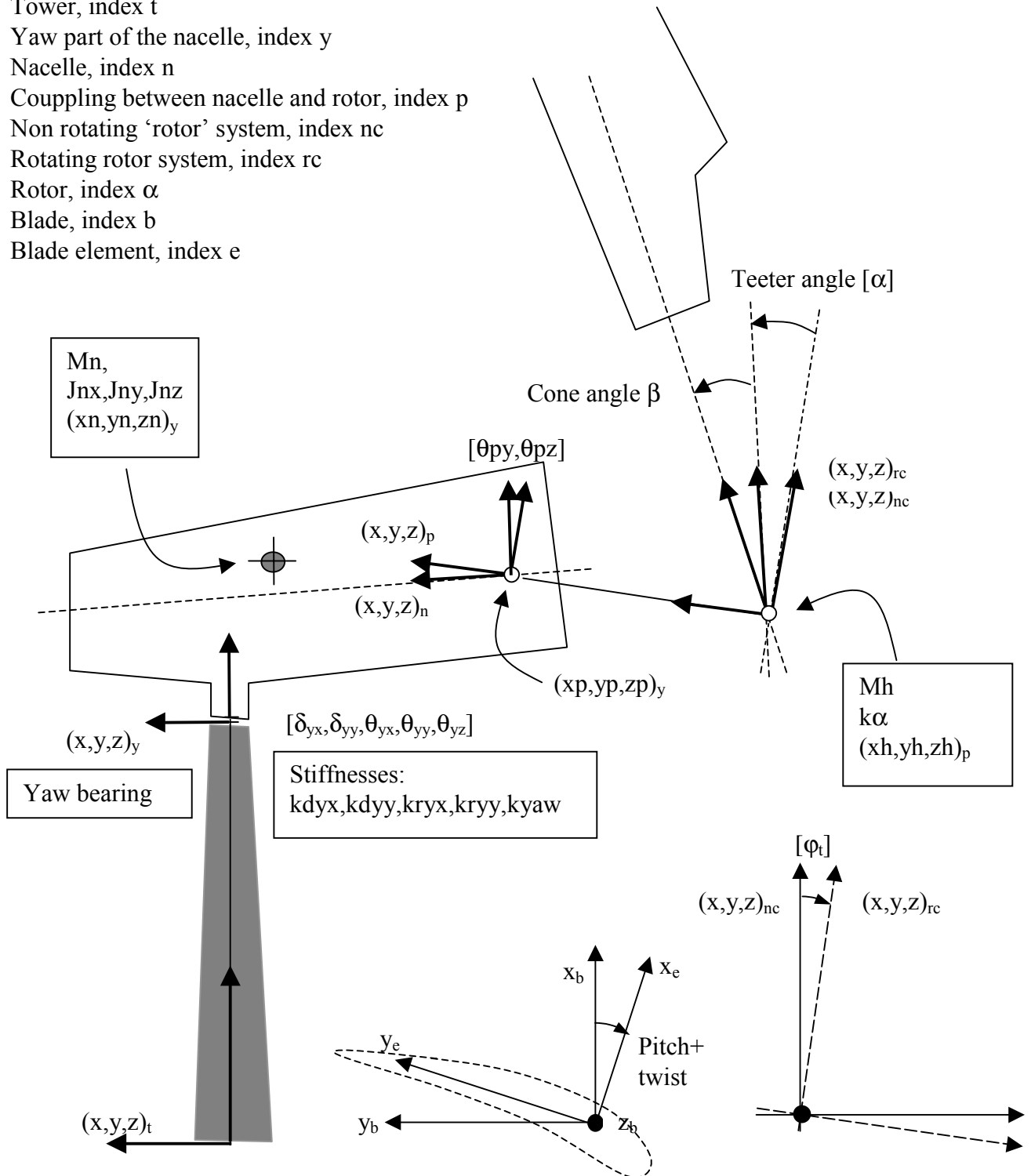- Blade, index b
- Blade element, index e

Fig 1

3. Tower and blade deflections.

Tower: the i:th tower mode dof q_{ti}

$$\overline{\delta}_t(t,z) = \sum_{i=nmt} q_{t,i}(t) \cdot \overline{d}_{t,i}(z)$$

$$\overline{\theta}(t,z)_t = \sum_{i=nmt} q_{t,i}(t) \, \overline{t}_{t,i}(z)$$

where

$$\overline{d}_{t,i}(z) = \{dx_{t,i}(z), dy_{t,i}(z), dz_{t,i}(z)\}$$

$$\overline{t}_{t,i}(z) = \{tx_{t,i}(z), ty_{t,i}(z), tz_{t,i}(z)\}$$

Blade: the j:th blade i:th mode dof q_{bji}

$$\overline{\delta}_{b,j}(t,r) = \sum_{i=nmb} q_{b,j,i}(t) \, \overline{d}_{b,j,i}(r)$$

where

$$\overline{d}_{b,j,i}(r) = \{dx_{b,j,i}(r), dy_{b,j,i}(r), tz_{b,j,i}(r)\}$$
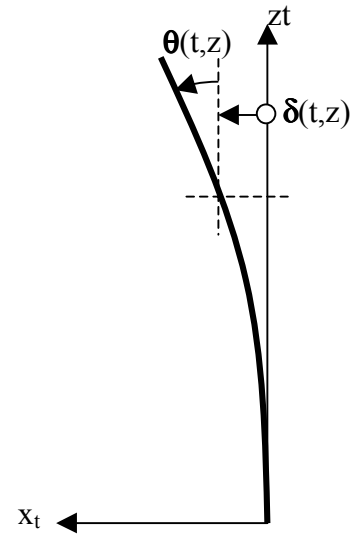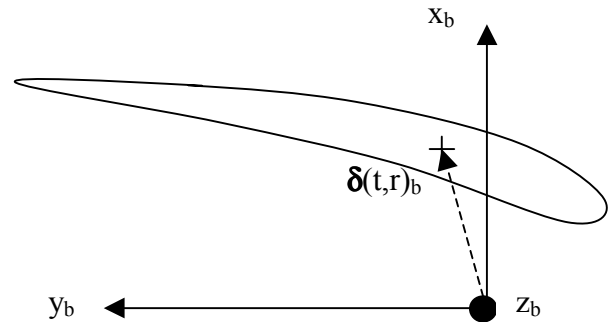
Fig 2

Fig 3

4. Degrees of freedom

Marked within [] in fig 1.

Blade: $q_{b,j,i}(t)$

Tower: $q_{t,i}(t)$

Yaw: $\delta_{yx}, \delta_{yy}, \theta_{yx}, \theta_{yy}, \theta_{yz}$

Primary shaft: θ_{py}, θ_{pz}

Rotor: φ_t, α

Generator: φ_g

In total there are 20 degrees of freedom which can be used within the actual discribed V824 model.

4. Principles of derivation of the dynamic equations

The derivation of the dynamic equations according to Lagrange equation for dynamics is based on kinetic energy (T) of all parts of the system and the potential energy (U) due to deformations of components and at couppling points. External loads (Fe), as aerodynamic blade forces, generator torque, control forces and gravity, contributes to the energy of the system. These forces are formulated as generalized forces (F_i), which can be interpreted as contributed work per degree of freedom. This is formulated below:

$$\frac{d}{dt}\left(\frac{\partial T}{\partial \dot{q}_i}\right) - \left(\frac{\partial T}{\partial q_i}\right) + \left(\frac{\partial U}{\partial q_i}\right) = F_i$$

where in principal

$$T = \frac{1}{2}\sum_k \left(\frac{d\mathbf{r}_k}{dt}^T \cdot \mathbf{M}_k \cdot \frac{d\mathbf{r}_k}{dt}\right)$$

$$U = \frac{1}{2}\sum_n \left(\boldsymbol{\delta}_n^T \cdot \mathbf{K}_n \cdot \boldsymbol{\delta}_n\right)$$

$$F_i = \frac{\partial W}{\partial q_i} = \sum_j \mathbf{F}e_j \cdot \frac{\partial \mathbf{r}_j}{\partial q_i}$$

where

$\mathbf{r}_i$= the i:th absolute position vektor
$\mathbf{M}_i$= inertia matrix for point i
$\boldsymbol{\delta}_i$= deformation vector of the i:th component
$\mathbf{K}_i$= stiffness matrix for the i:th component
$\mathbf{F}e_j$= external force at the j:the point
q_i= the i:th degree of freedom (dof)
j = the j: th point with external forces

Losses can be treated as external forces or formulated in terms of dissipation energi or power.

5. Transformations.

The formulation of the T and U energies as well as the generalized force can be carried out in terms of degrees of freedom (q_i). Fundamental of that procedure is transformation of coordinates of points from one system to another. Such a transformation of r_i of system *i* to system *i+1* can generally be written:

(1)

$$r_{i+1} = A_i(\theta_i) \cdot r_i + r_{0i}$$
where

θ_i= rotation between the *i* and *i+1* systems
r_{0i}= translation of the *i*-system to the *i+1*-system

There are several translations and rotations to consider when transforming a blade point to the fixed tower system. Refering to fig 1 the rotations are

- θ_{bz} = blade twist
- γ= pitch angel
- β= cone angel
- φ_b= blade angel, i.e π for blade number two of a two bladed turbine
- α= teeter angel
- φ_t= turbine angel
- τ= tilt angel
- θ_h = nacelle spring support (θ_x, θ_y, θ_z)
- θ_{yaw} = yaw angle
- θ_t= tower top angels (θ_{tx}, θ_{ty}, θ_{tz})

The deflection translations are:

- δ_b= blade deflections at point r_b (δ_{bx}, δ_{by},0)
- δ_h= nacelle spring support (δ_x, δ_y, δ_z)
- δ_t= tower top deflections (δ_{tx}, δ_{ty}, δ_{tz})

6. Modification of the equations.

The derived system of dynamic equations can be written:

$$\mathbf{A}_0 \cdot \ddot{\mathbf{q}} + \mathbf{b}_0 = \mathbf{f} \tag{2}$$

There are as many equations as there are degrees of freedom of the model, lets say nq, which are linear in the second derivative of $\mathbf{q}$ and where the quadric (nq,nq) matrix $\mathbf{A}_0$ and the vectors $\mathbf{b}_0$ and $\mathbf{f}$ are nonlinearly dependent on $\mathbf{q}$, d$\mathbf{q}$/dt and t. The $\mathbf{A}_0$ represents the inertia properties of the system, which generally is time dependent. Damping, gyroscopic and deformation forces are included in the $\mathbf{b}_0$ vector. External forces dominated by the aerodynamic blade forces and gravity can be found in the vector $\mathbf{f}$.

In order to make the equations effective and accurate for numerical calculations identification of common time dependent factors of terms of elements of the $\mathbf{A}_0$ matrix and the $\mathbf{b}_0$ vector have been used. The total inertia matrix $\mathbf{A}_0$ can be separated in parts which correspond to blade ($\mathbf{A}_{mb}$), tower ($\mathbf{A}_{mt}$) and all other rigid bodies ($\mathbf{A}_{mn}$). Summation is used along the flexible blades and the tower.

$$\mathbf{A}_0 = \sum_{ir}\left(\mathbf{Amb}_{ir} \cdot mb_{ir}\right) + \sum_{it}\left(\mathbf{Amt}_{it} \cdot mt_{it}\right) + \mathbf{Amn} \tag{3}$$

The $\mathbf{A}_{mb}$ matrix is the most extensive one of the matrices, which has been simplified as described below.

Elements (i,j) of the $\mathbf{Amb}_{ir}$ matrices above can be written as the sum of nt terms:

$$Amb_{ir,i,j} = \sum_{nt}\left(fmb_{ir,i,j,nt} \cdot gmb_{i,j,nt}(t)\right) \tag{4}$$

Each such term is in general a time dependent factor (function of the degrees of freedom), times a space (summation over ir) dependent constant. Putting this expression into the (i,j) element of $\mathbf{A}_0$ and changing order of the summations separates time and space dependent factors of each term.

$$A_{0,i,j} = \sum_{nt}\left[gmb_{i,j,nt}(t) \cdot \sum_{ir}\left(fmb_{ir,i,j,nt} \cdot mb_{ir}\right)\right] + \ldots = \sum_{nt}\left[gmb_{i,j,nt}(t) \cdot c_{i,j,nt}\right] + \ldots \tag{5}$$

Quite similar operations can be carried out for all other $\mathbf{A}$-matrices and $\mathbf{b}$-vectors as well. From calculation point point of view the advantage is that the space factors are constants along the whole calculation, which improves efficiency and accuracy. It is only the time factors which have to be updated at each time step. This means that there is potential to increase speed for calculation. The identification of the factor functions, as $fmb_{ir,i,j,nt}$ and $gmb_{i,j,nt}(t)$ is a very tedious task to do. The symbol handling and code generating system Mathematica® has been used for that.

7. The Vidyn system.

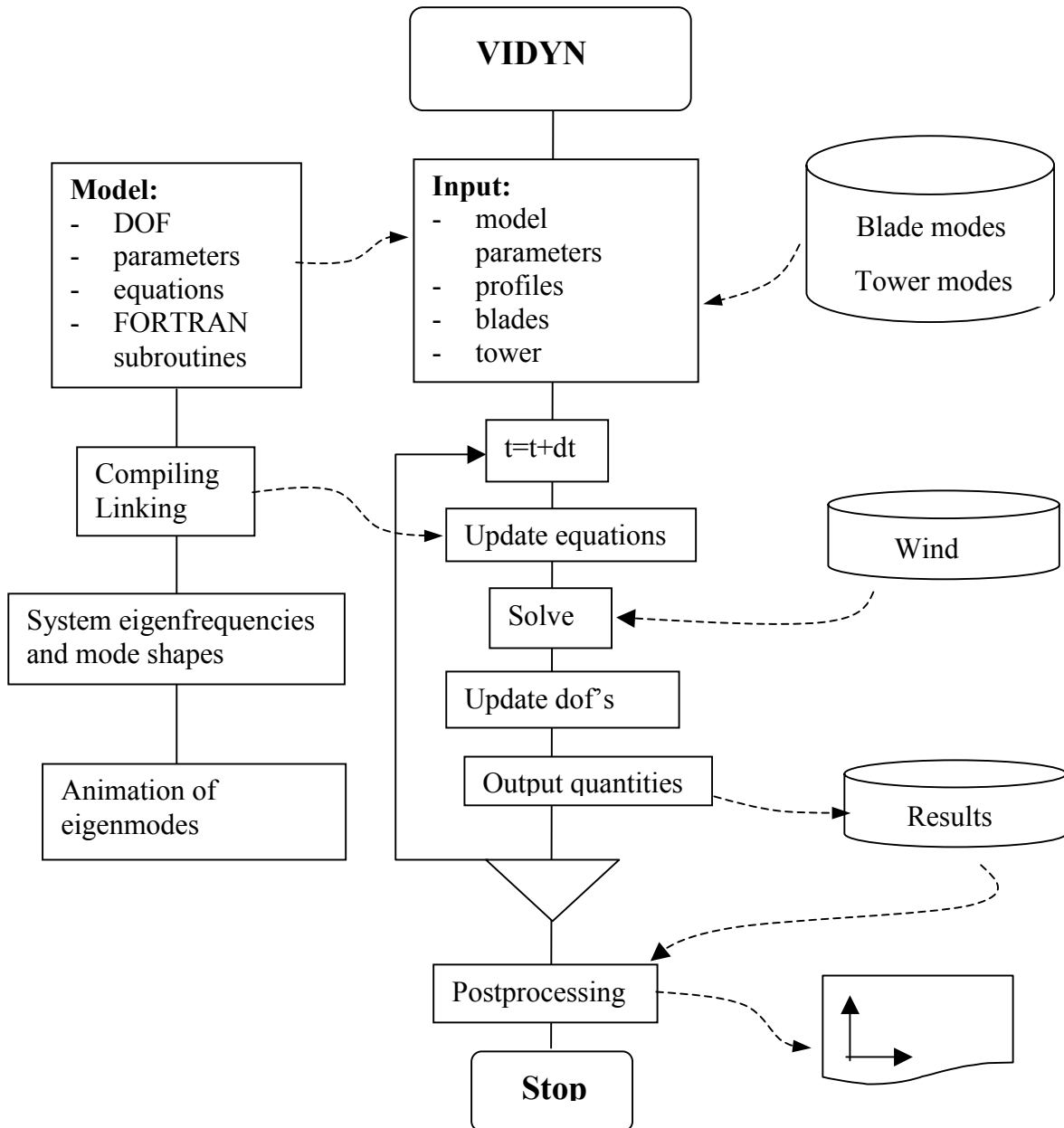A schematic layout of the Vidyn system is shown in fig 4 bvelow.

Fig 4 Layout of the Vidyn system

**AERODYNAMICS DRIVING THE STRUCTURAL DYNAMICS
IN THE WIND TURBINE SIMULATION MODEL "VIDYN"
SHORT SUMMARY**
Bjorn Montgomerie, FFA, Dec. 2000

1. Background
In this summary an aerodynamics model is described. It was developed at FFA during the last ten years. Its main application is to drive the dynamics in the aeroelastic code VIDYN which was developed at Teknikgruppen AB, Sweden. The aerodynamic methods used have a general validity to horizontal axis wind turbines.

2. Origins of the Aerodynamics Subroutine Package
The basic approach for the calculation of the aerodynamic forces, used for loading and performance, is the classic Blade Element Momentum (BEM) method. The original method was developed for

- Steady conditions
- The turbine disk being unconed, unyawed and untilted
- Attached blade flow
- The concentric tubular element areas being independent of each other

There are a few more simplifying assumptions underlying the basic BEM method as well.

In a sequence of co-operational projects in the European Union, a number of joint investigations were carried out, where real effects, such as deviations from what is stated in the list above, were analyzed using theoretical development, wind tunnel and full scale experiments. As a result the basic BEM method has been enriched with a patchwork of corrective measures.

3. The Composition of Methods
As mentioned above the basic BEM method is relied upon. Some additional considerations are briefly described below. A fuller description can be found in the references.

3.1 Variable wind
The planetary boundary layer is what wind turbines have to absorb to produce power. When the turbine is yawed and/or tilted the wake behavior depends on one certain wake angle. This angle is different from the oncoming average wind direction. The technique employed is to average the wind velocity over the disk area and to use this averaged velocity for calculation of an average induced axial velocity. From this the wake average direction is formed. Once the wake angle has been found it can be used in a simple expression for sinusoidal terms that will vary the induced velocity around the "clock".

But, time variation, of the oncoming wind, can also affect the disk average flow. The European project "Dynamic Inflow" was instrumental in providing the necessary database for development of methods in this respect. Here the induction is looked upon as being susceptible to time delays. In AERFORCE this is utilized such that annular tubes are treated as independent thus giving rise to a radial variation of the size of the delay.

For each time step of the simulation the described approach defines the setting for the blade element profiles, that in turn are subjected to the variable wind because of their azimuthal travel. Unsteady profile theory is employed in this context as described below.

3.2 Tip Losses
The tip loss factor F is calculated from Prandtl's original formula. The tip speed ratio is based on the velocity of the wind at the rotor disk (not in the wake). F is insensitive to yaw and tilt in the present implementation.

3.3 Dynamic Stall
Dynamic stall departs from the aerodynamic tables of CL, CD and Cm according to an implementation of the Beddoes-Leishman model. Thus, so far, there is no conversion from 2D to 3D in the aero tables.

3.4 Tower Interaction
The rotating blades will pass the proximity of the tower. One method each exists for downstream and upstream rotor placements. In the case of the upstream rotor the flow that hits the blades will have an additional influence from a 2D potential flow model of the circular tower. A dipole and a source are superimposed on the main flow, which is assumed to be homogeneous, presently disregarding the vertical wind gradient and turbulence of the inflowing wind. The dipole models the tower circular cross section shape, while the source represents the wake flow. The source is tuned on-line by the tower drag coefficient.

For the downstream location of the rotor another model is implemented. Here an empirical bell shaped function is employed to model the velocity deficit of the wake flow. The width, being empirically shaped, together with the tower drag coefficient dictate the depth of the "bell", thus defining a variable velocity deficit wind profile that is sensitive to the distance behind the tower.

4. References
[1] "AERFORCE: Subroutine Package for Unsteady Blade-Element/Momentum Calculations"
    FFA TN 2000-07
    Anders Björck

[2] "DYNSTALL: Subroutine Package with a Dynamic Stall Model"
    FFAP-V-110
    Anders Björck

[3] "Blade-Tower Interaction: Calculations Compared to Wind Tunnel Test Results
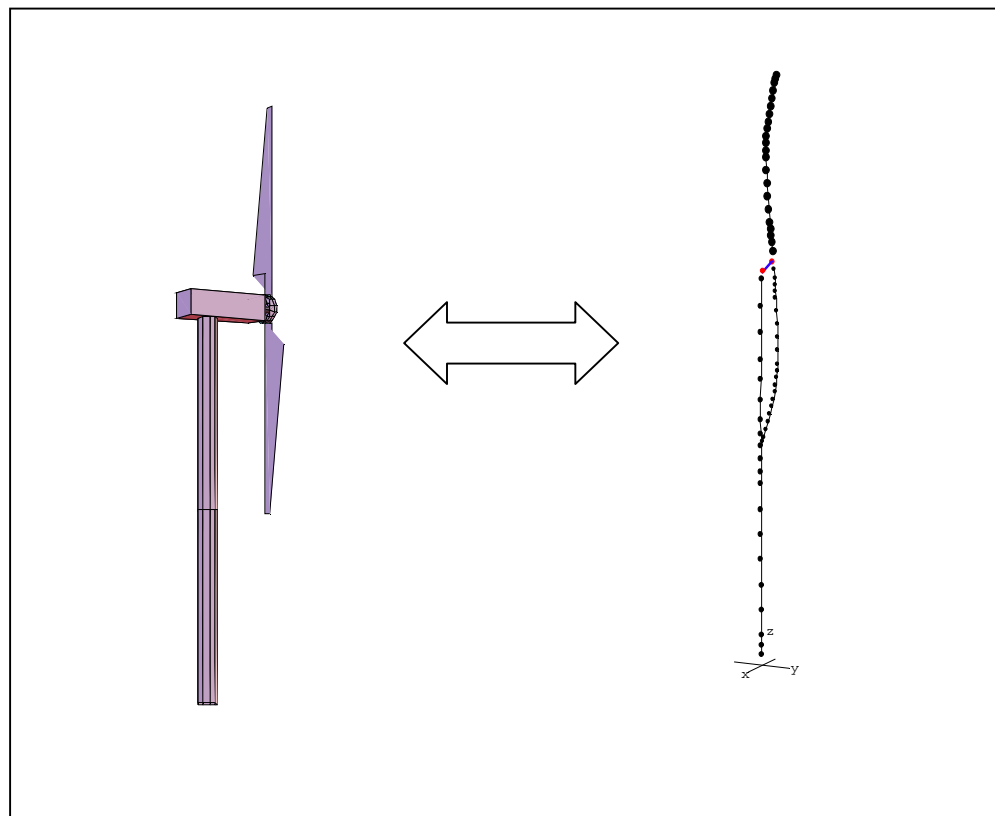   FFAP-V-107
    Anders Björck

[4] "Blade-Tower Interaction: Calculations with Two Tower Models Compared to Wind Tunnel Test Results"
    FFAP-V-124
    Anders Björck

Description of the structural model of the NREL wind tunnel test turbine.

A short summary.

November 2000
Hans Ganander

Content

Appendix I

Eight calculated eigenfrequencies at page 5-8

1. Introduction.

Aerodynamic tests have been carried out by NREL in the NASA Ames wind tunnel. A two bladed 10 [m] diameter turbine was used both as an upwind and a down wind turbine. The purpose of the project is primarily to improve knowledge about aerodynamic behaviour at different conditions [1], by comparing measurements and calculations. In this report the structure part of the aeroelastic Vidyn code [2] model of the test turbine is described. The general principles of the Vidyn code will also be found in [2]

The Vidyn structure model is based on three documents

- basic mashine data [3]
- mode shapes [4]
- frequency analysis [5]

Basic geometry, masses and tower properties are found in [3].

2. Blades

Blade mass and stiffness properties are determined to fit given frequencies and total mass. Properties of an untapered blade have been used, combined with indicated principal design. The dynamic properties of the used model blades are
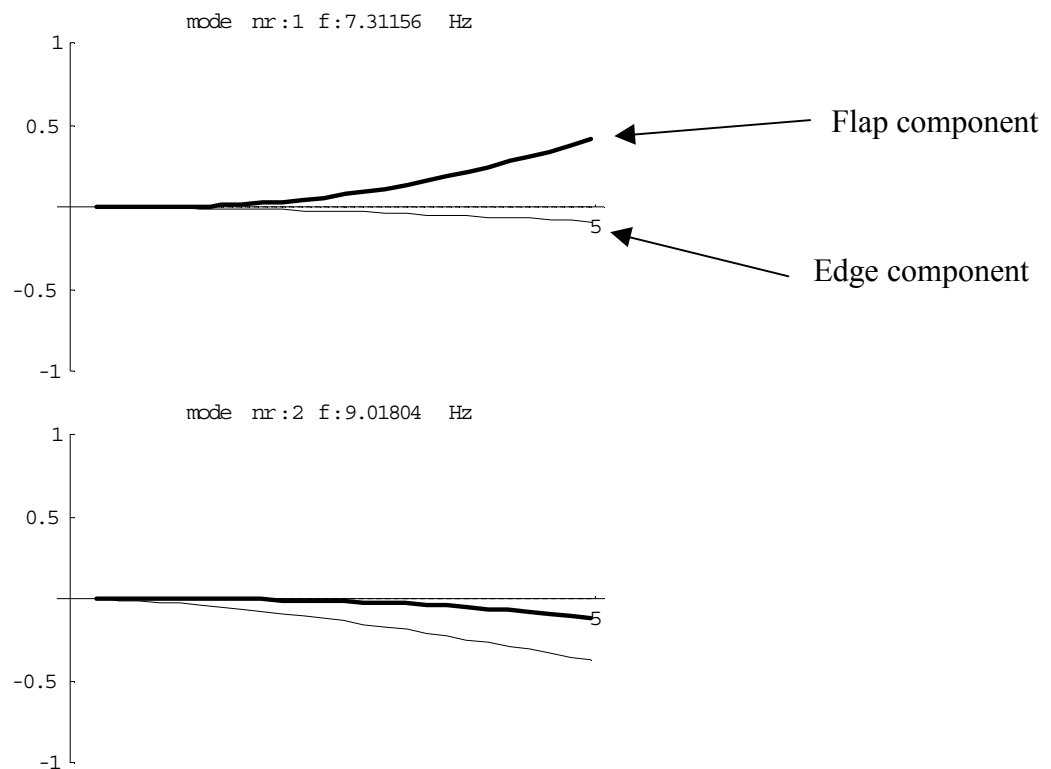

Fig 1 Model blade dynamic properties

These two frequencies correspond to the 1:st flap and the 1:edge frequencies. Due to blade twist and other deviations from symmetry the modes consists of two deformation components as can be seen in the fig 1.

3. Eigenfrequencies and tuning.

Stand still vibration tests were performed with the turbine locked in horizontal position. Teeter and yaw were also locked.

Measured eignfrequencies are used to tune the model eigenfrequencies. The idea is to assume that data about geometry and masses are known, as well as tower and blade flexibilities. Unknown stiffnesses at couplings between tower and nacelle, primary shaft and the rotor are determined to achieve as good agreement between measured and calculated frequencies as possible.

Eight eigenfrequencies of the tuned model are shown in app 1.

4. References

[1]: NREL/NWTC Aerodynamics Code Blind Comparison. September 2000.

[2]: Vidyn version V824. Description of the structure model and the new Vidyn system. Hans Ganander.Report TG-R-00-16. Teknikgruppen September 2000.

[3]: Basic Machine Parameters. Found at National Wind Technology Center (NWTC) web site, NASA Ames Wind Tunnel Tests.

[4]: Modal Test Movies and Results. Found at National Wind Technology Center (NWTC) web site, NASA Ames Wind Tunnel Tests.

[5]: Modal TestSummary. Found at National Wind Technology Center (NWTC) web site, NASA Ames Wind Tunnel Tests.

NREL Frequency Nr: 1   1.7 Hz
fi0 =1.5708 pitch =0.
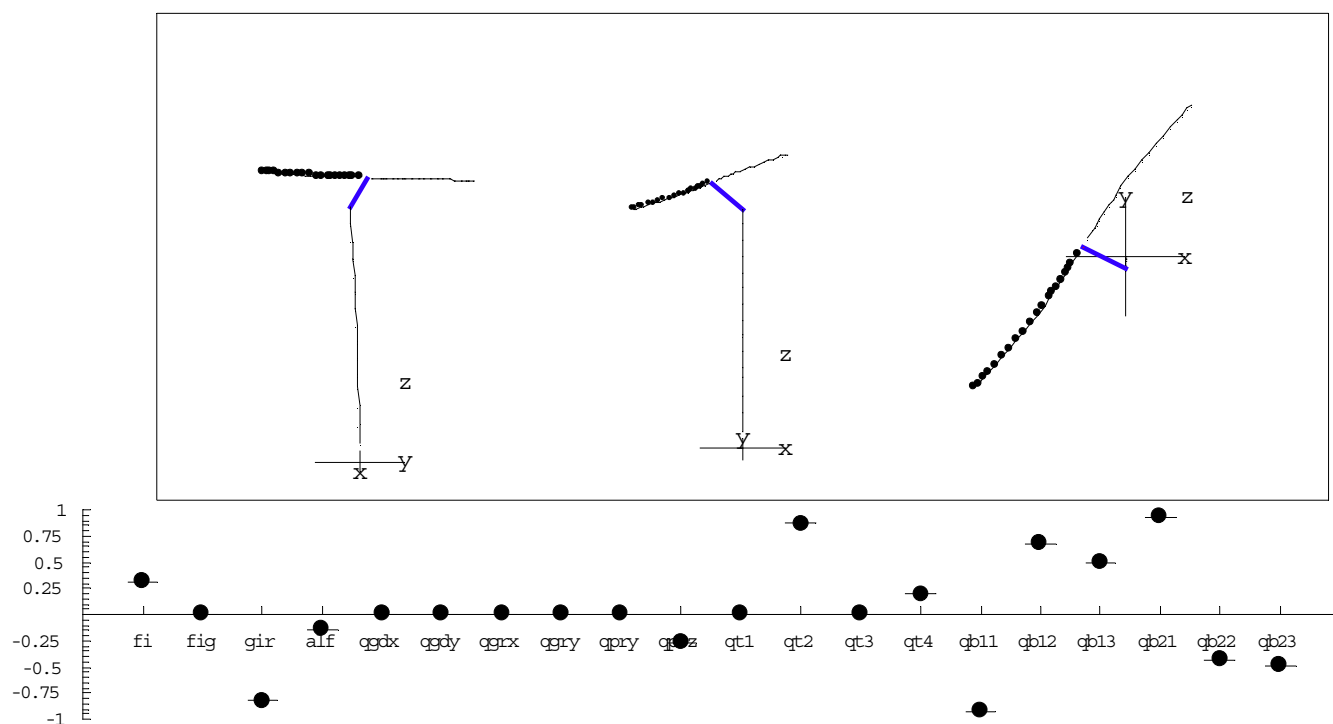kalf =7.4 kgdx =10. kgdy =10 kgrx =8. kgry =8. kpry =7. kprz =7. kgen =6. kyaw =6.
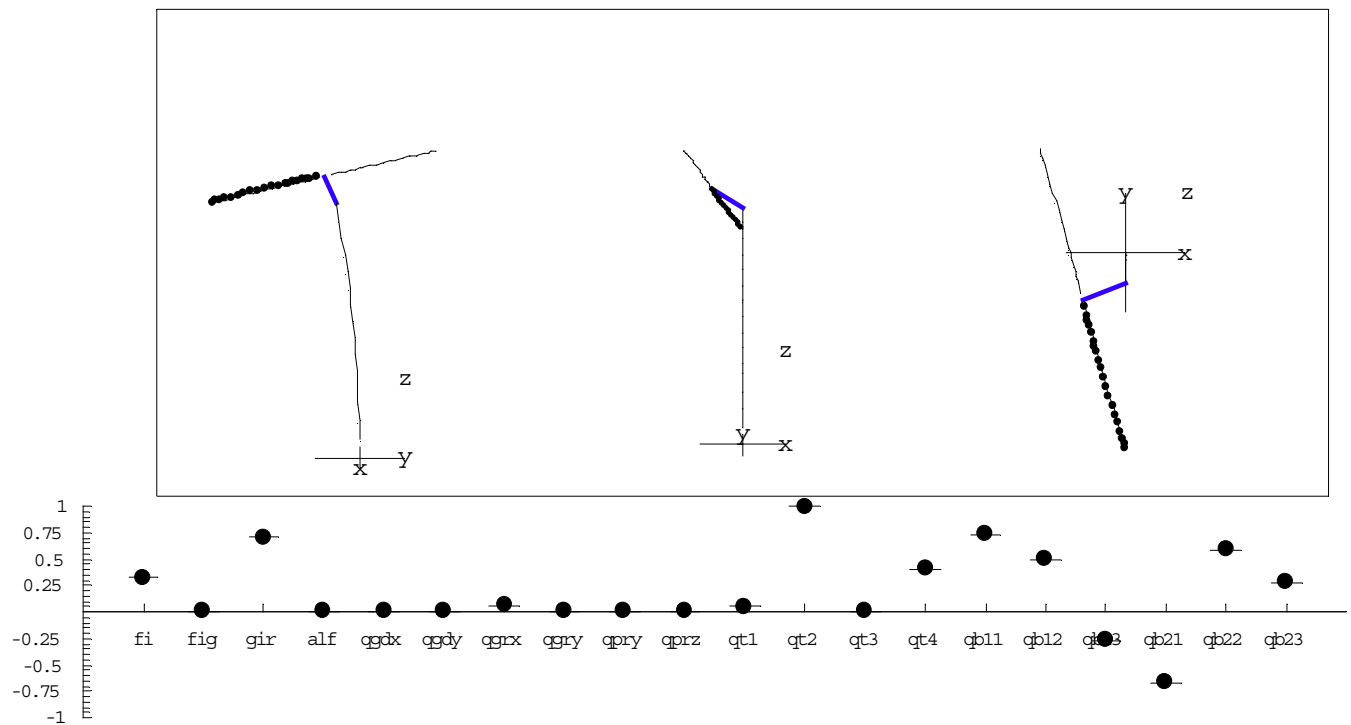
NREL Frequency Nr: 2   1.75 Hz
fi0 =1.5708 pitch =0.
kalf =7.4 kgdx =10. kgdy =10 kgrx =8. kgry =8. kpry =7. kprz =7. kgen =6. kyaw =6.
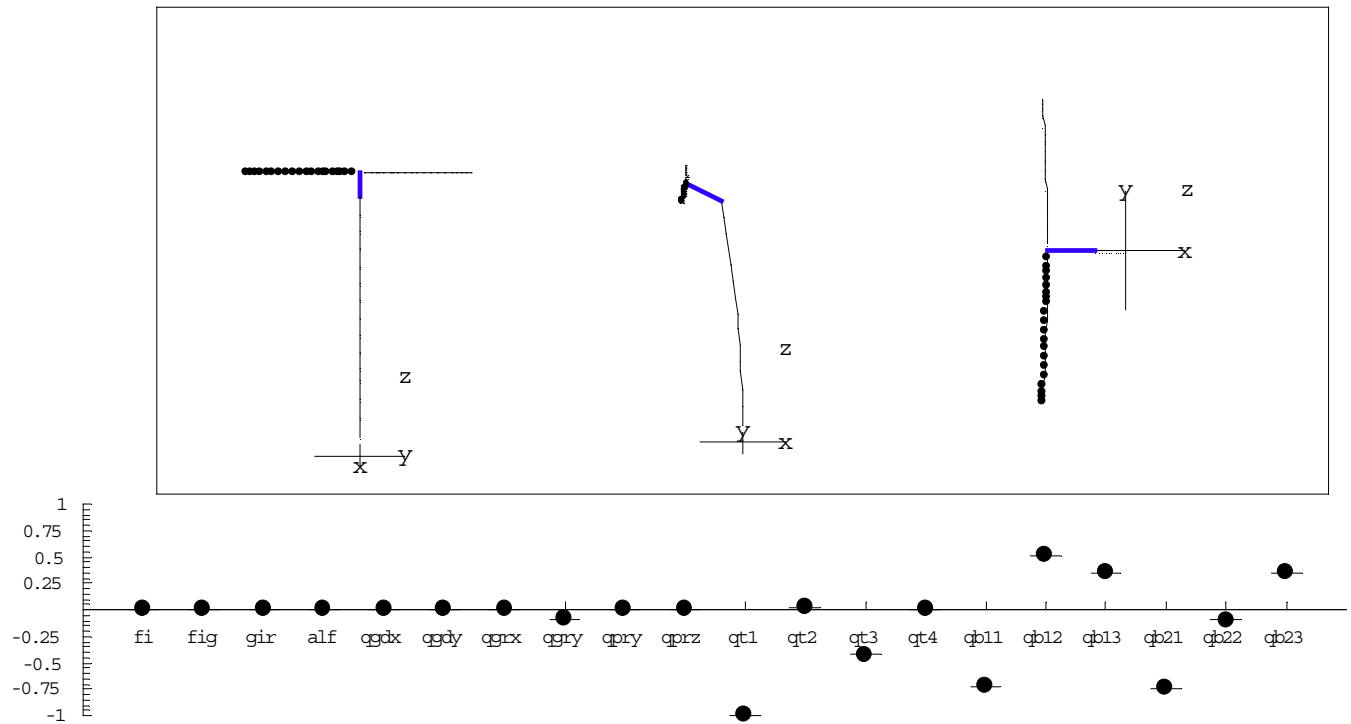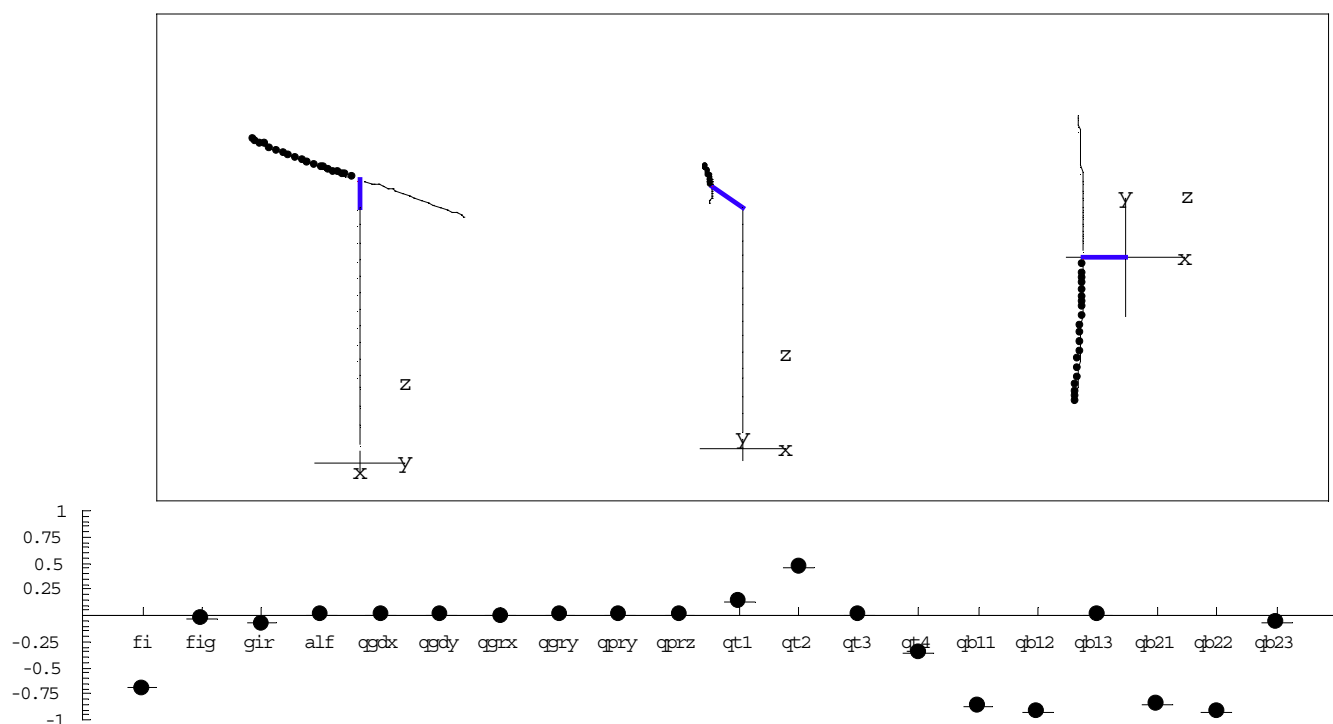
NREL Frequency Nr: 3 2.37 Hz
fi0 =1.5708 pitch =0.
kalf =7.4 kgdx =10. kgdy =10 kgrx =8. kgry =8. kpry =7. kprz =7. kgen =6. kyaw =6.

NREL Frequency Nr: 4 4.61 Hz
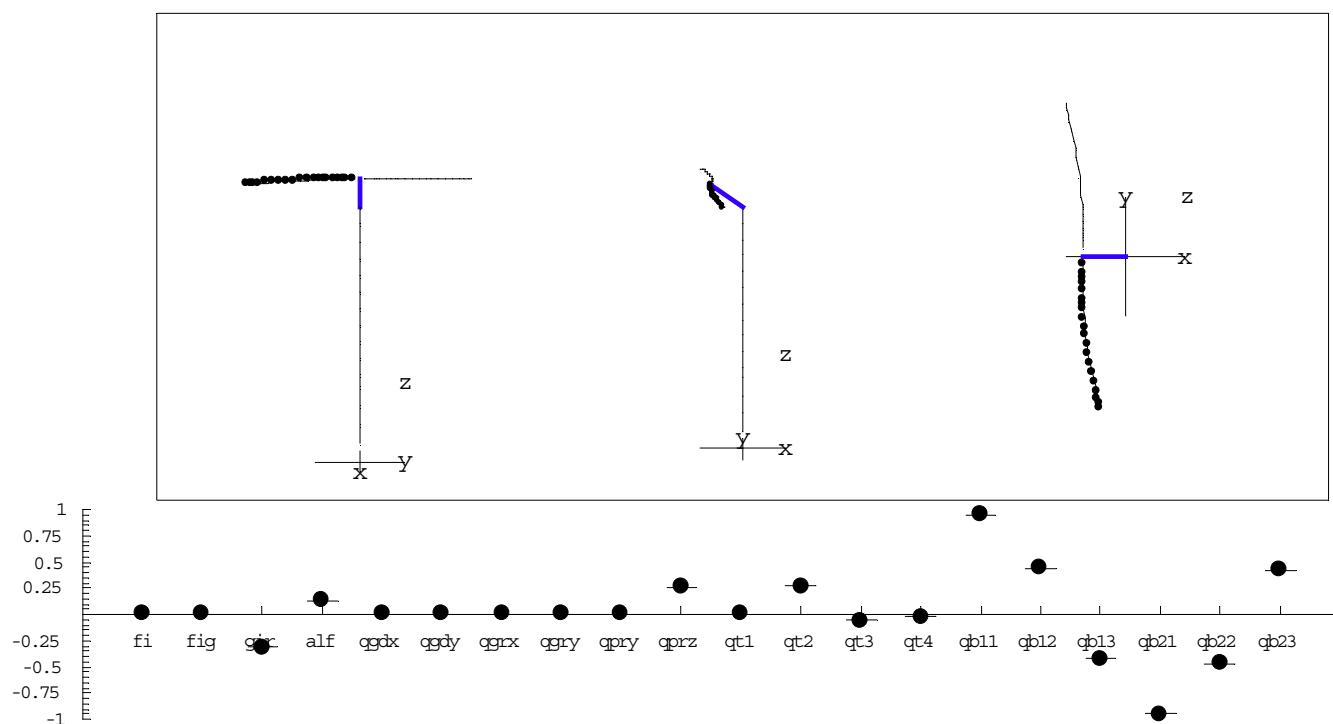fi0 =1.5708 pitch =0.
kalf =7.4 kgdx =10. kgdy =10 kgrx =8. kgry =8. kpry =7. kprz =7. kgen =6. kyaw =6.

NREL Frequency Nr: 5 7.1 Hz
fi0 =1.5708 pitch =0.
kalf =7.4 kgdx =10. kgdy =10 kgrx =8. kgry =8. kpry =7. kprz =7. kgen =6. kyaw =6.

NREL Frequency Nr: 6 7.31 Hz
fi0 =1.5708 pitch =0.
kalf =7.4 kgdx =10. kgdy =10 kgrx =8. kgry =8. kpry =7. kprz =7. kgen =6. kyaw =6.
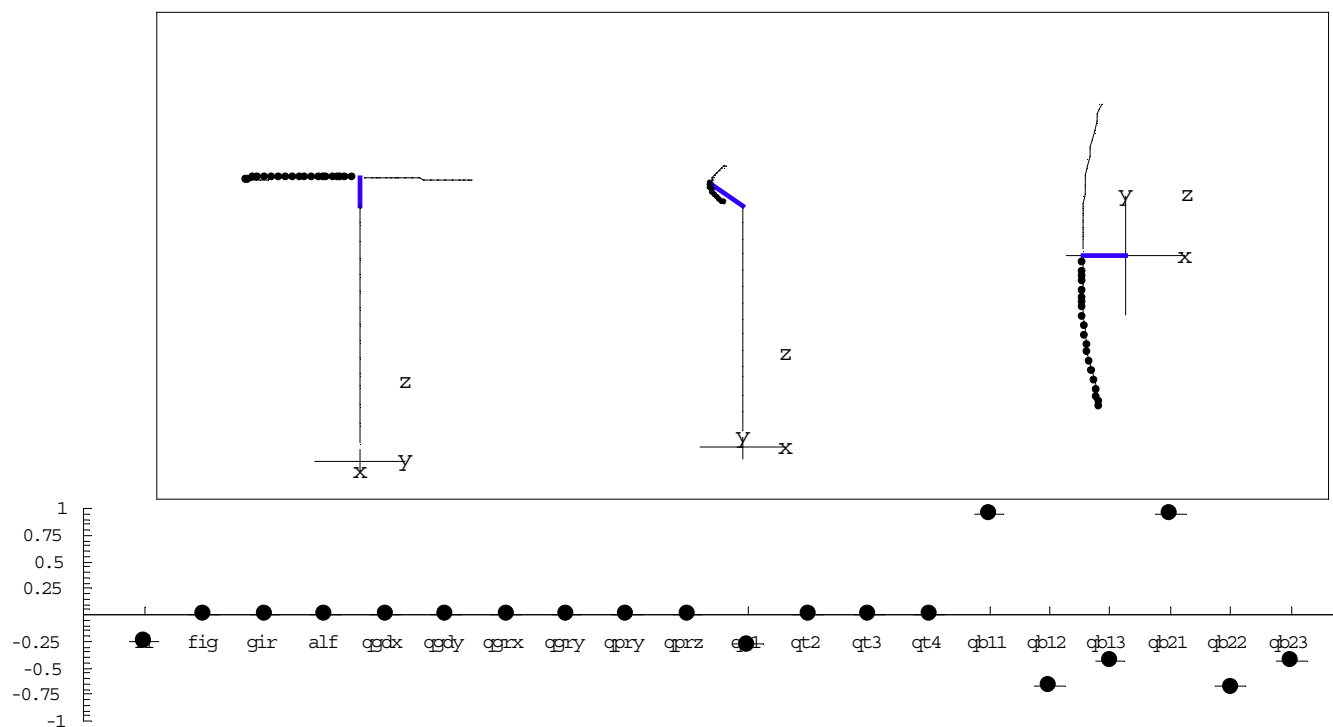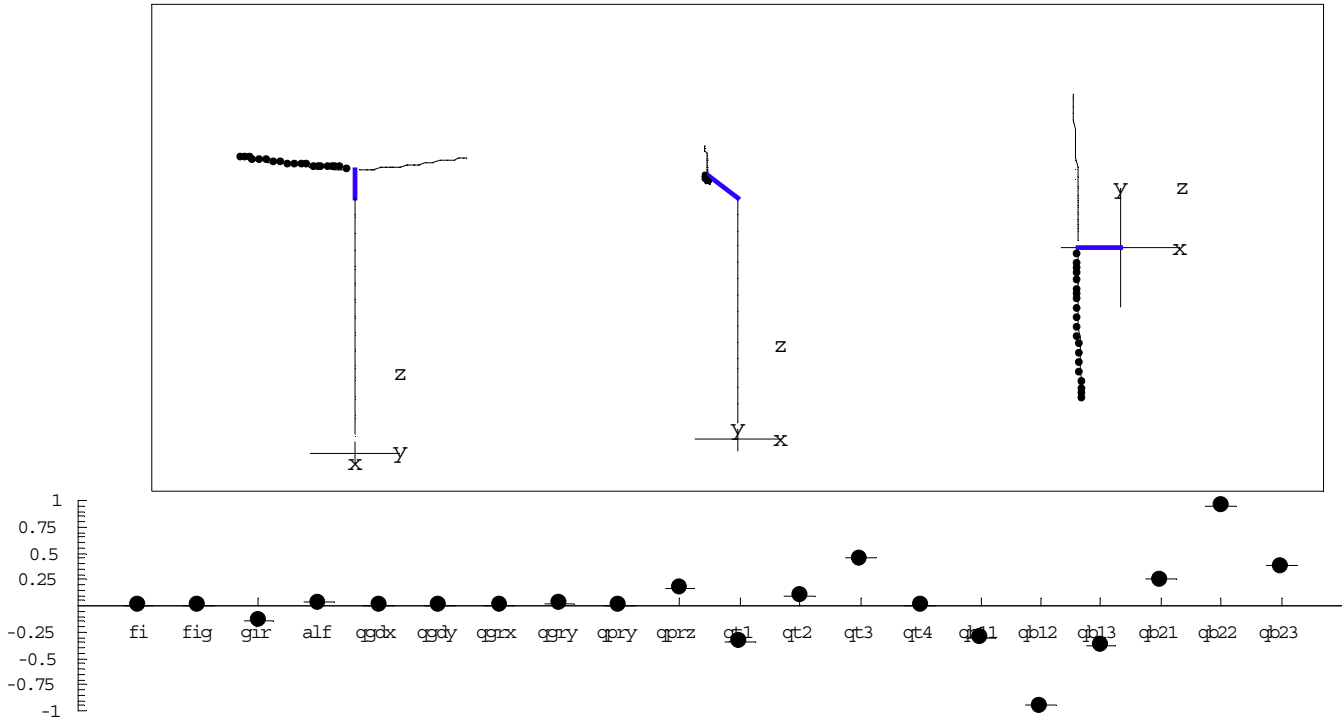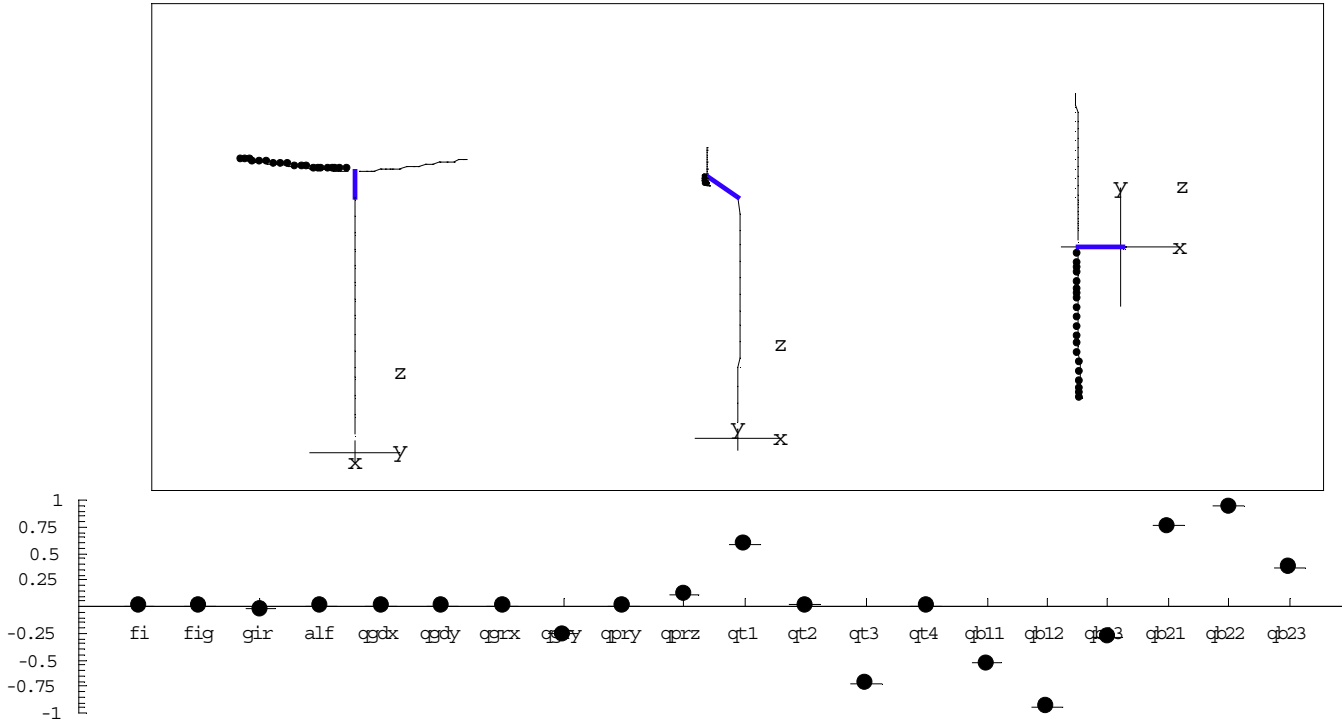
NREL Frequency   Nr: 7   9.17 Hz
fi0 =1.5708 pitch =0.
kalf =7.4 kgdx =10. kgdy =10 kgrx =8. kgry =8. kpry =7. kprz =7. kgen =6. kyaw =6.

NREL Frequency   Nr: 8   11.03 Hz
fi0 =1.5708 pitch =0.
kalf =7.4 kgdx =10. kgdy =10 kgrx =8. kgry =8. kpry =7. kprz =7. kgen =6. kyaw =6.

NREL/NWTC Aerodynamics Code Blind Comparison

Sørensen, N.N[†], Michelsen, J.A.[*]

[†] Wind Energy and Atmospheric
Physics Department
Risø National Laboratory
DK-4000 Roskilde, Denmark

[*] Department of Energy Engineering
Technical University of Denmark
DK-2800 Lyngby, Denmark

Abstract

An incompressible Reynolds Averaged Navier-Stokes solver, based on the pressure correction approach is described. The model is formulated in a rotating frame of reference attached to the blade, and the necessary fictitious forces are included as volume sources. The boundary layer turbulence is modeled by the SST $k - \omega$ model.
The Navier-Stokes solver is applied to the Combined Experiment Phase VI turbine, for six wind speeds (7, 10, 13.1, 15.1, 20.1 and 25.1 m/s) according to cases described by the NREL/NWTC Aerodynamics Code Blind Comparison. Both steady state and unsteady computations are performed.

Method

In the present work an incompressible Navier-Stokes solver is applied to predict the aerodynamics of the unsteady aerodynamics experiment phase-VI rotor at the National Renewable Energy Laboratory. In this investigation only the upwind configuration will be examined. The influence of the tower and nacelle on the rotor aerodynamics will to a first approximation be neglected. This highly simplifies the geometrical complexity of the flow problem, and the 1P interference between the blades and the tower and nacelle is also avoided by this simplification. Additionally, assuming zero vertical shear in the incoming flow and zero yaw misalignment, the blades see the same inflow conditions irrespectively of azimuth position of the rotor. These simplifications result in a simpler problem where only the rotor needs to be modelled. Even though instationarities from local flow separations on the blades may lead to flow unsteadiness, both steady and unsteady computations are carried out. In the present work only one of the blades is explicitly modelled in the computations. The remaining blade is accounted for using periodic boundary conditions, exploiting the 180 degrees symmetry of the two bladed rotor.

Navier-Stokes Solver

The in-house flow solver EllipSys3D is used in all computations presented in the following. The code is developed in cooperation between the Department of Energy Engineering at DTU and The Department of Wind Energy and Atmospheric Physics at Risø, see Michelsen [1], [2] and Sørensen [3].
The EllipSys3D code is a multiblock finite volume discretization of the incompressible Reynolds Averaged Navier-Stokes (RANS) equations in general curvilinear coordinates. The code uses a collocated variable arrangement, and Rhie/Chow [4] interpolation is used to avoid odd/even pressure decoupling. As the code solves the incompressible flow equations, no equation of state exists for the pressure, and the SIMPLE algorithm of Patankar [5] is used to enforce the pressure/velocity coupling. The EllipSys3D code is parallelized with MPI for executions on distributed memory machines, using a non-overlapping domain decomposition technique.
For rotor computations, a moving frame attached to the rotor blades is used, and the necessary fictitious forces are added to the governing equations. Polar velocities (v_r, v_θ and v_z) are used in order to allow simple treatment of periodic boundary conditions in the azimuth direction, Michelsen [6].
The solution is advanced in time using a 2nd order iterative time-stepping (or dual time-stepping) method. In each global time-step the equations are solved in an iterative manner, using underrelaxation. First, the momentum equations are used as a predictor to advance the solution in time. At this point in the computation the flowfield will not fulfill the continuity equation. The rewritten continuity equation (the so called pressure correction equation) is used as a corrector making the predicted flowfield satisfy the continuity constraint. This two step procedure corresponds to a single sub-iteration, and the process is repeated until a convergent solution is obtained for the timestep. When a convergent solution is obtained, the variables are updated, and we continue with the next time-step.
For steady state computations, the global time-step is set to infinity and dual timestepping is not used, this corresponds to the use of local time-stepping. In order to accelerate the overall algorithm, a three level grid sequence is used in the steady state computations.
The convective terms are discretized using a second order upwind scheme, implemented using the deferred correction approach first suggested by Khosla and Rubin [7]. Central differences are used for the viscous terms, where

only the normal terms are treated fully implicit in each sub-iteration, while the terms from non-orthogonality and the variable viscosity terms are treated explicitly. Thus, when the sub-iteration process is finished all terms are evaluated at the new time level.

The Jacobian J^* of the transformation, $\xi = \xi(r, \theta, z)$, $\eta = \eta(r, \theta, z)$ and $\zeta = \zeta(r, \theta, z)$ is given by:

$$J^* = \begin{vmatrix} r_\xi & r_\eta & r_\zeta \\ \theta_\xi & \theta_\eta & \theta_\zeta \\ z_\xi & z_\eta & z_\zeta \end{vmatrix} ,$$

and the volume of the finite volume cell J can be computed as the cell center radius r_{CC} times the Jacobian of the transformation.

In the polar frame of reference the metrics α^* are not of equal dimension, and in the following the area scaled metrics are used:

$$\begin{bmatrix} \alpha_{\xi r} \\ \alpha_{\eta r} \\ \alpha_{\zeta r} \end{bmatrix} = r_{CF} \begin{bmatrix} \alpha^*_{\xi r} \\ \alpha^*_{\eta r} \\ \alpha^*_{\eta r} \end{bmatrix} , \quad \begin{bmatrix} \alpha_{\xi \theta} \\ \alpha_{\eta \theta} \\ \alpha_{\zeta \theta} \end{bmatrix} = \begin{bmatrix} \alpha^*_{\xi \theta} \\ \alpha^*_{\eta \theta} \\ \alpha^*_{\zeta \theta} \end{bmatrix} , \quad \begin{bmatrix} \alpha_{\xi z} \\ \alpha_{\eta z} \\ \alpha_{\zeta z} \end{bmatrix} = r_{CF} \begin{bmatrix} \alpha^*_{\xi z} \\ \alpha^*_{\eta z} \\ \alpha^*_{\zeta z} \end{bmatrix} ,$$

where r_{CF} is the mean radius of the cell face.

The RANS equations in general curvilinear coordinates can be written as follows, where the density ρ is kept constant:

$$\frac{\partial Q}{\partial t} + \frac{\partial(E - E_v)}{\partial \xi} + \frac{\partial(F - F_v)}{\partial \eta} + \frac{\partial(G - G_v)}{\partial \zeta} = RHS ,$$

with

$$Q = J \begin{bmatrix} \rho \\ \rho v_r \\ \rho v_\theta \\ \rho v_z \end{bmatrix} , \quad E = \begin{bmatrix} C_1 \\ C_1 v_r + \alpha_{\xi r} p \\ C_1 \hat{v}_\theta + \alpha_{\xi \theta} p \\ C_1 v_z + \alpha_{\xi z} p \end{bmatrix} , \quad F = \begin{bmatrix} C_2 \\ C_2 v_r + \alpha_{\eta r} p \\ C_2 \hat{v}_\theta + \alpha_{\eta \theta} p \\ C_2 v_z + \alpha_{\eta z} p \end{bmatrix} , \quad G = \begin{bmatrix} C_3 \\ C_3 v_r + \alpha_{\zeta r} p \\ C_3 \hat{v}_\theta + \alpha_{\zeta \theta} p \\ C_3 v_z + \alpha_{\zeta z} p \end{bmatrix} ,$$

where $\hat{v}_\theta = \Omega r + v_\theta$ is the absolute velocity.

In the following, μ is the effective viscosity composed of the molecular viscosity and the turbulent eddy viscosity. For convenience the viscous terms are split in normal terms, crossterms, and terms arising form the variable viscosity:

$$E_v = E_v^n + E_v^c + E_v^v , \quad F_v = F_v^n + F_v^c + F_v^v , \quad G_v = G_v^n + G_v^c + G_v^v .$$

The normal diffusive term is given by the following expressions:

$$E_v^n = \frac{\mu \beta_{11}}{J} \begin{bmatrix} 0 \\ \frac{\partial v_r}{\partial \xi} \\ \frac{\partial v_\theta}{\partial \xi} \\ \frac{\partial v_z}{\partial \xi} \end{bmatrix} , \quad F_v^n = \frac{\mu \beta_{22}}{J} \begin{bmatrix} 0 \\ \frac{\partial v_r}{\partial \eta} \\ \frac{\partial v_\theta}{\partial \eta} \\ \frac{\partial v_z}{\partial \eta} \end{bmatrix} , \quad G_v^n = \frac{\mu \beta_{33}}{J} \begin{bmatrix} 0 \\ \frac{\partial v_r}{\partial \zeta} \\ \frac{\partial v_\theta}{\partial \zeta} \\ \frac{\partial v_z}{\partial \zeta} \end{bmatrix} .$$

where $\beta_{ij} = A A^T$, and A is given by:

$$A_{ij} = \begin{bmatrix} \alpha_{\xi r} & \alpha_{\xi \theta} & \alpha_{\xi z} \\ \alpha_{\eta r} & \alpha_{\eta \theta} & \alpha_{\eta z} \\ \alpha_{\zeta r} & \alpha_{\zeta \theta} & \alpha_{\zeta z} \end{bmatrix} .$$

The so called cross diffusion terms can be written as:

$$E_v^c = \frac{\mu}{J} \begin{bmatrix} 0 \\ \beta_{12} \frac{\partial v_r}{\partial \eta} + \beta_{13} \frac{\partial v_r}{\partial \zeta} \\ \beta_{12} \frac{\partial v_\theta}{\partial \eta} + \beta_{13} \frac{\partial v_\theta}{\partial \zeta} \\ \beta_{12} \frac{\partial v_z}{\partial \eta} + \beta_{13} \frac{\partial v_z}{\partial \zeta} \end{bmatrix} , \quad F_v^c = \frac{\mu}{J} \begin{bmatrix} 0 \\ \beta_{21} \frac{\partial v_r}{\partial \xi} + \beta_{23} \frac{\partial v_r}{\partial \zeta} \\ \beta_{21} \frac{\partial v_\theta}{\partial \xi} + \beta_{23} \frac{\partial v_\theta}{\partial \zeta} \\ \beta_{21} \frac{\partial v_z}{\partial \xi} + \beta_{23} \frac{\partial v_z}{\partial \zeta} \end{bmatrix} ,$$

$$G_v^c = \frac{\mu}{J} \begin{bmatrix} 0 \\ \beta_{31} \frac{\partial v_r}{\partial \xi} + \beta_{32} \frac{\partial v_r}{\partial \eta} \\ \beta_{31} \frac{\partial v_\theta}{\partial \xi} + \beta_{32} \frac{\partial v_\theta}{\partial \eta} \\ \beta_{31} \frac{\partial v_z}{\partial \xi} + \beta_{32} \frac{\partial v_z}{\partial \eta} \end{bmatrix} .$$

2

And the terms arising from the non constant viscosity:

$$
E_v^v = \mu \begin{bmatrix} 0 \\ \omega_{11}\alpha_{\xi r} + \omega_{21}\alpha_{\xi\theta} + \omega_{31}\alpha_{\xi z} \\ \omega_{12}\alpha_{\xi r} + \omega_{22}\alpha_{\xi\theta} + \omega_{32}\alpha_{\xi z} \\ \omega_{13}\alpha_{\xi r} + \omega_{23}\alpha_{\xi\theta} + \omega_{33}\alpha_{\xi z} \end{bmatrix} , \quad F_v^v = \mu \begin{bmatrix} 0 \\ \omega_{11}\alpha_{\eta r} + \omega_{21}\alpha_{\eta\theta} + \omega_{31}\alpha_{\eta z} \\ \omega_{12}\alpha_{\eta r} + \omega_{22}\alpha_{\eta\theta} + \omega_{32}\alpha_{\eta z} \\ \omega_{13}\alpha_{\eta r} + \omega_{23}\alpha_{\eta\theta} + \omega_{33}\alpha_{\eta z} \end{bmatrix} ,
$$

$$
G_v^v = \mu \begin{bmatrix} 0 \\ \omega_{11}\alpha_{\zeta r} + \omega_{21}\alpha_{\zeta\theta} + \omega_{31}\alpha_{\zeta z} \\ \omega_{12}\alpha_{\zeta r} + \omega_{22}\alpha_{\zeta\theta} + \omega_{32}\alpha_{\zeta z} \\ \omega_{13}\alpha_{\zeta r} + \omega_{23}\alpha_{\zeta\theta} + \omega_{33}\alpha_{\zeta z} \end{bmatrix} .
$$

where $\omega_{ij} = AB$, and the B matrix is given by:

$$
B_{ij} = \begin{bmatrix} \frac{\partial v_r}{\partial \xi} & \frac{\partial v_r}{\partial \eta} & \frac{\partial v_r}{\partial \zeta} \\ \frac{\partial v_\theta}{\partial \xi} & \frac{\partial v_\theta}{\partial \eta} & \frac{\partial v_\theta}{\partial \zeta} \\ \frac{\partial v_z}{\partial \xi} & \frac{\partial v_z}{\partial \eta} & \frac{\partial v_z}{\partial \zeta} \end{bmatrix} .
$$

Finally, the right-hand-side consisting of the fictitious forces resulting from rotation around the z-axis and the extra terms resulting form the use of the polar reference frame is given by:

$$
RHS = \begin{bmatrix} 0 \\ \frac{\rho J \hat{v}_\theta^2}{r} + \frac{J}{r^2}(2\mu v_r + 3\mu \frac{\partial v_\theta}{\partial \theta} + v_\theta \frac{\partial \mu}{\partial \theta}) \\ -\frac{\rho J v_r \hat{v}_\theta}{r} - \frac{J}{r^2}(-\mu v_\theta + 3\mu \frac{\partial v_r}{\partial \theta} - v_\theta r \frac{\partial \mu}{\partial r} + 2v_r \frac{\partial \mu}{\partial \theta}) \\ 0 \end{bmatrix} .
$$

The convective fluxes are given by the following expressions:

$$
\begin{aligned}
C_1 &= \rho(v_r\alpha_{\xi r} + v_\theta\alpha_{\xi\theta} + v_z\alpha_{\xi z}) , \\
C_2 &= \rho(v_r\alpha_{\eta r} + v_\theta\alpha_{\eta\theta} + v_z\alpha_{\eta z}) , \\
C_3 &= \rho(v_r\alpha_{\zeta r} + v_\theta\alpha_{\zeta\theta} + v_z\alpha_{\zeta z}) .
\end{aligned}
$$

Red-black Gauss-Seidel point relaxation is employed for the momentum equations. Within the relaxation, coupling between the three equations arises only from the centrifugal and Coriolis terms. The solution of the Poisson system arising from the pressure correction equation is accelerated using a multi-grid method.

In the present work the turbulence in the boundary layer is modelled by the $k-\omega$ SST eddy viscosity model by Menter [8]. The details of the model will not be given here, we will only state that the model is chosen because of the very promising results for 2D separated flows, Wilcox [9], Menter [10]. The equations for the turbulence model are solved after the momentum and pressure correction equations in every sub-iteration. No corrections for rotation are included in the present implementation of the $k-\omega$ model. In the present computations the flow is considered to be fully turbulent, and the laminar/turbulent transition process is not considered.

Computational Mesh

Using the 180 degree symmetry of the problem, the grid is only generated around a single blade. As seen from Figure 1, the outer boundary of the computational domain is spherical and is located approximately 5 rotor diameters away from centre of rotation in all directions.

The mesh consists of three main components, see Figure 2: First an inner 5-block O-O-topology is used locally around the blade (the pink section), secondly a 3-block outer section is wrapped around the inner O-O-section (the green section). Both these two block configuration covers only 120 degrees in the azimuth direction. Finally a 4-block configuration is used to cover the remaining 60 degrees of the computational domain, this section is simply generated by rotating the 'periodic plane' of the 120 degree section (the red section) . In total the mesh consists of 12 blocks of 64^3 or a total of 3.1×10^6 cells.

The size of the inner O-O section is shown in Figure 2, the up and downstream faces are place approximately 1 meter away from the rotor plane.It has 64 cells in the direction normal to the surface, 256 cells in the chordwise direction, and 64 cells in the spanwise direction. To facilitate the resolution of the tip of the blade a 64x64 block is placed a the tip. The total number of cells for the 5 block inner O-O-section is 1.3×10^6 cells. In order to resolve the boundary layer the y^+ values at the wall is kept below 2 everywhere on the blade surface.

3

Boundary Conditions

In the computations fully developed conditions are applied at the downstream end of the spherical domain where the flow leaves the domain. A t the inner cylindrical face near the rotational axis, Euler conditions are applied, while no-slip conditions are applied at the surface of the rotor blade. F ully implicit periodic conditions are applied at the 180 degrees cyclic boundaries. A t the upstream part of the spherical domain, the undisturbed wind speed is specified.

In the present computations a very large computational domain is used, and no attempt was made to include the effects of the tunnel walls. With the present computational domain, placing the farfield boundary approximately 5 rotor diameters aw ay from the rotor blades, no correction for the presence of the rotor is necessary

Results

F or all computations presented in the following the Risø IBM SP-2 parallel computer was used, it is equipped with eleven 300 MHz Pow er-3 SC Thin Nodes, with each 2 CPU's. The memory usages is approximately 1 Gb per 1 million points or a total of 3 Gb for the present mesh.

The steady state computations are continued for approximately 4500 iterations, and take appro ximately 30 hours per case on a 4 processor IBM SP-2. Looking at the pow er production as function of iteration number, it can be seen that after approximately 1500 iterations the solution becomes periodic. The unsteady computation uses the steady state flowfield as starting condition and carries out 830 timesteps per revolution for 3.4 revolutions, which takes appro ximately 40.8 Cpu hours, using 4 processors on the IBM SP-2.In the present computations 3 subiterations are used per timestep.

F rom the Navier-Stok es computation the time averaged pressure at the surface of the blades is readily available, and in Figure 3 to 8 the pressure distributions at five span wise locations along the blade are shown for the six computations.

Finally, the limiting streamlines are shown on the suction sides of the blades in Figure 9 to 14. These are obtained by releasing particles close to the surface of the blade, and moving them according to the local skin friction. It is observ ed that separated areas exists at all windspeeds. A peculiar behaviour for the 10 m/s wind speed case is observ ed near $r/R=0.30$, where the separation line suddenly moves tow ard the leading edge. F or the 20 and 25 m/s cases, the blade is totally stalled.

References

[1] J.A. Michelsen. Basis3D - a Platform for Development of Multiblock PDE Solvers. Technical Report AFM 92-05, Technical University of Denmark, 1992.

[2] Michelsen J.A. Bloc k structured Multigrid solution of 2D and 3D elliptic PDE's. T echnical Report AFM 94-06, Technical University of Denmark, 1994.

[3] N. N Sørensen. General Purpose Flow Solver Applied to Flow ov er Hills. Risø-R- 827-(EN), Risø National Laboratory, Roskilde, Denmark, June 1995.

[4] Rhie C. M. *A numerical study of the flow past an isolate d airfoil with separation.* PhD thesis, Univ. of Illinois, Urbane-Champaign, 1981.

[5] P atank ar S. V. and Spalding D. B.A Calculation Prodedure for Heat, Mass and Momentum Transfer in Three-Dimensional Parabolic Flows. *Int. J. Heat Mass Transfer*, 15:1787, 1972.

[6] J.A. Michelsen. General curvilinear transformation of the Navier-Stok es equations in a 3D polar rotating frame. T echnical Report ET-AFM 98-01, Technical University of Denmark, 1998.

[7] Khosla P. K. and Rubin S. G. A diagonally dominant second-order accurate implicit scheme. *Computers Fluids*, 2:207–209, 1974.

[8] Menter F. R. Zonal Two Equation k-ω T urbulence Models for Aerodynamic Flows. AIAA-paper-932906, 1993.

[9] Wilcox D. C. A Half Century Historical Review of the K-ω Model. AIAA-91-0615, 1991.

[10] Menter F. R. P erformance of P opular T urbulence Models for Attached and Separated Adverse Pressure Gradient Flows. *AIAA Journal*, 30(8):2066–2072, August 1992.
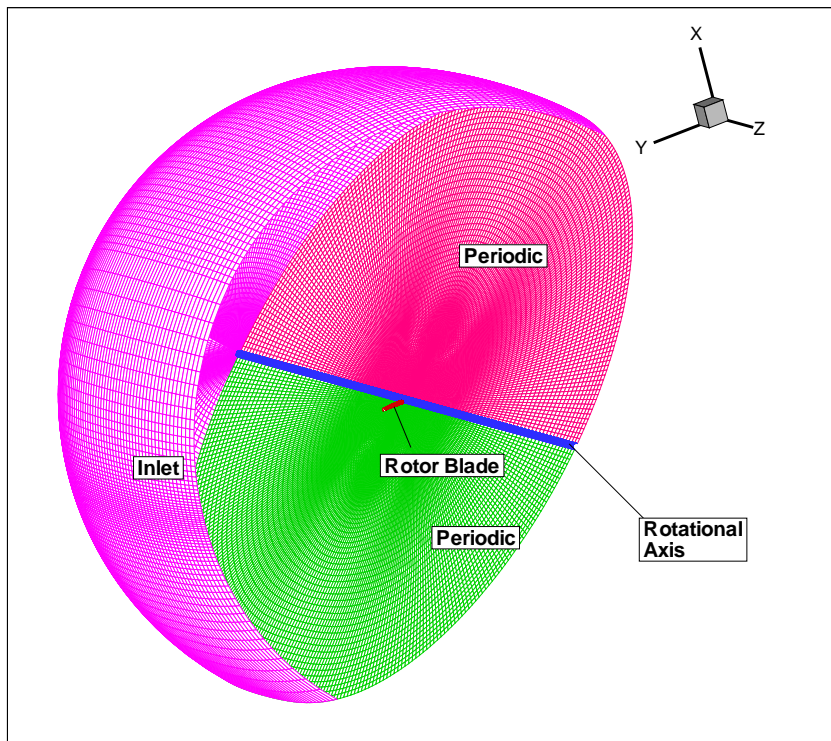
Figure 1: Computational mesh used in the computations. The inlet part of the spherical outer part of the mesh is shown (pink), the tw o 180 degrees periodic planes (green and red), the rotational axis (blue), and the rotor blade.
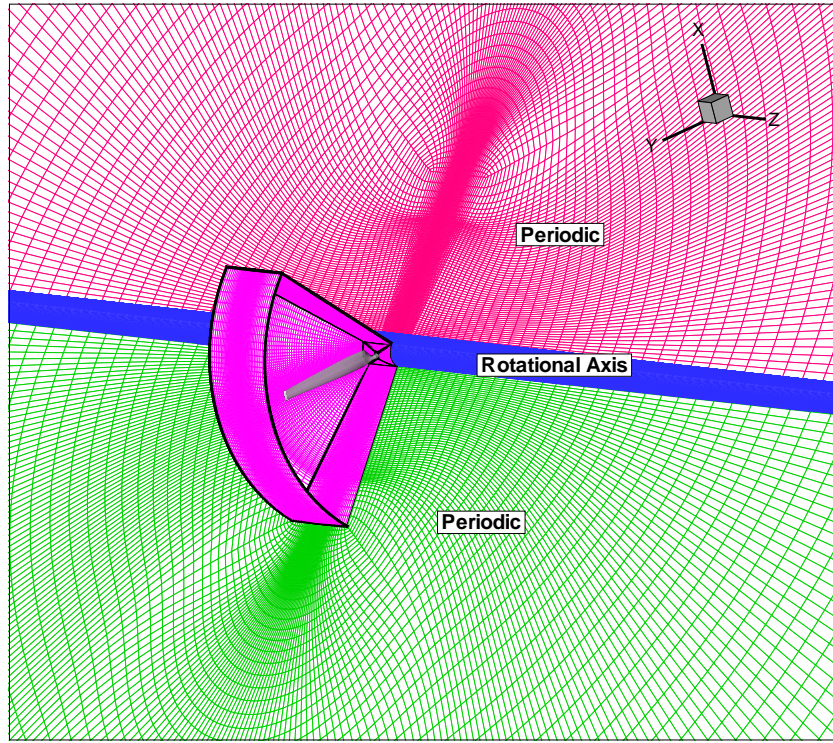
Figure 2: Detail of the computational mesh near the rotor. The five block O-O-mesh around the rotor is sho wn with pink color, the three block wrapping around the O-O-section is shown with green, and finally the 4 block extension is shown with red.
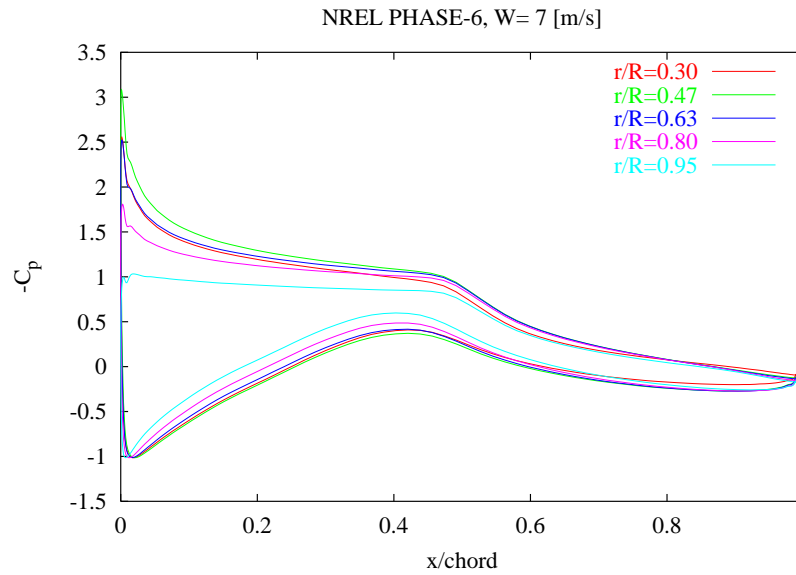
Figure 3: Predicted pressure distributions for the 7 m/s upwind case
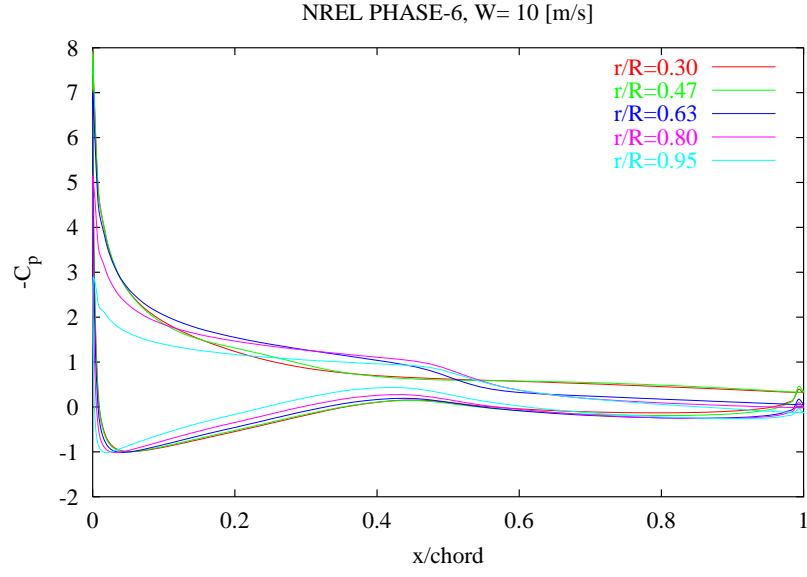
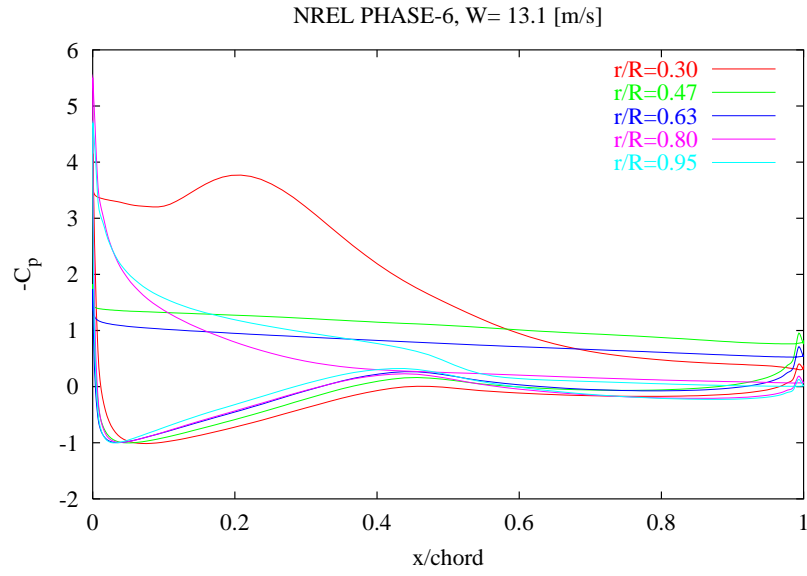Figure 4: Predicted pressure distributions for the 10 m/s upwind case

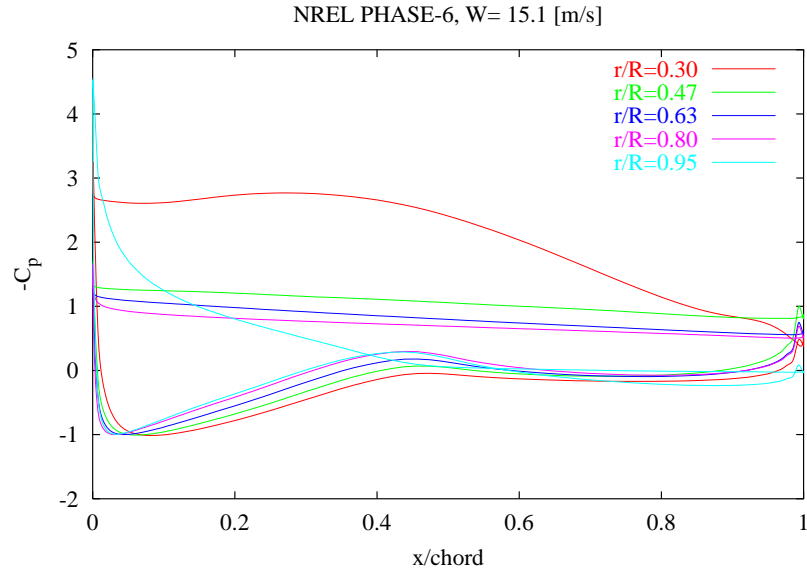Figure 5: Predicted pressure distributions for the 13.1 m/s upwind case

Figure 6: Predicted pressure distributions for the 15.1 m/s upwind case
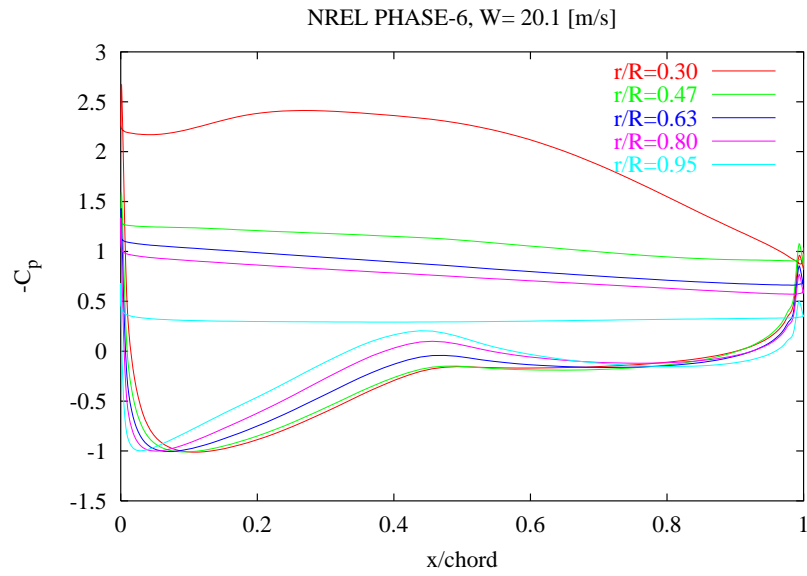

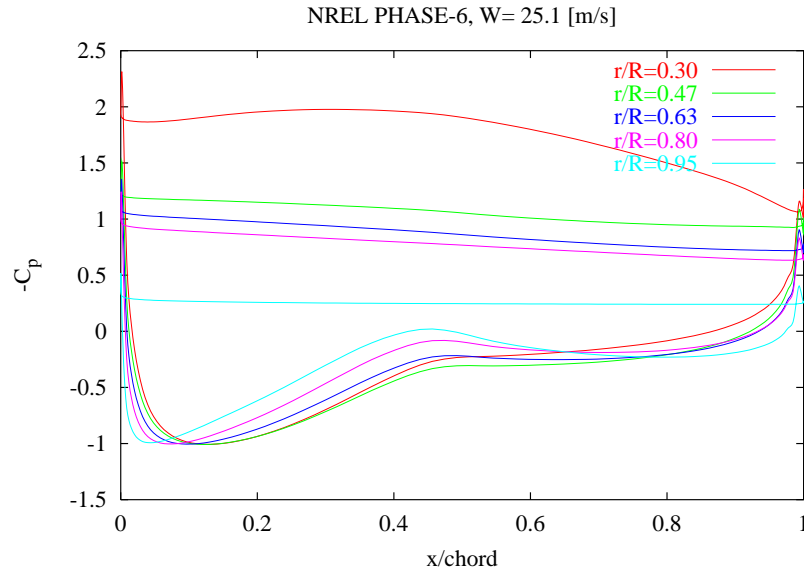Figure 7: Predicted pressure distributions for the 20.1 m/s upwind case

Figure 8: Predicted pressure distributions for the 25.1 m/s upwind case

Figure 9: Limiting stream lines on the blade for the unsteady computation of the 7 m/s case.

**NREL PHASE-6, W= 10 [m/s], Limiting Streamlines
RISOE, EllipSys3D Computation**

Figure 10: Limiting stream lines on the blade for the unsteady computation of the 10 m/s case.

**NREL PHASE-6, W= 13.1 [m/s], Limiting Streamlines
RISOE, EllipSys3D Computation**

Figure 11: Limiting stream lines on the blade for the unsteady computation of the 13.1 m/s case.

**NREL PHASE-6, W= 15.1 [m/s], Limiting Streamlines
RISOE, EllipSys3D Computation**

Figure 12: Limiting stream lines on the blade for the unsteady computation of the 15.1 m/s case.

**NREL PHASE-6, W= 20.1 [m/s], Limiting Streamlines
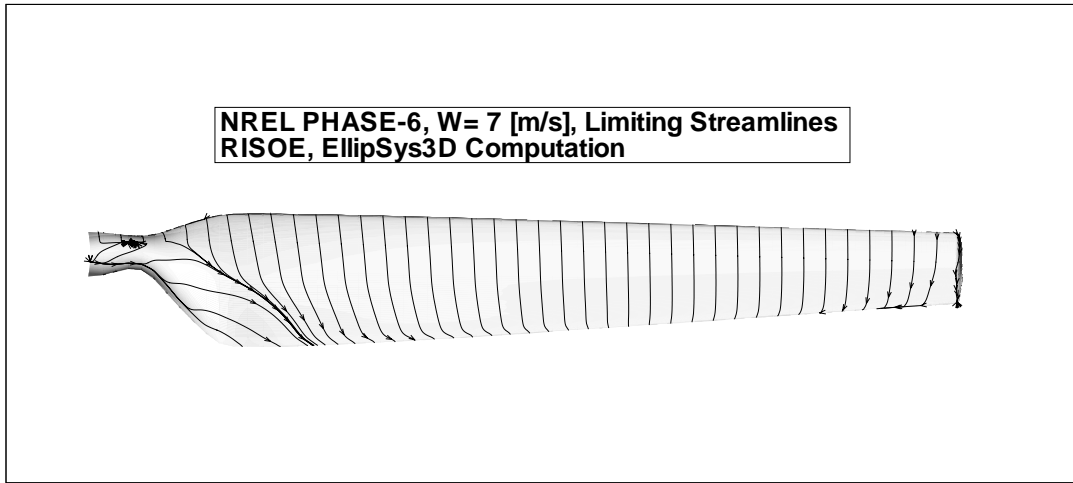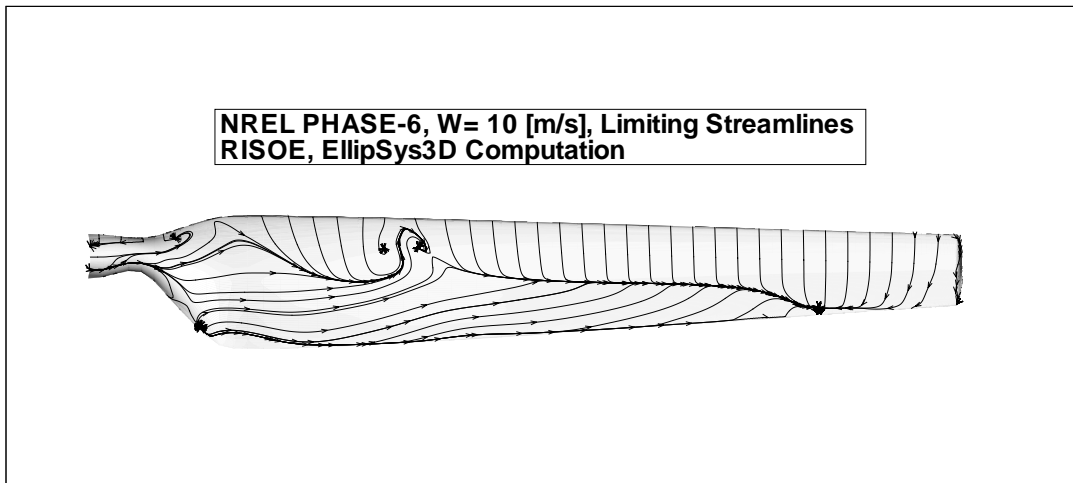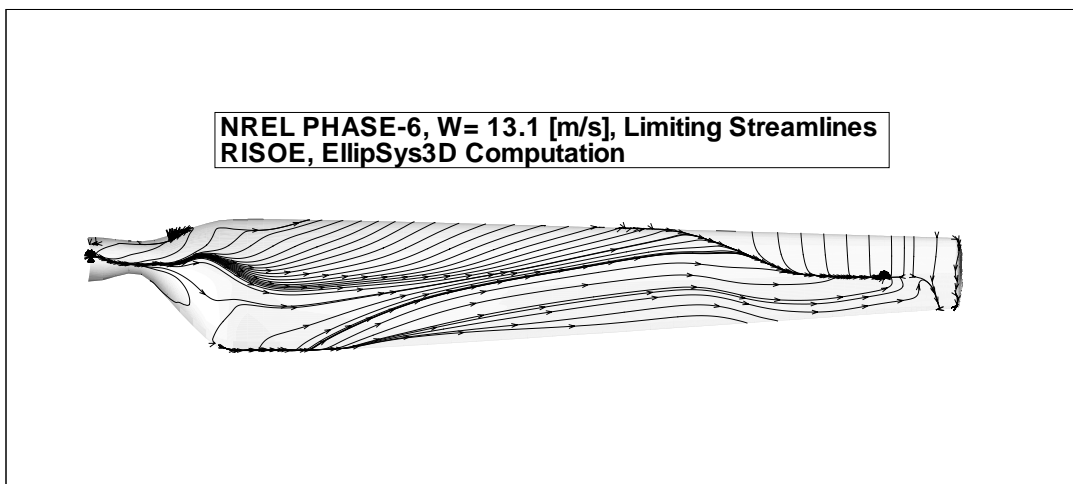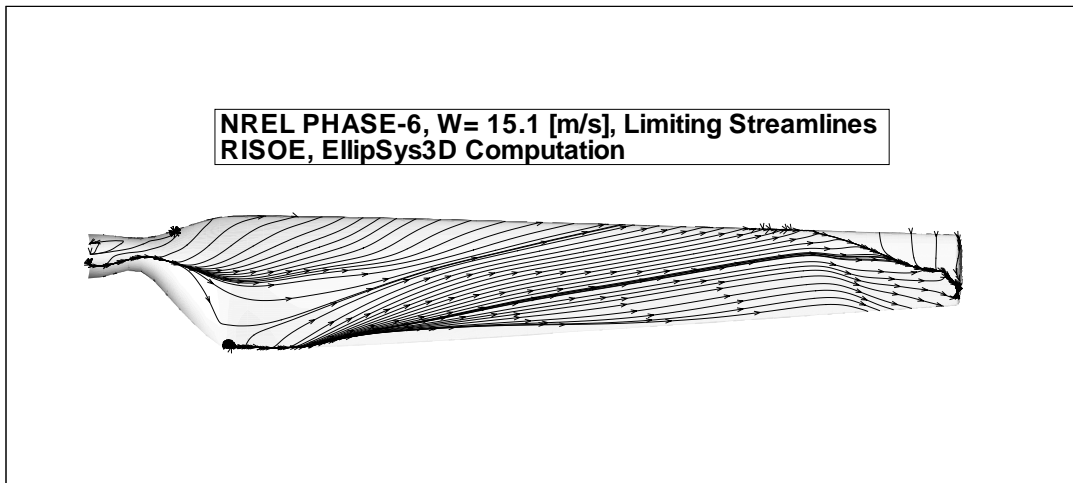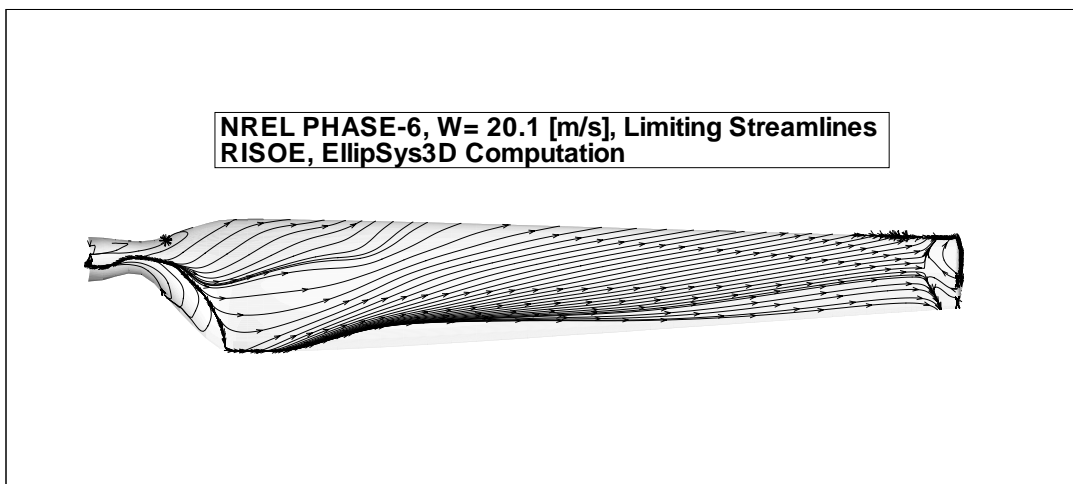RISOE, EllipSys3D Computation**

Figure 13: Limiting stream lines on the blade for the unsteady computation of the 20.1 m/s case.

Figure 14: Limiting stream lines on the blade for the unsteady computation of the 25.1 m/s case.
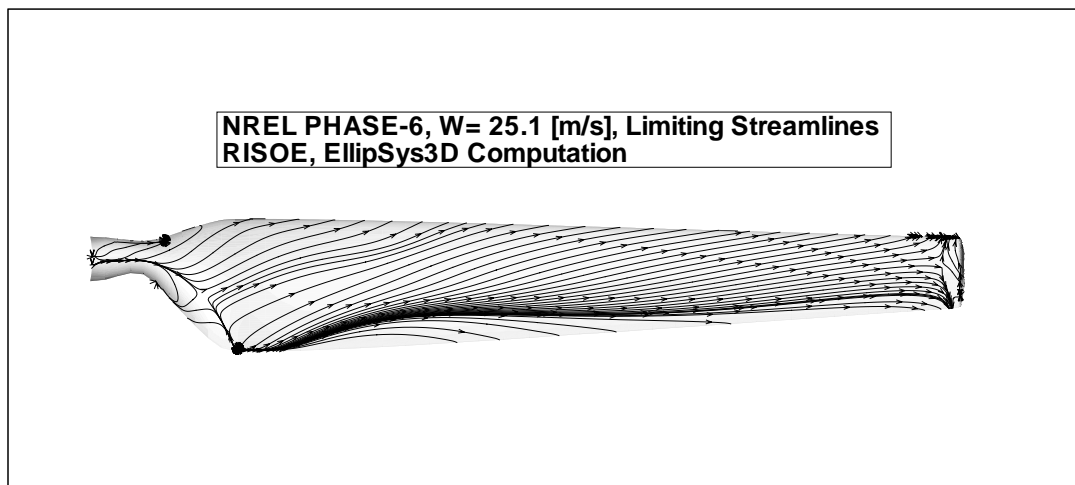
Code describtion and airfoil data used
for the NREL 10m Wind Turbine

Ph.D. Student Robert Mikkelsen
Technical University of Denmark, DTU
Department of Energy Engineering, Fluid Mechanics   Email: rm@et.dtu.dk
Nils Koppels Allé, Building 403   Phone: +45 4525 4156
DK-2800 Lyngby, Denmark   Fax :   +45 4593 0663

Code description

A computational model that combines the actuator disc principle with the axi-symmetric, incompressible Navier-Stokes equation were used. The model is describted in detail in Sørensen et al. [1,2], and is a vorticity-swirl velocity-stream function formulation of the Navier-Stokes equation where the forces is applied from airfoil characteristics using a Blade Element approach. Tip-correction is compensated for by using the Prandtl formula.

Computational domain and boundary conditions

The computational domain was chosen to be 30R long with the disc placed 10R downstream of the inlet. The lateral boundary was set to 3R as a slip wall with no mass-flux across, uniform flow at the inlet and a Neumann condition at the outlet. The grid contained 100 cells in axial direction, streached towards the disc and in the radial direction a 120 linearly distributed cells were used, where the rotor is resolved by 40 cells.

Wind turbine geometry

The geometry data listed in table 1 were used to sub divide the rotor into 40 linearly distributed elements.

Table 1

r (m)	twist(g)	chord(m)
0.0000	0.0000	0.2180
0.5080	0.0000	0.2180
0.6600	0.0000	0.2180
0.8830	0.0000	0.1830
1.0080	6.7000	0.3490
1.0670	9.9000	0.4410
1.1330	13.4000	0.5440
1.2570	20.0400	0.7370

```
1.3430  18.0740   0.7280
1.5100  14.2920   0.7110
1.6480  11.9090   0.6970
1.9520   7.9790   0.6660
2.2570   5.3080   0.6360
2.3430   4.7150   0.6270
2.5620   3.4250   0.6050
2.8670   2.0830   0.5740
3.1720   1.1500   0.5430
3.1850   1.1150   0.5420
3.4760   0.4940   0.5120
3.7810  -0.0150   0.4820
4.0230  -0.3810   0.4570
4.0860  -0.4750   0.4510
4.3910  -0.9200   0.4200
4.6960  -1.3520   0.3890
4.7800  -1.4690   0.3810
5.0000  -1.7750   0.3580
```

A global pitch of 4.775^o is specified whereby the angle between the rotor plane and tip chord is 3°.

Airfoil data

The data that was used were provide at http://wind2.nrel.gov/amestest/. The 2D data was extracted from measurement made at Delft University of Technology low speed laboratory low turbulence wind tunnel with a Reynolds No. of 1.000.000. A peak in the data at angle 11.21^o was removed and the data was extended from 20.16^o to 90° assuming a flat C_L up to 40° and thereafter decreasing to $C_L=0$ at 90°. C_D was extrapolated to 1.3 at 90°. As the loading in the aerodynamic model is based on forces form airfoil data, the result strongly depends on this. The data used are shown in table 2.

Table 2

Angle^o	C_L	C_D
-1.0400	0.0190	0.0095
-0.0100	0.1390	0.0094
1.0200	0.2580	0.0096
2.0500	0.3780	0.0099
3.0700	0.4970	0.0100
4.1000	0.6170	0.0100
5.1300	0.7360	0.0097
6.1600	0.8510	0.0095
7.1800	0.9130	0.0127
8.2000	0.9520	0.0169
9.2100	0.9730	0.0247

```
10.2000   0.9520   0.0375
12.2300   1.0070   0.0636
13.2200   1.0310   0.0703
14.2300   1.0550   0.0828
15.2300   1.0620   0.1081
16.2200   1.0430   0.1425
17.2100   0.9690   0.1853
18.1900   0.9380   0.2280
20.1600   0.9230   0.2840
25.0000   0.9230   0.4200
30.0000   0.9220   0.5500
40.0000   0.9110   0.7500
50.0000   0.8000   0.9000
70.0000   0.5000   1.1500
90.0000   0.0000   1.3000
```

Results

Only stationary computations of the cases

s0700000
s1000000
s1300000
s1500000
s2000000
s2500000

are performed. The results are put into the EXCEL file.

References

[1] J. N. Sørensen, C. W. Kock, "A Model for the Unsteady Rotor Aerodynamics", J. Wind Eng. Ind. Aerodyn., **58**, 259-275,1995

[2] R. Mikkelsen, J. N. Sørensen and W. Z. Shen, "Modelling and Analysis of the Flow Field Around Coned Rotors", proc. 13th IEA symp. 1999.

Description of the Hybrid Code and Post-processing Methods used for the NREL 10-m Wind Turbine

Guanpeng Xu, Ph.D. Candidate
Lakshmi N. Sankar, Regents Professor, Principal Investigator (PI)
School of Aerospace Engineering
Georgia Institute of Technology
Atlanta, GA 30332

Code Description

The blind comparison cases were simulated using the Georgia Tech Hybrid code developed for the use of horizontal axis wind turbines (HAWT). The present authors developed this hybrid code under the National Renewable Energy Laboratory (NREL) Contract No. XCX-7-16466-02.
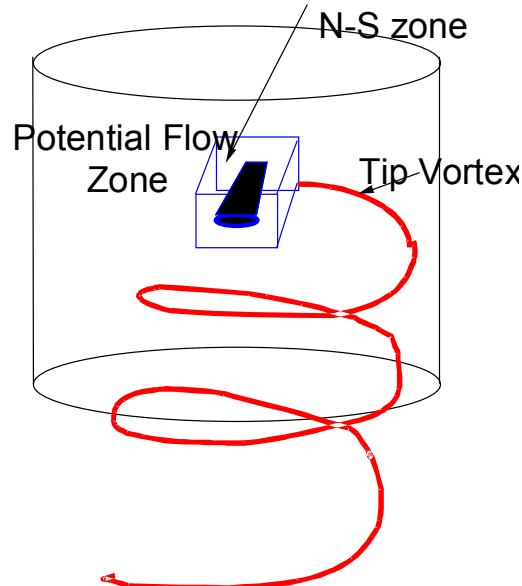

Figure 1 The Hybrid Methodology

The Hybrid code combines Navier-Stokes/potential flow methodology for modeling three-dimensional unsteady viscous flow over (HAWT) configurations. In this approach, the costly viscous flow equations are solved only in a small viscous flow region surrounding the blade. The rest of the flow field is modeled using a potential flow methodology. The tip vortices are modeled using a free wake approach, which allows the vortices to deform and interact with each other. The effects of turbulence models and transition models, the wake geometry, and numerical procedures for non-axial (yaw) conditions had also been studied. A full featured hybrid code, which can use either the Boldwin-Lomax turbulence model or the Sparlart-Allmaras model, can use either the Eppler transition prediction model or the Michel transition model, and can simulate either axial or yaw conditions, has been developed.

The details of the hybrid methodology and related research activities have been documented in Reference 1, and 2, and the progress reports submitted to NREL. These may be found at www.ae.gatech.edu/~lsankar/NREL.

Input Data

Since the hybrid code is based on the first principles, the Navier-Stokes/full-potential equations are solved in a domain enclosing the HAWT rotor. Only the far field boundary, and the rotor/blade geometry need to be input. The rotor/blade geometry was used to generate a body-fitted H-O grid in the computation domain. The far field boundary conditions, specifically the rotor rpm, wind speed, temperature, air density, were specified in an input file in a non-dimensional manner.

The new rotor in the blind comparison has two tapered, twisted blades. The rotor radius is 5.03 meter with the S809 airfoil over most of the blade radius. The blades are rotating at 72 RPM. The blade tip pitch angle is 3°. The linearly tapered blade has 30° nonlinear twist. Figure 2 shows the twist distribution of the tapered blade.
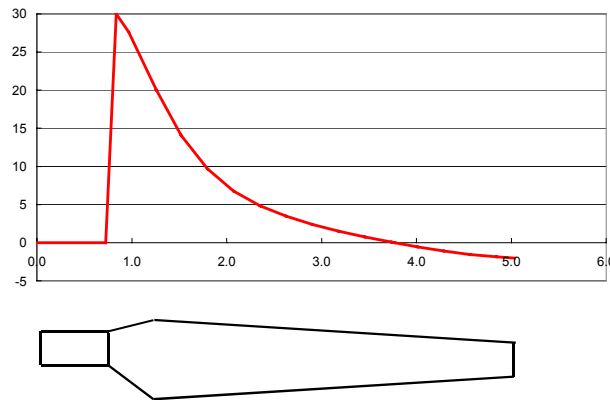
Fig. 2 Twist Distribution of the Tapered/Twisted Blade

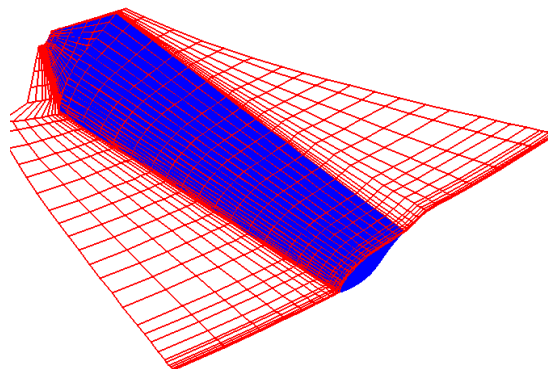A H-O grid was generated for the simulation of the NREL new 10-m rotor. Figure 3 shows the grid on the overall blade.

Figure 3 H-O Grid on Tapered and Twisted Blade

Measured air properties and rotor rpm were used.

Post-Processing

The complete flow field properties over the computation domain were obtained from the CFD analysis. The data submitted in required form were extracted by following method:

Air speeds at radius location 0.30R, 0.47R, 0.63R, 0.8R and 0.95R, at a point 0.80 local chord ahead of the blade leading edge and 0.03 meter below the chord line were extracted for computing the dynamic pressure and the aerodynamics coefficients at the span-wise location. The interested point for air speed and inflow angle measurement at a typical radial location is shown below as figure 4.
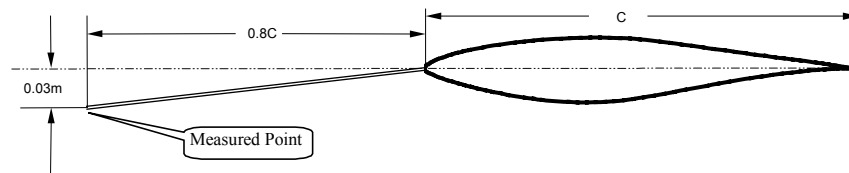
Fig. 4 Measured Point at a Typical Span-wise Location

The air-speed was taken as is at the specific point in the converged flow field. No further correction was applied. The aerodynamics coefficients and load were computed based on the equations provided by NREL in the Blind Comparison Overview.

Comments

Since the hybrid code solves the computational domain using the first principles, the results contain the complete fluid field properties in the domain. In addition to obtaining a handful of numbers as in the spreadsheet submitted, we may visualize the 3-D flow field, generate pressure map of interest, study separation and transition, and draw both quantitative and qualitative conclusions after seeing the flow pattern.

References:

1. Guanpeng Xu and Lakshmi N. Sankar, 'Computational Study of Horizontal Axis Wind Turbines,' Journal of Solar Energy Engineering, Feb. 2000. (Also presented on the 37th AIAA/ASME as AIAA 99-0042)

2. Guanpeng Xu and Lakshmi N. Sankar, 'Effects of Transition and Free-stream Unsteadiness on the Performance of Horizontal Axis Wind Turbines,' AIAA 2000-0048.

NREL/NWTC Aerodynamics Code Blind Comparison

CRES/NTUA GENUVP model

Description of the flow model:
(See cres-ntua-genuvp.ps)
GEUVP is a free-wake model based on a vortex blob approximation of the wake. The presence of the solid bodies is introduced by means of classical panel methods. As regards, loads, they are either calculated as in blade element models using 2D airfoil data or by means of coupled boundary layer approximations in a section-by-section procedure.

Domain discretisation: Surface paneling of each component separately.

Model inputs: Blade geometry, inflow and operational conditions, structural and control data (e.g. pitch regulation, free yaw etc.)

Solution algorithm and physics: Unsteady, free-wake modeling based on vortex blob approximations. The solution is obtained from a 2nd order time marching scheme (Adams-Bashford). Aerostructural coupling is based on multi-body dynamics and finite – element approximations of each structural component separately. It includes the blades, the drive train and the tower as beam structures subjected to bending, torsion and extension. Controls of the pitch, yaw, teeter rpm can be included.

Model assumptions: Viscous-inviscid interaction.

Performance attitudes: On a SGI Origin 200, one time step would require 2min (11 spanwise strips). The memory usage is dependent on the total number of time steps. A full 10min aeroelastic calculation would last 4 days and would require no more than 100Mb.

GENUVP: A Vortex Particle Free Wake Aerodynamic Model and its application to the Performance Analysis of Horizontal Axis Wind Turbines

Spyros G. Voutsinas

National Technical University of Athens

September 2000

Contents

1   Introduction

The response of an HAWT to dynamic inflo w conditions is a special case of the aerodynamic performance problem of rotors. In terms of its basic ph ysical features, the corresponding flow is an example of a three-dimensional and non-linear vortex or rotational flow [1÷4]. Assuming the fluid incompressible and inviscid, the spatially distributed vorticity will correspond to the wakes generated by the flow around the blades. For a theoretical analysis of the dynamic inflow effects, vortex methods are among the most cost effective numerical models [5÷19]. Within this con text, a computational en vironment has been developed by the name GENUVP (GENeral Unsteady Vortex Particle method). GENUVP is an unsteady code based on the vortex particle approximation of the free vorticity. In brief the modelling is defined along the following guidelines:

> According to Helmholtz's decomposition theorem [20] the v elocity field is made up of an irrotational part representing the disturbance due to the presence of the solid boundaries and a rotational part representing the disturbance due to the wakes. In order to determine the irrotational part a Neumann boundary value problem for the Laplace equation is solved. On the other hand the rotational part of the velocity field is determined directly as con volution of the vorticity contained in the wakes. As the fluid is assumed in viscid, there is no link between the irrotational and the rotational part of the velocity field. In order to bring these parts into contact, a link can be defined that models the vorticity emission process observ ed in real flows. Mathematically this link is based on the Kutta condition (more exactly on an appropriate formulation of Kelvin's theorem). The fulfilment of the Kutta condition, permits to define quan titavely the conversion of the bound-vorticity into free-vorticity. This mec hanism constitutes the in viscid analog of the vorticity produ ction process already existing in all the conventional aerodynamic models.

Vortex models as described in the sequel, are basically in viscid and therefore a good part of the underlying physics regarding the aerodynamic beha vior of HAWT is suppressed. Probably the most importan t issue, is the calculation of loads in case of stall. In this connection, it is possible to impro ve the performance of vortex models based on the double wake concept [21]. It consists of letting vorticity to be released not only from the trailing edge but also from the separation line along the blades. In the model proposed in [21], the extra vorticity released at separation is determined by means of a semi-empirical stall model (namely the extended ONERA model). A further impro vement could be seeked b y introducing boundary layer corrections. This was done for the case of a 2D airfoil, using a strong viscous-inviscid interaction model whic h follows the guidelines first proposed by Drela and included in the well known XFOIL code [22]. Such a calculation has been included in GENUVP in a section-by-section procedure. A fully 3D boundary layer model is still to be constructed. A ttempts in this direction ha ve been done at MIT [23÷25] giving promising results.

   The ultimate step to wards a detailed aerodynamic analysis of HAWTs is definitely the use of viscous models. During the last few y ears, groups in Europe and USA have started producing interesting results based on Navier-Stokes solvers [26]. The indeed high computational cost of suc h models, prohibits for the time being, the use of CFD in practice. So until computers become fast enough so that a viscous calculation becomes cost effective, vortex methods could be used as an intermediate approach between engineering and viscous ones.

2   Form ulation of the problem

W e consider the unsteady flow of an inviscid and incompressible fluid around a com bination of N three-dimensional bodies B_k with boundaries S_k, $k = 1(1)N$ that form the configuration of a wind turbine. Each component of the configuration can be regarded as either a non-lifting body or as a lifting one according to its operational characteristics. Non-lifting bodies are the nacelle and the tower of the turbine whereas the blades are lifting bodies in the sense that they generate wakes. This holds for an upwind rotor. For a downwind rotor, the wake of the tower is to included, since it will affect the flow over the blade during its passage by the tower. According to the geometrical assumptions made, the blades can be modeled either as lifting surfaces (thin wing assumption) or as thic k wings. In order to keep the level of the computational requiremen ts reasonable, thickness effects for the blades could be neglected.

Let $D \subset R^3$ denote the flow field, S its boundary and $\vec{\nu}$ the outward unit normal to S (Figure 1). Moreover let $\vec{u}(\vec{x};t)$ $\vec{x} \in D$, $t \geq 0$ denote the velocity field. According to Helmholtz's decomposition theorem [20], $\vec{u}(\vec{x};t)$ takes the form:

$$\vec{u}(\vec{x};t) = \vec{U}_*(\vec{x};t) + \nabla\phi(\vec{x};t),\, \vec{x} \in D,\, t \geq 0 \tag{1}$$

where $\vec{U}_*(\cdot;t)$ is a given div-free velocity field and $\phi(\cdot;t)$ the disturbance velocity potential. The term $\vec{U}_*(\cdot;t)$ is set to include the inflow velocity $\vec{U}_\infty(\cdot;t)$ as well as the velocity induced by the free vorticity. Therefore $\vec{U}_*(\cdot;t)$ represents the rotational part of the flow. As regards the scalar potential $\phi(\cdot;t)$, it is defined so as to give the absolute perturbation velocity when differentiated with respect to a fixed co-ordinate system.

For an incompressible fluid, the velocity potential will be the solution of a boundary value problem for the Laplace equation. However the presence of lifting bodies imposes the introduction of the wakes they generate as active boundaries of the flow. Let S_{W_k}, $k = 1(1)N_B$ denote the vortex sheets shed by the N_B lifting bodies, and $\vec{\nu}_{W_k}$ their outward unit normals respectively (In the sequel the subscript "W" will be used to denote quantities corresponding to the wakes of the flow). Clearly

$$\partial D \equiv S = S_T + \bigcup_{k=1}^{N_B} S_k + \bigcup_{k=1}^{N_B} S_{W_k} \tag{2}$$

Within the framew ork of the potential flow theory the velocity potential can be represented by means of surface singularity distributions [18]. For non-lifting bodies, source distributions $\sigma(\cdot;t)$ are used, whereas for lifting bodies the source distribution is supplumented with a dipole distribution $\mu(\cdot;t)$ which is also extended over the wake of the body.

In this connection it is reminded that a dipole distribution $\mu(\vec{x}); \vec{x} \in \Sigma$ defined on a surface Σ , introduces a discontinuity of the scalar potential (Figure 2):

$$\mu(\vec{x}) = -[\phi](\vec{x}),\, \vec{x} \in \Sigma \tag{3}$$

whereas the potential itself is given by:

$$\phi_\mu(\vec{x}_0) = -\int_\Sigma \frac{\vec{\nu}(\vec{x}) \cdot (\vec{x}_0 - \vec{x})}{4\pi|\vec{x}_0 - \vec{x}|^3} d\Sigma(\vec{x}) \tag{4}$$

From equation (4) the corresponding velocity field $\vec{u}_\mu(\cdot)$ is obtained by differentiation. Using Stokes theorem, $\vec{u}_\mu(\cdot)$ takes the form [18]:

$$\vec{u}_\mu(\vec{x}_0) = \nabla_o\phi_\mu(\vec{x}_0) \quad = \quad \int_\Sigma \frac{\nabla_\Sigma\mu(\vec{x}) \wedge \vec{\nu}(\vec{x})}{4\pi|\vec{x}_0 - \vec{x}|^3} \wedge (\vec{x}_0 - \vec{x})d\Sigma(\vec{x}) \; +$$
$$\oint_{\partial\Sigma} \mu(\vec{x})\frac{d\vec{l}(\vec{x}) \wedge (\vec{x}_0 - \vec{x})}{4\pi|\vec{x}_0 - \vec{x}|^3} \tag{5}$$

where $\nabla_0(\cdot)$ denotes differentiation with respect to $\vec{x}_0$. It is known that as $\vec{x}_0$ approaches Σ the velocity becomes discontinuous. In particular if $[\vec{u}_\mu]$ denotes the velocity discontinuity defined on Σ,

$$[\vec{u}_\mu](\vec{x}) \cdot \vec{\nu}(\vec{x}) \quad = \quad 0,\, \vec{x} \in \Sigma$$
$$\vec{\nu}(\vec{x}) \wedge [\vec{u}_\mu](\vec{x}) \quad = \quad \nabla_\Sigma\mu(\vec{x}) \wedge \vec{\nu}(\vec{x}) = \vec{\gamma}(\vec{x}),\, \vec{x} \in \Sigma \tag{6}$$

where $\vec{\gamma}(\vec{x})$ denotes the intensity of the surface vorticity and $\nabla_\Sigma(\cdot)$ the superficial differential operator. From (5) and (6) we deduce that a surface on which a dipole distribution is defined, corresponds to a vortex sheet, i.e. a surface with tangential velocity discontinuity.

Following the notations defined above, by means of Green's theorem the following representation theorem for the velocity potential $\phi(\vec{x}_o; t)$, $\vec{x}_o \in D$, $t \geq 0$ is obtained:

$$\phi_\mu(\vec{x}_0; t) = \int_{S_T} \sigma_T(\vec{x}; t) \cdot \frac{1}{4\pi|\vec{x}_0 - \vec{x}|} dS(\vec{x}) \qquad (I)$$

$$+ \sum_{k=1}^{N_B} \int_{S_k} \sigma_k(\vec{x}; t) \cdot \frac{1}{4\pi|\vec{x}_0 - \vec{x}|} dS(\vec{x}) \qquad (I)$$

$$- \sum_{k=1}^{N_B} \int_{S_k} \mu_k(\vec{x}; t) \cdot \frac{\vec{\nu}(\vec{x}) \cdot (\vec{x}_0 - \vec{x})}{4\pi|\vec{x}_0 - \vec{x}|^3} dS(\vec{x}) \qquad (II)$$

$$- \sum_{k=1}^{N_B} \int_{S_{W_k}} \mu_{W_k}(\vec{x}; t) \cdot \frac{\vec{\nu}_{W_k}(\vec{x}; t) \cdot (\vec{x}_0 - \vec{x})}{4\pi|\vec{x}_0 - \vec{x}|^3} dS_W(\vec{x}) \qquad (III) \qquad (7)$$

where,

- $\sigma_T(\cdot; t), \sigma_k(\cdot; t)$ denote the source distributions of the tower and the k-th blade respectively (term I),

- $\mu_k(\cdot; t)$ denotes the dipole distribution of the k-th blade (term II),

- $\mu_{W_k}(\cdot; t)$ the dipole distributions of the vortex sheet originating from the k-th blade (term III)

Due to the unsteady character of the inflow conditions, the unknown distributions $\sigma_k(\cdot; t)$, $\mu_k(\cdot; t)$ and $\mu_{W_k}(\cdot; t)$ are time dependent. Besides that as the vortex sheets S_{W_k} are freely moving material surfaces, the geometry of the problem is also time varying. Consequently the problem to be solved is a free-boundary evolution problem with unknowns the surface distributions $\sigma_k(\cdot; t)$, $\mu_k(\cdot; t)$ and $\mu_{W_k}(\cdot; t)$ as well as the geometry of the vortex sheets S_{W_k} .

In order to determine the unknown fields of the problem we dispose two types of conditions:

(a) the kinematic ones and more specifically the non-entry conditions on all the solid surfaces, and the conditions of material motion of the vortex sheets

(b) the dynamic conditions, i.e. the requirement of zero pressure jump throughout the vortex sheets.

Let $\vec{U}_B(\cdot; t)$ denote the rigid body velocity distribution defined on the solid boundaries of the configuration. Then the non-entry conditions on all the solid surfaces take the form:

$$\frac{\partial \phi}{\partial \nu}(\vec{x}; t) = \vec{\nu}(\vec{x}; t) \cdot [\vec{U}_B(\vec{x}; t) - \vec{U}_*(\vec{x}; t)], \; \vec{x} \in S_k(t), \; k = 1(1)1 + N_B \qquad (8)$$

The application of the Neumann condition (8) for the the potential $\phi(\cdot; t)$ given by (7), leads to an integral equation which, when applied over S_k, produces the necessary algebraic equations for determining the source distributions. For a given panelling of S_k and a piecewise constant distribution of sources, a discrete system is obtained by imposing (8) to the centers of all panels. Of course this system will also include the dipole distributions which are also unknown. As regards $\mu_k(\cdot; t)$ over the blade surfaces, they are assumed to be piecewise constant over each spanwise strip of the blades. Moreover, for each specific strip, $\mu_k(\cdot; t)$ is assumed to vary linearly with respect to the surface length, modulated by the circulation of the strip considered. Therefore, this specific choice of $\mu_k(\cdot; t)$ leaves as free parameters (and unknowns), the spanwise circulation distribution, i.e. one unknown per strip. In order to determine the circulation distribution, the well known Kutta condition is applied. It consists of imposing zero pressure jump at the trailing edge of the blade.

Finally there is also the contribution of the dipole distribution defined on the wakes of the blades, $\mu_{W_k}(\cdot; t)$. Each of these distributions, is closely related to the circulation distribution of the corresponding lifting body, and so they can be defined only by means of the dynamic conditions of the problem. Let,

$$\vec{x}_W \in S_W : \vec{x}_W = \vec{x}_W(\xi^1, \xi^2; t), \; \xi^1 \in [-1, 1], \; \xi^2 \geq 0, \; t \geq 0 \qquad (9)$$

denote a parametric representation of a vortex sheet S_W shed from a lifting component of the configuration along its trailing and possibly its tip edges, i.e. the vorticity emission line (Figure 4). Clearly S_W can be regarded as a surface generated by the sequence of material lines leaving the emission line. In order to keep track with the history of the vortex shedding, a point $\vec{x}_W(\xi^1, \xi^2; t)$ is identified as the position at time t of a material element that was shed at time ξ^2 and at the point along the emission line defined by ξ^1 . Consequently $\vec{x}_W(\xi^1, t; t)$ represents the current position of the emission line. Moreover the lines $\xi^1 = ct$ are formed by the material elements shed by the same point of the emission line. Having

4

defined the history of the vortex sheets, the zero pressure jump condition can be recast in an explicit form, permitting the determination of the remaining unkno wns$\mu_{W\,k}(\cdot;t)$. In this connection let us first consider the dynamics of a vortex sheet $\Sigma(t)$, i.e. a moving surface carrying a dipole distribution $\mu(\cdot;t)$. Let

$$\vec{x} \in \Sigma(t) \ : \ \vec{x}_\Sigma(\xi;t), \xi = (\xi^1, \xi^2) \in A \subseteq R^2, t \geq 0 \tag{10}$$

denote the Lagrangian representation of $\Sigma(t)$. The evolution of $\Sigma(t)$ is defined by its equation of motion (11a) and the zero pressure jump condition (11b) obtained by applying Bernoulli's equation to the two faces of $\Sigma(t)$:

$$\frac{d\vec{x}_\Sigma(\xi;t)}{dt} = \vec{U}_m(\vec{x}_\Sigma;t)$$

$$\tag{11}$$

$$\frac{\partial [\phi]}{\partial t}(\vec{x}_\Sigma;t) + \vec{U}_m(x_\Sigma;t) \cdot [\vec{u}_\mu](\vec{x}_\Sigma;t) = 0$$

In (11) $\vec{U}_m(\cdot;t)$ and $[\vec{u}_\mu](\cdot;t)$ denote the mean and the jump of the v elocity field, both defined as *surface* fields, i.e. for points of $\Sigma(t)$ only. From (3) and (6b) we have that: for $\xi \in A, t \geq 0$, $\mu(\xi;t) = -[\phi](\xi;t)$ and $[\vec{u}_\mu](\xi;t) = \nabla_\Sigma \mu(\xi)$. Thus if,

$$\frac{d_m}{dt}(\cdot) = \frac{\partial}{\partial t} + (\vec{U}_m \cdot \nabla_\Sigma)(.) \tag{12}$$

is the superficial material time deriv ative, then (11b) yields the following condition:

$$\frac{d_m \mu}{dt}(\cdot) = 0 \tag{13}$$

which states that the dipole distribution of a vortex sheet is conserved materially and thus (13) is equivalent to Kelvin's theorem.

Coming bac k to wind turbine configurations, condition (13) can be used with respect to S_{W_k} in two ways. In accordance to the time history defined by (9),

$$\mu_W(\vec{x}_W(\xi^1, \xi^2;t);t) = \mu_W(\vec{x}_W(\xi^1, `\xi^2;\xi^2);\xi^2) \tag{14}$$

Equation (14) simply states that the in tensity of the dipole distribution carried by the material elemen tξ is equal to the value this element had when it was first shed from the emission line of the body. Therefore, all d.o.f. of μ_{W_k} on S_{W_k} (usually the nodal values over the panelling of S_{W_k}), will be known from previous time steps, except those along the corresponding emission lines, which by continuity are set equal to the values of $\mu(\cdot;t)$ to be determined as discussed earlier from the Kutta condition. So the system of equations for all the unknown singularity distributions, is completed.

In order to conclude the formulation of the problem, we have to add the equations of motion for the vortex sheets defining the wakes of the lifting components of the configuration:

$$\frac{d\vec{x}_W}{dt} = \vec{U}_*(\vec{x}_W;t) + \nabla\phi(\vec{x}_W;t) - \vec{U}_B(\vec{x}_W;t) \tag{15}$$

Theoretical results as well as numerical evidence suggest that in time, the ev olution of a free vortex sheet S_W results the loss of its geometrical smoothness. In order to o vercome this difficult y, a generalization of the vorticity field is introduced. Based on (6) the generalized vorticity field associated with a vortex sheet Σ can be defined :

$$\vec{\omega}_\Sigma(\vec{x};t) = \nabla \wedge \vec{u}_\mu(\vec{x};t) = \underbrace{\delta_\Sigma(\vec{x} - \vec{x}_\Sigma) \cdot [\nabla\mu(\vec{x}_\Sigma;t) \wedge \vec{\nu}(\vec{x}_\Sigma;t)]}_{surface\ \ vorticity} +$$

$$\tag{16}$$

$$\underbrace{\delta_{\partial\Sigma}(\vec{x} - \vec{x}_{\partial\Sigma};t)\vec{\tau}(\vec{x}_{\partial\Sigma};t)}_{line\ \ vorticity}$$

where $\delta_\Sigma(\cdot)$ and $\delta_{\partial\Sigma}(\cdot)$ denote the surface and line Dirac functions defined on the interior and the boundary of $\Sigma(t)$ respectively and $\vec{\tau}(\cdot,t)$ the unit tangential to $\partial\Sigma$ vector (Figure 2). It is noted that if $\mu(\cdot;t)$ is constant then there is no surface term. The above generalization permits the application of the vortex particle approximation. More specifically the surface and line v orticities carried by the wake surfaces S_{W_k} are considered as generalized spatially distributed vorticity.

3 The Computational Model

Since the problem is formulated in time, a time marching scheme was defined. Let Δt denote the time step of the scheme. According to the analysis given in the previous section, all information concerning the vortex sheets of the flow, is known from previous steps, except of the *near part*, i.e. the part generated during the current time step. Consequently different approximations can be used for the near ("new" part) and the far ("old" part) region of the free vortex sheets. More specifically the vortex sheet assumption is retained only for the near region of every wake. On the contrary the rest, i.e. the "old" part, is transformed into free spatial vorticity, in the sense that a vortex particle approximation is introduced.

In this connection, let $S_{W_k}^\Delta, S_{W_k}^*, k = 1(1)N_B$ denote the near and far part respectively of the vortex sheet of the k-th lifting body (Figure 5). Accordingly the wake potential (term (III) in (7) is decomposed into two parts: the potential $\Phi_W^\Delta(\cdot;t)$ induced by the near parts and the potential Φ_W^* induced by the far parts of all vortex sheets:

$$\phi(\vec{x};t) = \Phi + \Phi_W^\Delta + \Phi_W^*$$

$$\Phi_W^\Delta = \sum_{k=1}^{N_B} \Phi_{W_k}^\Delta(\vec{x};t) \tag{17}$$

$$\Phi_W^* = \sum_{k=1}^{N_B} \Phi_{W_k}^*(\vec{x};t)$$

Then according to (6) and (16),$\nabla\Phi_W^*(\cdot;t)$ can be identified to the rotational part of the flow $\vec{U}_\omega(\cdot;t)$:

$$\vec{U}_\omega(\vec{x}_0;t) = \int_{D_\omega(\vec{x};t)} \frac{\vec{\omega}_W(\vec{x};t) \wedge (\vec{x}_0 - \vec{x})}{4\pi|\vec{x}_0 - \vec{x}|^3} dD(\vec{x}) \tag{18}$$

where $D_\omega(\cdot;t)$ denotes the support of the free vorticity $\vec{\omega}_W(\cdot;t)$ given by

$$\vec{\omega}_W(\vec{x};t) = \nabla \wedge \vec{U}_\omega(\vec{x};t) = \sum_{k=1}^{N_B} \sum_{e=1}^{E_{W_k}} \vec{\omega}_{W_k}^e(\vec{x};t)$$

$$\vec{\omega}_{W_k}^e(\vec{x};t) = \delta_{S_{W_k}^e}(\vec{x} - \vec{x}_{S_{W_k}^e}) \cdot [\nabla\mu_{W_k}^e(\vec{x};t) \wedge \vec{\nu}(\vec{x}_{S_{W_k}^e};t)]$$
$$+ \delta_{\partial S_{W_k}^e}(\vec{x} - \vec{x}_{W_k}) \cdot \mu_{W_k}^e(t) \cdot \vec{\tau}_W^e(\vec{x}_W;t) \tag{19}$$

where E_{W_k} denotes for every lifting body the number of panels on its near wake.

The above interpretation of $\nabla\Phi_W^*(\cdot;t)$ leads to some modifications of equations (7) and (10). At first in (7) $\phi(\cdot;t)$ should be identified with the sum $(\Phi + \Phi_W^\Delta)(\cdot;t)$ of (17). This means that wherever the contribution of the wakes appears, it should be restricted only to the near parts $S_{W_k}^\Delta$. Finally in (7) as well as in (10) $\vec{U}_\omega(\cdot;t)$ should be included into $\vec{U}_*(\cdot;t)$.

As regards the discrete problem, $\vec{U}_\omega(\cdot;t)$ as well as its evolution is approximated by means of the vortex particle approximations of the form:

$$\vec{\omega}_W(\vec{x};t) \cong \sum_{j \in J(t)} \vec{\Omega}_j(t) \cdot \zeta_\epsilon(\vec{x} - \vec{Z}_j(t)) \tag{20}$$

where $\vec{\Omega}_j(t)$ and $\vec{Z}_j(t)$ denote the intensities and positions of the vortex particles, $J(t)$ the index set for the vortex particles and $\zeta_\epsilon(r)$ the cut-off function :

$$\zeta_\epsilon(r) = \frac{1}{\epsilon^3} e^{(-\frac{r}{\epsilon})^3} \tag{21}$$

Using (20), $\vec{U}_\omega(\cdot;t)$ takes the form:

$$\vec{U}_\omega(\vec{x};t) = \sum_{j \in J(t)} \frac{\vec{\Omega}_j(t) \wedge [\vec{x} - \vec{Z}_j(t)]}{4\pi|\vec{x} - \vec{Z}_j|^3} f_\epsilon(\vec{x} - \vec{Z}_j(t)) \tag{22}$$

6

where

$$f_\epsilon(r) = 1 - e^{-\left(\frac{r}{\epsilon}\right)^3} \tag{23}$$

Thus instead of calculating the geometry of the vortex sheets and the dipole distributions they carry, we follow the evolution of the vortex particles defined by the following dynamic equations:

$$\frac{d\vec{Z}_j(t)}{dt} = \vec{u}(\vec{Z}_j;t) - \vec{U}_B(\vec{Z}_j;t), \; j \in J(t) \tag{24}$$

$$\frac{d\vec{\Omega}_j(t)}{dt} = (\vec{\Omega}_j(t) \cdot \nabla)\vec{u}(\vec{Z}_j;t) - \frac{1}{2}\vec{\Omega}_j(t) \wedge (\nabla \wedge \vec{U}_B(\vec{Z}_j;t)) \tag{25}$$

Equations (24) and (25) concern the evolution of the far parts of the wakes. As the near parts still retain their character as vortex sheets their determination is different. Let $\vec{U}_{em}$ denotes the mean velocity at a point $\vec{X}_{em}$ along the vorticity emission line of a lifting body. The geometry of the near part of the corresponding wake S_W^Δ is determined kinematically through the following relation:

$$\vec{X}^\Delta = \vec{X}_{em} + \Delta t \cdot \vec{U}_{em} \tag{26}$$

where $\vec{X}^\Delta - \vec{X}_{em}$ denotes the width of $S_{W_k}^\Delta$ in vectorial form (Figure 5). Finally the intensity of the dipole distribution of $S_{W_k}^\Delta$ is determined by means of condition (13).

Due to the time dependent character of the problem, the wakes as well as the vortex particles they include in their far parts, will be constructed gradually. This means that vortex particles will be created as the near parts of the wakes evolve. In order to make this approach compatible with the dynamics of vortex sheets, $\vec{\Omega}_j(t)$ and $\vec{Z}_j(t)$ are defined as follows:

$$\vec{\Omega}_j = \int_{P_j} \vec{\omega}_W dS \qquad \vec{\Omega}_j \wedge \vec{Z}_j = \int_{P_j} \vec{\omega}_W \wedge \vec{x} dS \tag{27}$$

In the above relations, the integration covers for every vortex particle the surface of an element of the near part of the wake considered.

THE FLOW CHART OF THE GENUVP MODEL
For every time step $(H - t = n \cdot \Delta t)$

A. POTENTIAL CALCULATIONS
$\vec{u} = \vec{U}_\infty + \nabla\Phi + \nabla\Phi_W^\Delta + \vec{U}_\omega$

0 Initialize S_W^Δ and Φ_W^Δ (H-through the values of along the emission lines of the lifting bodies)

Iterative schemes for the near wake:

1 Calculate Φ (H-fulfilment of non-entry boundary conditions)

2 Calculate the emission velocities $\vec{U}_{em}$ along the emission lines

3.1 Correct S_W^Δ

3.2 Correct $[\Phi]_W^\Delta$ (H-fulfilment of the Kutta condition)

4. Check for convergence: $\delta[\Phi]_W^\Delta < \epsilon$

5. FIRST OUTPUT: Force and velocity calculations.

B. VORTICITY CALCULATIONS

1. Create new vortex particles

2. SECOND OUTPUT: Wake structure and velocity profiles in the wake

3. Move and deform all the Vortex Particles

3.1 Calculate the velocities and deformations induced at the Vortex Particle locations

3.2 Check for Vortex-Solid surface interaction and correct accordingly

3.3 Produce the new far-wake

4 References

1. Batchelor G.K. (1967) "An introduction to fluid dynamics", Cambridge University Press.

2. Saffman, P.G. (1981) "Dynamics of vorticity", J.Fluid Mech. Vol.106, pp.49-58

3. Saffman, P.G., Baker, G.P. (1979) "Vortex interactions", Ann. Rev. Fluid Mech., Vol.11, pp.11-122.

4. Guiraud, J.P., Zeytounian, R.Kh. (1982) "Vortex sheets and concentrated vorticity. A variation on the theme of asymptotic modelling in fluid mechanics", in Vortex motion, ed. H.G.Hornung, E.A.Muller, Friert. Vieweg & Sohn.

5. Leonard, A. (1980) "Vortex methods for flow simulation", J. Comp. Physics, Vol.37, pp.289-335.

6. Leonard, A. (1985) "Computing three-dimensional incompressible flows with vortex filaments", Ann. Rev. Fluid Mech., Vol.17, pp.523-559

7. Hoeijmakers (1986) "Numerical Simulation of Vortical Flows", Introduction to vortex dynamics, VKI Lecture Notes.

8. Smith, J.H.B. (1986) "Vortex flows in aerodynamics", Ann. Rev. Fluid Mech. Vol.18, pp.221-242 (See also: Smith, J.H.. (1986) "Modelling 3D Vortex Flows in Aerodynamics", Introduction to vortex dynamics, VKI Lecture).

9. Belotserkovskii, S.M. (1977) "Study of the unsteady aerodynamics of lifting surfaces using the computer", Ann. Rev. Fluid Mech., Vol.9, pp.469-494. (See also Belotserkovskii, S.M., Nisht, M.I. (1973) "Nonstationary nonlinear theory of a thin wing of arbitrary planform", Izv. AN SSSR. Mekhanika Zhidkosti i Gaza, Vol.8, No.4, pp.100-108 and Golovkin, V.A., Golovnin, M.A. (1978) "Numerical solution for separated inviscid incompressible flow past an arbitrary body", 6th Int. Conf. Numerical Methods in Fluid Dynamics, Springer Verlag).

10. Kandil, O.A., Chu, LC., Yates, E.C. (1980) "Hybrid vortex method for lifting surfaces with free vortex flow", AIAA paper 800070 (See also: Kandil, O.A., Mook, D.T., Nayfeh, A.H. (1976) "Nonlinear prediction of Aerodynamic loads on lifting surfaces", J. Aircraft, Vol.13, No.1, pp.22-28).

11. Maskew, B. (1980) "Predicting aerodynamic characteristics of vortical flows on three-dimensional configurations using a surface singularity panel method", AGARD C.P.208

12. Katz, J. (1982) "Large scale vortex lattice model for the locally separated flow over wings", AIAA J., Vol.20, No.12, pp.1640-1646 (See also: Levin, D., Katz, J. (1981) "Vortex-lattice method for the calculation of the nonsteady separated flow over Delta wings", J. Aircraft, Vol.18, No.12, pp.1032-1037)

13. Wagner, S.N., Schottl, Ch. (1990) "Validation of the aeroelastic simulation program for horizontal axis wind energy converters", Proc. ECWEC'90, p.296, Madrid, Spain (See also the references cited therein).

14. Rechbach, C. (1977) "Calcul numerique d'ecoulements tridimensionnels instationnaires avec nappes tourbillon naires", Recherche Aerospatiale, No 5, pp.289-298

15. Cantaloube, B., Huberson, S. (1984) "Calcul d'ecoulements de fluide incompressible non visqueux autour de voilures tournantes par une methode particullaire", Recherche Aerospatiale, No.5, pp.403-415.

16. Zervos, A., Huberson, S., Hemon, A. (1988) "Three- dimensional free wake calculation of wind turbine wakes", J. Wind Engineering and Industrial Aerodynamics, Vol.27, pp.65-76

17. Huberson, S., Zervos, A. (1988) "A 3D vortex particle model for the Darrieus rotor", submitted for publication

18. Voutsinas, S.G. (1990) "Theoretical and numerical analysis of three dimensional subsonic inviscid flows", PhD. Thesis, NTUA, Dept. Mech. Engineering.

19. Zervos, A., Voutsinas, S.G. (1991) "Numerical simulation of three-dimensional vortical flows", NTUA Report.

20. Richardson, S.M., Conrish, A.R.H. (1977) "Solution of three-dimensional incompressible flo w problems", J. Fluid Mec h. Vol.82, part 2, pp.309-319

21. Voutsinas, S. G., Riziotis, V. A. (1996) "Vortex Particle Modelling of Stall on Rotoros. Application to Wind T urbines", ASME Conference on Fluid Engineering, San Diego, California, U.S.A..

22. Voutsinas S. G., Riziotis V. A., (1999) "A Viscous-Inviscid Interaction Model for Dynamic Stall Simulations on Airfoils", 37th Aerospace Sciences Meeting and Exhibit, Reno, Jan uary 11-14, 1999, AIAA paper 99-0038.

23. Milewski, W.M. (1997) "Three Dimensional Viscous Flo w Computations Using the Integral Boundary Layer Equations Simultaneously Coupled with a Low order Panel Method", MIT PhD

24. Mughal, B.H. (1992) "A calculation method for the three dimensional boundary la yer equations in integral form" , MIT MSc

25. Mughal, B.H. (1998) "In tegral methods for three-dimensional boundary la yers", MIT PhD

26. Chaviaropoulos, T. (2000) "Viscous and aeroelastic effects on wind turbine blades" Final Report of the JOR3-CT98-0208, VISCEL project.
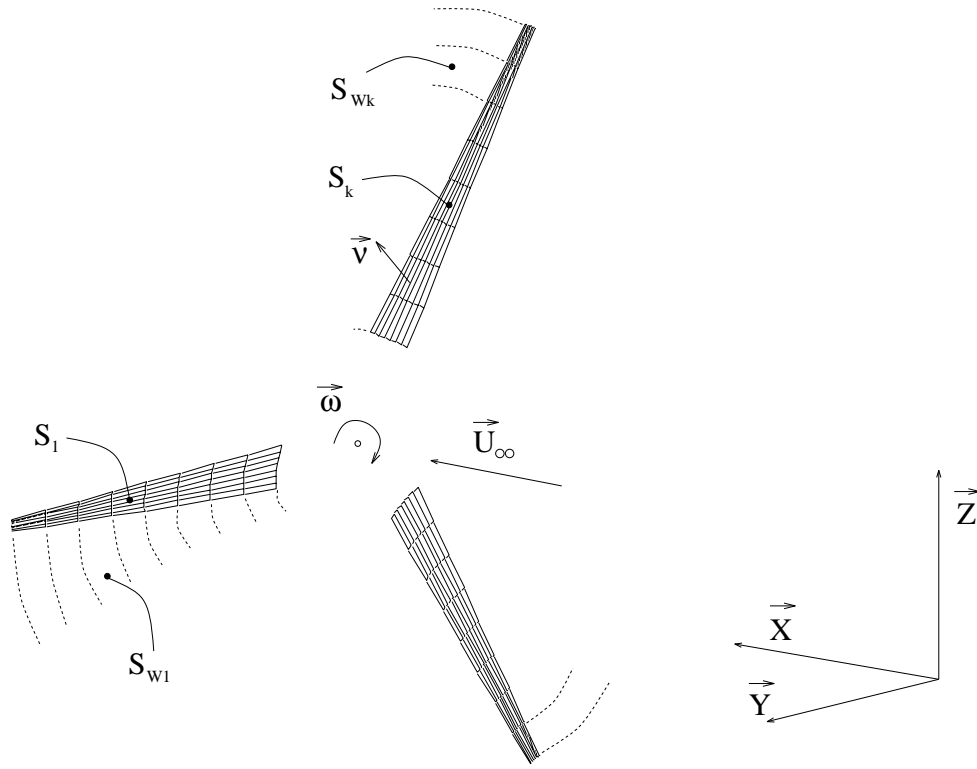
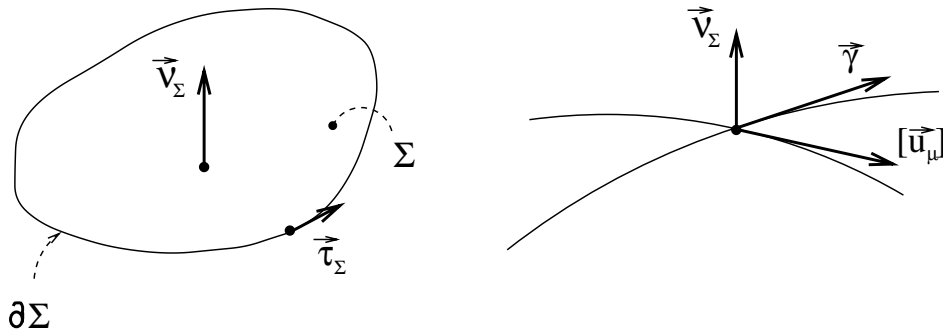Figure 1: The basic notations

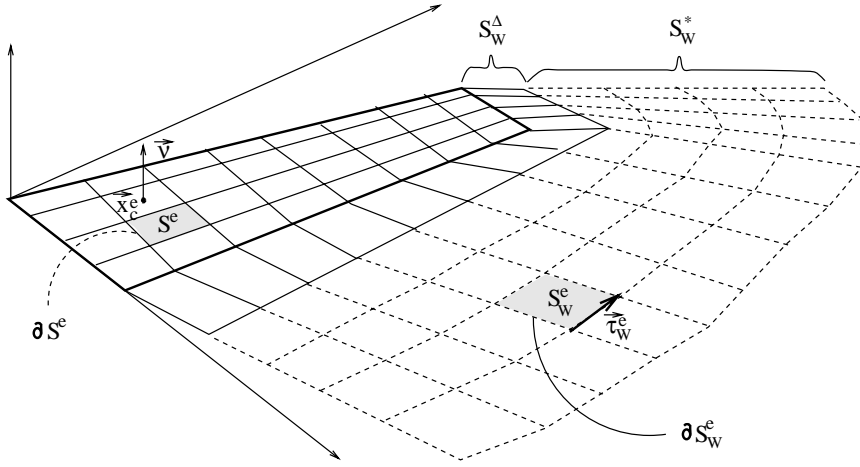Figure 2: Equivalence between a dipole and a surface vorticity distribution
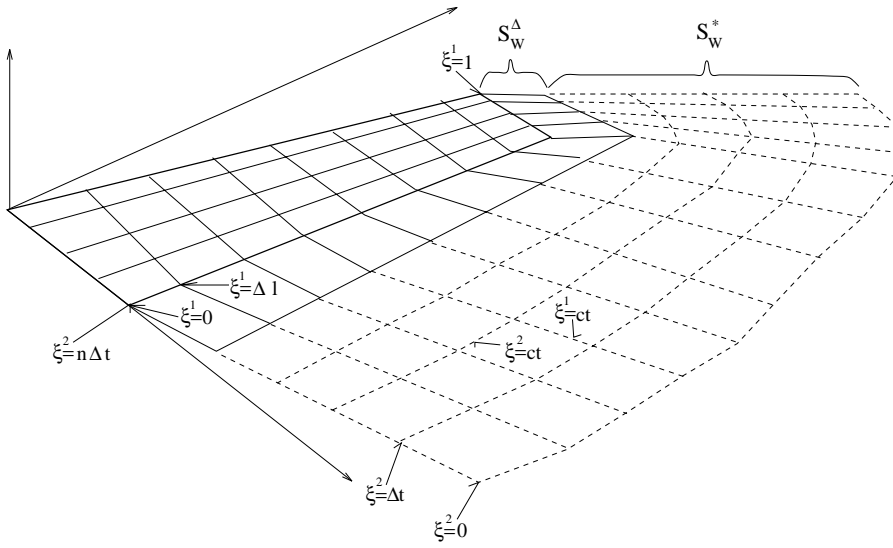
Figure 3: The notations of the grid used

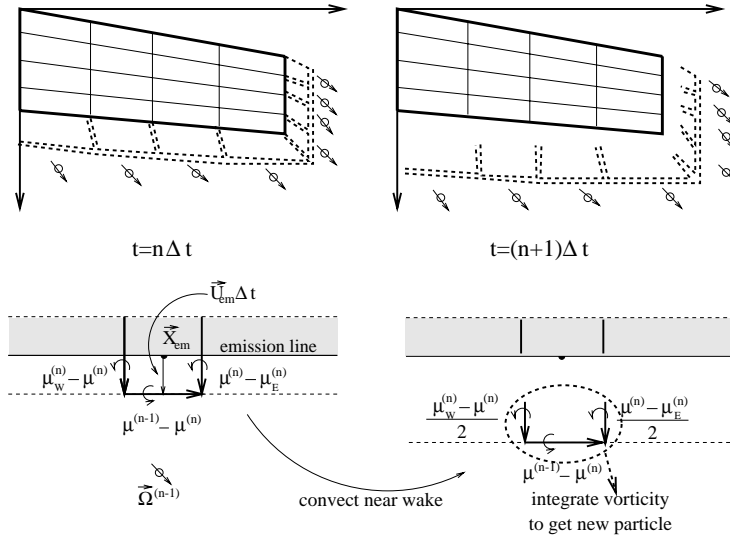Figure 4: The notations for the wake of a lifting surface

Figure 5: The hybrid scheme

Overview of the HAWTDAWG Model
– A Model for Aerodynamic Performance of HAWTs

Tongguang Wang and Frank. N. Coton
Department of Aerospace Engineering
University of Glasgow
Glasgow G12 8QQ, U.K.

INTRODUCTION

The HAWTDAWG (Horizontal Axis Wind Turbine Directly Allocated Wake Geometry) model has been developed at the University of Glasgow for a number of years. This unsteady model involves an application of a prescribed wake scheme. In the technique, the blade is modelled as a series of blade elements, from which trail vortex filaments whose strengths correspond to the differences in bound circulation. In addition, shed vorticity is introduced to account for the temporal variations in bound vorticity. These trailed and shed vorticities are modelled as a discretised, sequential mesh of finite, straight-line vortex filaments extending from the blades. The method uses prescription functions to specify the wake structure. Vortex theory is applied to obtain estimates of the velocities at the blades induced by the wake. This information is used to generate blade-bound vorticity and wake trailed and shed vorticity distributions, as well as to provide the basis for the construction of the wake. Therefore, an iterative procedure is required to obtain converged wake geometry and blade loading [1,2].

A prescribed velocity deficit profile is included in the onset flow for downwind rotors to account for the tower shadow effects [3].

The Beddoes-Leishman dynamic stall model [4] is coupled to the prescribed wake scheme to provide estimates of the unsteady aerodynamic loads acting on the blades [2]. A three-dimensional stall delay model has been incorporated within the Beddoes-Leishman unsteady model to modify the 3-D rotational effects. The manner in which this was achieved is discussed in detail by Wang and Coton [5]. In this way, the unsteady aerodynamic response of the blade can be directly computed from the coupled unsteady 3-D prescribed wake model.

MODELLING OF BLADE AND WAKE

In the model, the blade is divided into N_E elements, which are defined by (N_E+1) element boundaries. The control point of the blade element is positioned at the quarter chord of the mid-span of each element. The code has been designed for its users to input the radial positions of the element boundaries according to their needs, either in an arc-cosine distribution of the boundaries or in another specific distribution in order to obtain a prescribed series of control points.

For azimuthal discretisation, a revolution of the rotor is equally divided into N_T time steps. Thus. there are (N_E+1) helical vortex filaments in the wake trailing from each blade element boundary and convecting downstream to infinity. These vortex filaments are composed of straight-line elements, each of which corresponds to a time step. When the wake vortex element is downstream far enough, its induction at the blade is negligible. For this reason, the far wake is cut off after N_C cycles and beyond this cut-off point the wake is neglected. Thus, each trailing vortex filament has ($N_T \bullet N_C$) elements. Across the trailing vortex filaments are the shed vortices.

MODEL INPUTS

The model inputs include flow conditions (inflow velocity, yaw angle, air density), blade and rotor geometric parameters (number of blades, radius, rotational angular speed, blade chord and pitch spanwise distribution), discretisation parameters (number of blade elements N_E, number of azimuth positions per cycle N_T, and number of wake cycles N_C), and two-dimensional aerodynamic aerofoil data (lift and drag coefficients), etc.

In order to include the tower shadow effects for downwind rotors, tower diameter and rotor overhang should be input. In the present code blind comparison, a cosine function has been used to model the velocity deficit behind the tower and the maximum deficit taken as 30% of the onset flow velocity. The tower shadow width has been set at 2.5 times the tower diameter in the calculation.

Implementation of the Beddoes-Leishman unsteady model requires a number of empirical constants, which are obtained from static and unsteady aerofoil test data.

The 3-D rotational effects on the unsteady blade loads is presented based on the stall delay model of Selig-Du [6], which has been coupled to the unsteady method on the basis of the 3-D consideration. The 3-D correction for the chordwise force requires the input of the ordinates of the aerofoil upper surface.

PERFORMANCE ATTRIBUTES

In order to compromise the computational time and the accuracy of the results, the inputs such as N_E, N_T and N_C must appropriately chosen, because the computation time strongly depends on these parameters, and is approximately proportional to ($N_C N_E N_T^2$). In the present calculation, for the code blind comparison, N_E=16, and N_C varies from 5 at a low tip speed ratio to 10 at a high tip speed ratio. For the upwind rotor cases, N_T has been set to 18, corresponding to an azimuth interval of 20 degrees. This time step is then refined to 10 degrees in the unsteady aerofoil model. To obtain a reasonable representation of tower shadow effects, N_T has been chosen to be 36 for the downwind rotor cases.

For N_E=16, N_T=18 and N_C=5, the CPU time for a converged output is approximately 178 seconds on a Sun-Sparc workstation. The maximum memory is 8MB and maximum swap 15MB.

POST PROCESSING

The calculated results from the model are output at every azimuth angle of 10 degrees for the present case. In order to meet the requirement by the output file format of NREL/NWTC, the results from the model have been reconstructed at an azimuth interval of 1 degree using a cubic-spline which interpolates (passes exactly through) the set of data output from the model. The mean, standard deviation, maximum and minimum values for each column have also been calculated.

REFERENCES

1. Robison, D.J., Coton, F.N., Galbraith, R.A.McD. and Vezza, M., Application of a prescribed wake aerodynamic prediction scheme to horizontal axis wind turbines in axial flow, *Wind Engineering*, **19**(1), 1995, 41—51.
2. Coton, F.N. and Wang, T., The prediction of HAWT performance prediction in yawed flow using an unsteady prescribed wake model, *Proc. I. Mech. E. Part A, J. of Power and Energy*, **213**(1), 1999, 33—43.
3. Wang, T. and Coton, F.N., An unsteady aerodynamic model for HAWT performance including tower shadow effects, *Wind Engineering*, **23**(5), 1999, 255—268.
4. Leishman, J.G. and Beddoes, T.S., A semi-empirical model for dynamic stall, *J. of American Helicopter Soc.*, **34**(3), 1989, 3—17.

5. Wang, T. and Coton, F.N., Prediction of the unsteady aerodynamic characteristics of horizontal axis wind turbines including three-dimensional effects, *Proc. I. Mech. E. Part A, J. of Power and Energy*, **214**, 2000 (To appear in the November Issue).
6. Du, Z. and Selig, M.S., A 3-D stall-delay model for horizontal axis wind turbine performance prediction, *AIAA—98—0021*, 1998.

SHORT DESCRIPTION OF THE METHOD AND THE TEST CASE

The numerical method used to calculate the flow around the NREL/NWTC wind generator solves the complete 3D steady, Reynolds-averaged momentum equations by the finite volume approach. A two block, Chimera-type domain decomposition is employed to discretize the computational space, Fig. 1. A C-type mesh covers the blade whereas a cylindrical mesh comprises the outer block and covers the field around the generator. The grid in the first block is orthogonal curvilinear on transverse sections, created by applying a conformal transformation of the blade section on the unit circle. In the outer domain the flow variables refer to an orthogonal cylindrical system. A two zonal, k-ε eddy viscosity model has been used to model the Reynolds stresses. The standard k-ε model is used far from the solid boundaries, while a one-equation k-model based on the mixing length approximation is applied near the wall and up to the solid boundary. A SIMPLE-like pressure correction procedure is followed to calculate the pressure field and successive solutions are performed independently in the two blocks until convergence is achieved.

The method has been applied in one configuration of the proposed. The characteristics of the test case (S1000000-downwind)) are :

Yaw angle : 0
Wind speed: 10m/s
Air density: 1.246 kg/m**3
Rpm: 72.1
Blade flap:0
Tip pitch angle: 3
External Radious: 5.029m

The computational grid past the blade had 498x31x75 nodes where the first number denotes the nodes parallel to the contour, the second normal to it and the third represents the transverse sections. The external boundary was placed at a distance of 1.3 the radius of the blade R. After the solution has converged, the first near wall nodes had a mean value of y^+ equal to 0.75, i.e. they were lying in the viscous sub-layer region. The external cylindrical grid consistsed of 172(circumferential) x 86 (radial) x 171(x-axis) nodes, and extended from –2R to 6R in the longitudinal (x) direction. All computations were carried out in an ORIGIN-2000 SGI computer, using one processor.
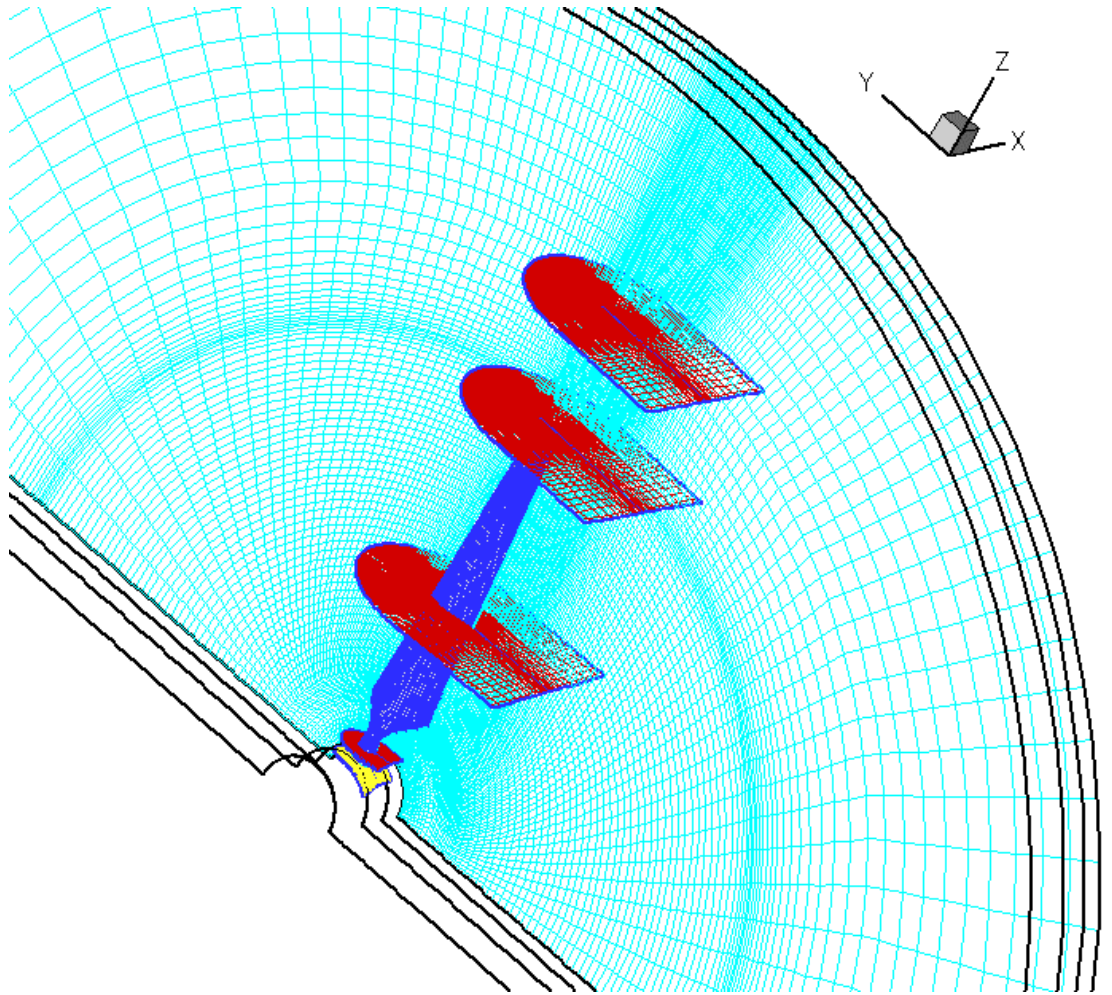
Fig.1 The two-block grid configuration